TOP-FUEL DRAGSTER WING DESIGN USING CFD AND ITS INFLUENCE ON VEHICLE DYNAMIC PERFORMANCE

By

TONY MICHAEL BURATTI

Bachelor of Science

Oklahoma State University

Stillwater, Oklahoma

1998

Submitted to the Faculty of the
Graduate College of
Oklahoma State University
in partial fulfillment of
the requirements for
the Degree of
MASTERS OF SCIENCE
December, 2000

TOP-FUEL DRAGSTER WING DESIGN USING CFD

AND ITS INFLUENCE ON VEHICLE

DYNAMIC PERFORMANCE

Thesis Approved:

Thesis Advisor

Dean of the Graduate College

ACKNOWLEDGEMENTS

I am deeply grateful to my parents, Richard M. and Joyce K. Buratti, for their love, support and encouragement. They have instilled in me the value of hard work and dedication which has helped me to become who I am today. Special thanks goes to my grandmother, Frances Henson, for her love and support that she has provided.

I also extend my appreciation to the faculty and staff of the Mechanical and Aerospace Engineering department at Oklahoma State University who have adopted me and encouraged me to be successful. I would also like to thank the other members of my committee, Dr. David G. Lilley and Dr. Gary E. Young, for their suggestions and comments throughout this research.

Mr. Brian Vermillion of Advanced Racing Composites has provided support through his knowledge, information, and insight into the racing community. I appreciate all his time and resources that he has provided in support of my research and education. I would also like to thank Dr. Kajal K. Gupta of NASA Dryden Flight Resource Center for his support and sponsorship.

Lastly, I wish to express my sincere appreciation to my graduate advisor, Dr. Andrew S. Arena Jr., for his continual support and guidance throughout the last couple of years. He has been inspirational through his teachings and will continue to serve as a great mentor throughout my professional career.

TABLE OF CONTENTS

Chapter Page

Chapter Page

LIST OF TABLES

LIST OF FIGURES

Figure Page

Figure Page

Figure Page

NOMENCLATURE

CFD	Computational Fluid Dynamics
NHRA	National Hot Rod Association
A	Aerodynamic reference area-projected frontal area of the vehicle
AR	Aspect Ratio
C_D	Coefficient of drag
C_L	Coefficient of lift
D_{free}	Free diameter of the tire, unrestrained, inches
F_v	Vertical tread force, lbf, impact momentum
L.E.	Leading Edge
M_{grd}	Mass of tread, lb_m/g, W/g
$\dot{M}_{grd}$	Mass rate of tread, $lb_m/g \cdot \sec$
N_i	Rear axle input speed, RPM
N_r	Real axle speed, RPM, $N_i/3.2$
P	Specific effective power
Re	Reynolds number
RPM	Revolutions per minute
S	Wing area
SR	Slip Ratio

a	Distance to vehicles cg from the front wheels
b	Wing span
c	Chord length of an airfoil
d	Distance from the vehicle cg to vehicles center of pressure
g	Acceleration due to gravity
h	Height of endplate
m	Mass of the vehicle
s	Horizontal distance traveled
$\dot{s}$	Longitudinal velocity
$\ddot{s}$	Longitudinal acceleration
s_L	Aerodynamic radius, $s_L = \frac{m}{\frac{1}{2}\rho A C_L}$
Λ, Δ	Fraction of lift on driving wheels including weight transfer effect
γ	Traction coefficient
η	Vehicle driving efficiency
λ	Fraction of weight on driving wheels including weight transfer effect
μ	Coefficient of rolling resistance
ρ	Air density

CHAPTER 1

1. INTRODUCTION

1.1 Background

The dynamics of a Top-Fuel Dragster Car, depicted in Figure 1-1, are quite complicated to model and pose problems for many research areas of interest. The Top-Fuel Dragster is the fastest of drag racing vehicles. It accelerates at almost 4 longitudinal g's completing a quarter mile run in less than five seconds. It reaches over 100 mph in less than a second and finishes the run with speeds in excess of 320 mph. They are powered by a supercharged engine that puts out over 6000 horsepower and the massive tires spin at almost 8000 rpm. For a single run these dragsters consume more than 5 gallons of nitro methane fuel. The vehicles weight is around 2150 pounds, including the driver, giving it a phenomenal power to weight ratio that puts it in a class like no other.

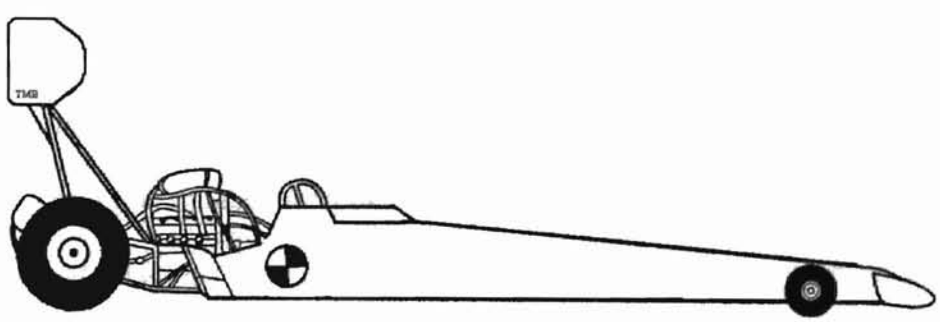

Figure 1-1: Schematic of a top-fuel dragster

Lift and drag are very important factors for this type of racing event. Many components are responsible for creating this lift and drag but only a couple greatly affect the dragsters performance. These components include the body, rear wheel dynamics, and the rear wing.

The performance of the enormous rear tires, 36.0" x 17.0"-16's, add to the complexity of the problem. During the run the tires stretch and deform due to a large engine torque of around 4500 ft-lbs as well as the rotational inertial of the tire tread. Normal operating pressure is 4 psig to 5 psig creating a tire footprint of over 250 square inches at the start of the run. The tire constantly changes in size and can expand adding an additional 4.5 inches to the diameter during a run. The rotational inertia of the tire delivers a down force to the car. On the other hand, the flow over the wheels has a great affect on the performance of the car because it results in a positive lift at the rear axle.

The rear wing is used to increase the amount of down force to the rear tires. Increasing this down force increases the normal force between the tire and track surface, which theoretically should increase the potential to use the engine power to accelerate the dragster. If there is little normal force then there is potential for the car to experience wheel slip and thus not have traction to accelerate.

The reason every top fuel dragster team doesn't make a rear wing that has an enormous amount of down force is the fact that when lift is generated so is drag. This drag is referred to as induced drag and is a function of the square of the velocity. This increase in drag therefore takes more horsepower away from the acceleration horsepower and results in a reduced maximum speed that can be achieved during the run. The question is therefore how much down force is needed and at what time during the run is the maximum amount of down force critical?

1.2 Research Objective

The emphasis of the present work is two fold. First is to develop an accurate dynamic model for a quarter mile run of a top-fuel dragster. The model will be as complete as possible accounting for the significant forces encountered on the vehicle. The performance of the vehicle will be determined by the elapsed time and final speed.

The second portion of this work will be to study the effects that the aerodynamic characteristics of a dragster and rear wing have on the performance of the dragster using the model. From this data an alternative wing will be designed and analyzed. This data will be entered into the model and compared to the current style of wings being used.

Most emphasis has gone into improving the rear wing characteristics but this will not necessarily improve the performance of the dragster. The dynamic solver will be used to determine if the new wing will improve the performance of the overall vehicle. Therefore the focus will be in improving the performance of the car and not just focus on improving the rear wing characteristics. A computational fluid dynamic (CFD) solver will be used to analyze the wing characteristics and this information will be used in the dynamic dragster model.

CHAPTER 2

2. LITERATURE REVIEW

This literature review covers several aspects of a dragster. First two dynamic models will be discussed in detail and one will be modified and used for the current research. Second the dynamics of the tires will be discussed to find out more about modeling the tire dynamically and all the modeling problems that it might pose. The other part of the tire research review will be on the aerodynamics of the tires since they are large and rotate at high rpm. To end the chapter other aerodynamic studies will be done for different wing designs talking about the general style of dragster wing used now and the rules limiting the wings.

2.1 Dynamics of Vehicles

It is good to first look at the interaction between the vehicles aerodynamic characteristics and wheel dynamics and see how they affect the overall vehicle performance. Better and improved vehicle performance is what is truly desired and not just the improvement of the components. Granted the improvements in components can lead to better vehicle performance but how much and at what time during the run is the question. The dynamics of the vehicles and how it is affected by the dynamics and aerodynamics of the tires, the aerodynamic surfaces, and the aerodynamics of the vehicle's body is what is looked at next.

2.1.1 Tire Tread Momentum Theory

Because Top-Fuel Dragsters accelerate at over 4 longitudinal g's for several seconds this means that there is an effective tire friction factor of over 4 [Hallum, 1994]. This is not possible and therefore Hallum offers a theory on his tread momentum principle.

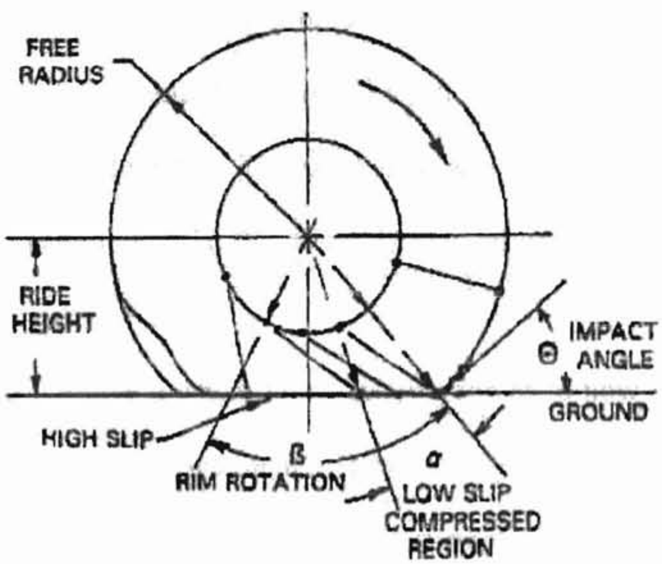

Figure 2-1: Drag Tire Schematic

A schematic of a dragster tire is depicted in Figure 2-1 above. In this schematic the tire contact angles, tread radius, tread sidewall twisting-straightening, and rotational angles are all shown. Hallum states that the normal force applied to the ground under the compressed area is about equal to the rate of change of vertical tread momentum at the contact. This force, for one tire is given by equation (2-1).

$$F_v = \dot{M}_{grd} \cdot V_{grd} \cdot \sin\theta \tag{2-1}$$

where
$$\dot{M}_{grd} = \cdot M_{grd}\left(\frac{N_r \cdot RPM}{60}\right)$$

$$V_{grd} = \pi \cdot \left(\frac{D_{free}}{12}\right)\left(\frac{N_r}{60}\right)$$

For this method there are three initial inputs into the system, which are start line ride height (16.5 inches), rear axle RPM at initiation (0 RPM), ground velocity (0 ft/sec), and acceleration due to rear static weight times the tire friction. The rear axle RPM and ground velocity are from real data but it would seem that the ground velocity would be something that should be calculated. The ride height was assumed and a constant friction factor was used. The output is the tread horizontal momentum change and the acceleration of the dragster.

This model did not give a whole lot of information as to how it works and proved difficult to use when trying to implement. Therefore a different model was sought and discovered that would prove more beneficial to the current research effort.

2.1.2 Critical Speed Model

A different model was proposed by [Hawks and Sayre, 1973] in which they study the optimum straight-line performance of an automobile. They introduce the equations of motion for a straight-line acceleration including both the aerodynamic lift and pitching moment. Their results concluded that aerodynamic down force can improve performance if the acceleration is limited by traction and that aerodynamic lift is beneficial when power is the limiting factor.

Most of the trends in those days, when considering high-performance automobile design, was to place emphasis on producing down force for the purpose of improving cornering speeds. It was thought that these aerodynamic devices that were being used degraded straight-line performance due to the drag but then it would be made up in the cornering.

Hawks and Sayre found that, in certain circumstances, the straight-line performance improved along with the cornering speed due to the introduction of these aerodynamic down force generating devices. There studies looked at the performance of three vehicles - an AA/FD Competition Fuel Dragster, a Ford Galaxie sedan, and the Lola T-140 Formula A car with several different aerodynamic devices.

It was found that below a certain speed, referred to as the critical speed, the vehicle can spin its wheels. This force corresponds to the friction coefficient multiplied by the normal force on the tires. When there are aerodynamic forces acting on the vehicle then the force becomes a function of the vehicles speed squared. This increase in down force comes with the penalty of increased drag due to the induced drag of the aerodynamic surfaces as discussed previously. If the increase in driving force is greater than the increase in drag then an improvement in performance will result.

Some of the assumptions that were made for this model include a rigid body in rectilinear motion; the automobile is driven through one pair of wheels; acting on the automobile are the driving force, the rolling resistance, the aerodynamic forces of lift and drag, and the aerodynamic pitching moment; and there is an ideal transmission. It was also assumed that below the critical speed, wheel spin is impending and the driving force is dependent on the product of the friction coefficient and the normal force on the driving wheel. Above this critical speed the driving force is proportional to the maximum power and inversely proportional to the speed. The rolling resistance is assumed to be constant for simplicity.

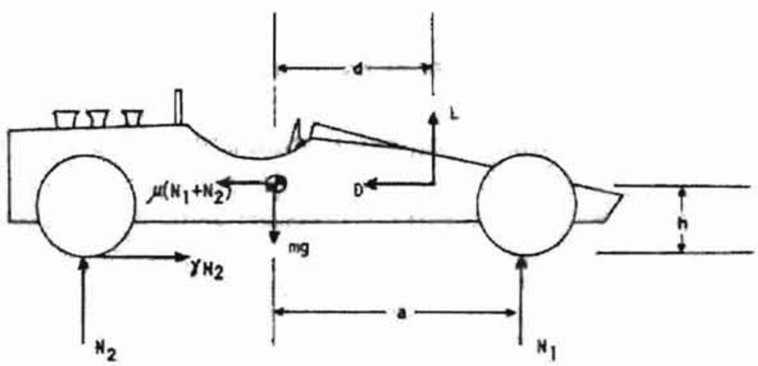

Figure 2-2: Schematic of an AA/FD Dragster with Forces [Hawks and Sayre, 1973]

When looking at the model in a more detailed manner the schematic of an AA/FD Dragster and the forces acting upon it should be used and is depicted in Figure 2-2. Using the vertical force equation and the moment equation to find the normal loads on the tires, the equation of motion in the longitudinal direction can be derived. The longitudinal acceleration for a speed that is less than the critical speed is shown in equation (2-2).

$$\ddot{s} = [\gamma\lambda - \mu]g - \frac{1}{2}\frac{\rho A}{m}[C_D + (\gamma\Lambda - \mu)C_L]\dot{s}^2 \qquad (2\text{-}2)$$

Equation (2-3) is the acceleration where the speed is greater than the critical speed.

$$\ddot{s} = \frac{\eta \mathrm{P}}{m\dot{s}} - \mu g - \frac{1}{2}\frac{\rho A}{m}\left[C_D + \mu C_L\right]\dot{s}^2 \tag{2-3}$$

where
$$\lambda = \frac{a}{1 - h\gamma}$$

$$\Lambda = \frac{a - d}{1 - h\gamma}$$

Since the critical speed is the speed at which the traction-limited driving force equals the power-limited driving force it can be found by equating (2-2) and (2-3). The resulting equation is a cubic equation in critical speed where the critical speed is the smaller positive root of equation (2-4).

$$\dot{s}^3 - \frac{\lambda g}{\Lambda} s_L \dot{s} + \frac{\mathrm{P} s_L}{m \Lambda \gamma} = 0 \tag{2-4}$$

where s_L is the aerodynamic radius and is given by

$$s_L = \frac{m}{\frac{1}{2}\rho A C_L}$$

For the current research effort the critical speed model will be modified and used in order to look at particular components of the dragster and how they affect the performance. Actual parameters will be used when known but other parameters will be estimated to develop a good model. This model will be validated using top-fuel dragster data. Further research will be done to show patterns of the affects that changing the aerodynamic characteristics have on the performance. The model will also be used to look at a current wing used and see what types of changes can be made to it, if any, that will help lower the elapsed time and increase top speed.

2.2 Characteristics and Dynamics of Rotating Wheels

The tire is one of the most important considerations of the racecar because it is the linkage between the vehicle and the racing surface. There are many studies on the dynamics of tires and the various things that affect the performance of the tire. The bulk of the studies in this area have been for passenger cars but some of this can be used for the current research. There will also be some discussion of the dynamics and aerodynamics of various parts of the vehicle. After talking about passenger car tires and the dynamics and aerodynamics, a section dealing with just top-fuel dragster tires will be discussed.

2.2.1 Dynamics of Tires

The main bulk of the material for the dynamics of tires deals with lateral forces or cornering forces. The research done in this field is for passenger tires and deals mainly with trying to model a tire for passenger cars. For example several researchers look at tire interaction with different surface terrain, how things differ when there is an uneven vehicle, how the effects of braking and cornering affect traction, the effects of wheel orientation, temperature and pressure variations, and various combinations of each.

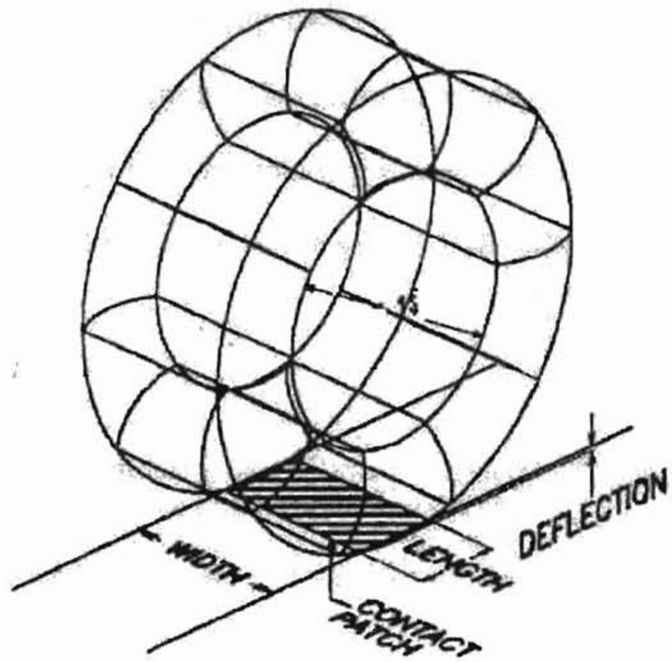

Figure 2-3: Schematic of the Contact Patch

The concern for the current research is that for straight-line acceleration where it deals with the longitudinal forces. When accelerating there are longitudinal forces between the tire and the ground that arise in an area referred to as the tire footprint as can be seen in Figure 2-3. The longitudinal forces have similarities to the lateral or cornering forces inasmuch as there is an elastic distortion region, referred to as longitudinal stretching, and a sliding or frictional region [Milliken and Milliken, 1995]. In addition to these longitudinal forces there are other important forces that arise that come from the aerodynamics of the tires.

2.2.2 Tire Aerodynamic Studies

Tire aerodynamics are not the main focus of this work but for modeling purposes it is necessary to understand some of the characteristics of the tires when developing an accurate dynamic model. Wheel aerodynamics is a topic that is not fully understood. The information that is generated is based upon research done for the automotive industry. A lot of time has been put into experimental wind tunnel setups where the concern becomes ground interference. Once placed in the wind tunnel, a tire setup can consist of several things:

1. The tire can be stationary (not allowed to rotate) varying the gap distance between the floor and the bottom of the tire.
2. It can be powered by a motor and vary the gap between the floor and the bottom of the tire.
3. The wind tunnel has a movable floor and the wheel is powered by a motor and placed on the moving floor.

All these tests in the wind tunnel are used to try to match existing tire aerodynamic data. It might not be possible to have the ideal setup in the wind tunnel because they might not have a moving floor, they might not be able to power the wheel, etc. The ideal setup would be to have a wind tunnel vehicle that is able to rotate the wheels at their appropriate speeds with zero ground clearance.

Studies have been done looking at the first setup where the tire is stationary and the gap is varied. It was shown by using wool tufts around the wheels that for the stationary wheels the difference between a sealed and unsealed ground clearance was almost imperceptible [Stapleford and Carr, 1970]. It was stated that the boundary layer effect restricted the flow of air under the wheels when the gap was opened. But when the wheels were rotating, as in the second setup mentioned above, an additional airflow was induced through these gaps and the flow pattern had changed considerably. The principal effect of the rotation was an asymmetric pressure distribution causing a large negative lift to be generated in accordance with the Magnus effect, which is discussed next.

For inviscid flow past a cylinder has a symmetric flow pattern and by symmetry the lift and drag are zero. But for a rotating cylinder it will drag some of the fluid around producing circulation. This in effect causes the flow to be asymmetric and the average pressure is greater on the upper half of the cylinder than on the lower half of the cylinder causing lift to be generated. This is known as the Magnus effect and is pictured in Figure 2-4. This figure was provided by [Munson, Young, and Okiishi, 1994].

In the figure, the first picture (a) is of a uniform upstream flow past a cylinder without circulation. The second picture (b) is a free vortex at the center of the cylinder while the last picture (c) is the combination of the free vortex and uniform flow past a cylinder. This combination gives nonsymmetrical flow and thus produces lift.

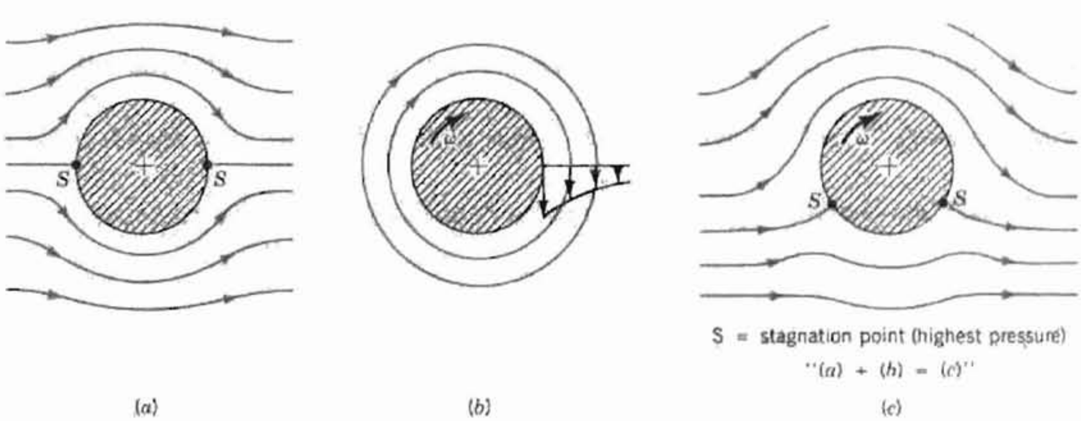

Figure 2-4: Schematic of Magnus Effects

Further explanation is given by [Katz, 1995] where he talks about and shows the difference in separation points for a rotating and non-rotating wheel in a wind tunnel. As seen in Figure 2-5 the separation point on the rotating wheel (left) occurs much sooner than the separation point on the stationary wheel (right). This figure was provided by [Katz, 1995].

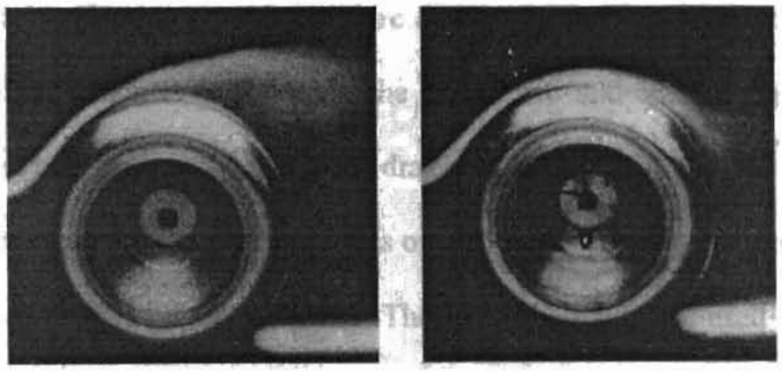

Figure 2-5: Experimental Study of Flow Past a Stationary and Rotating Wheel [Katz, 1995]

This early separation for the rotating wheel can be explained by studying Figure 2-6 which was provided by [Milliken and Milliken, 1995]. For the stationary wheels the suction pressure is greater on the top of the wheels and thus causes a greater positive lift upwards. When the rotation is introduced the separation point is further upstream reducing the suction pressure and thus reducing this positive lift. The figure below is from wind tunnel tests and the rotating wheel had an effective "zero" ground clearance while the stationary wheel had a 0.25 inch ground clearance [Stapleford and Carr, 1969].

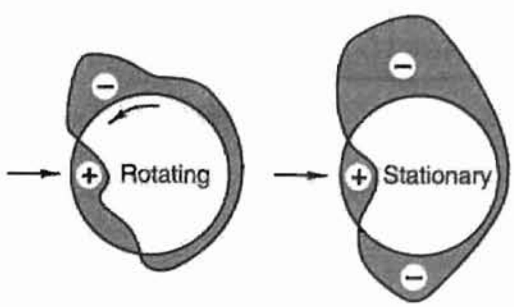

Figure 2-6: Pressure Distribution Around the Wheels of a Vehicle

Another thing that greatly affects the characteristics of tire performance is Reynolds number. A little bit of information was provided by [Cogotti, 1983] about the effects of Reynolds number. He also provides his tire data along with the corresponding critical Reynolds number, which is based upon the turbulence and surface roughness. This critical Reynolds number greatly affects the drag coefficient.

When looking at the Re number effects on a smooth cylinder, as seen in Figure 2-7, the coefficient of drag is greatly affected. The figure below is not used for any data in this work but it is merely to show how great Re number effects can be on an object similar to the dragster tire. The figure was provided by [Munson, Young, Okiishi, 1994]. The calculated Re number for the top-fuel dragster tire at a top speed of 330 mph, based upon its diameter, is 9.25×10^6.

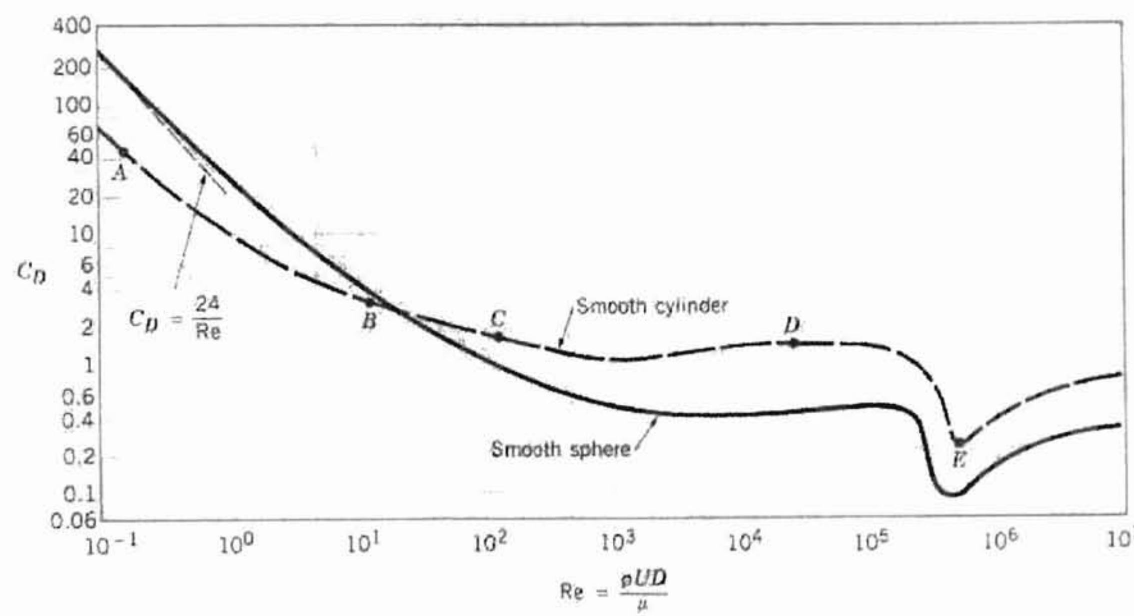

Figure 2-7: Reynolds Number Effects on the Coefficient of Drag [Munson, Young, Okiishi, 1994]

The letters in the previous figure correspond to flow patterns in Figure 2-8, below. The wheel would see a similar flow pattern as it speeds up but in this case there is no ground effects present and the cylinder is not spinning so the flow pattern is for visual purposes only. This helps show the different flows that are encountered during the dragsters run which make the analysis that much more difficult.

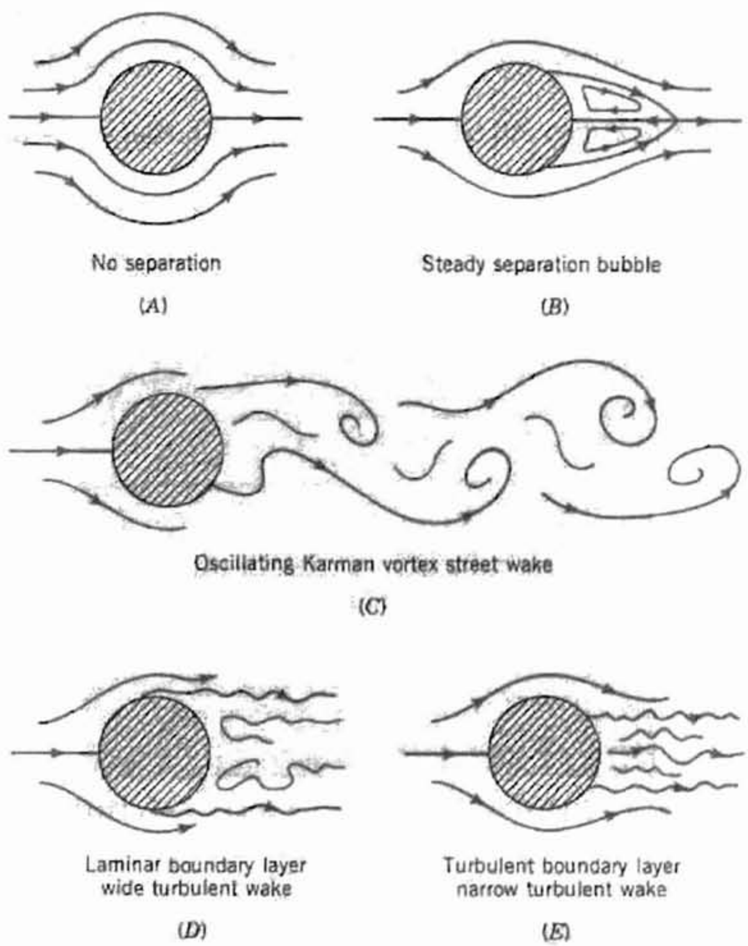

Figure 2-8: Flow Pattern Around a Smooth Cylinder at Various Re Number

One thing in common with all of these papers is that they all seem to come to the conclusion that wheel aerodynamics are very difficult to measure experimentally and their full interaction with the rest of the vehicle is still in a state of confusion. This was mainly for passenger type tires without the added complications of the top-fuel dragster tire where the high torque, low pressure, high speeds, and large tire deformations add to the complexity of the problem.

2.2.3 Top-Fuel Dragster Tires

As mentioned before the top-fuel dragster has enormous rear tires, 36.0" x 17.0"-16's as seen in Figure 2-9. The side walls of the 36-inch diameter tire are very flexible and weighs around 47 pounds. The main tread of the tire comes in at a weight of around 30 pounds for its 17-inch width.

Figure 2-9: Static View of a Top-Fuel Dragster Tire

With a large engine torque of around 4500 ft-lbs coupled with the normal operating tire pressure of 4 psig to 5 psig gives way to the large 4.5 inches of diameter expansion that the tire sees. In Figure 2-10, there is a static picture before a burnout as well as a picture of the same vehicle during the burnout. The tire has changed shape dramatically both in the width and the diameter of the tire.

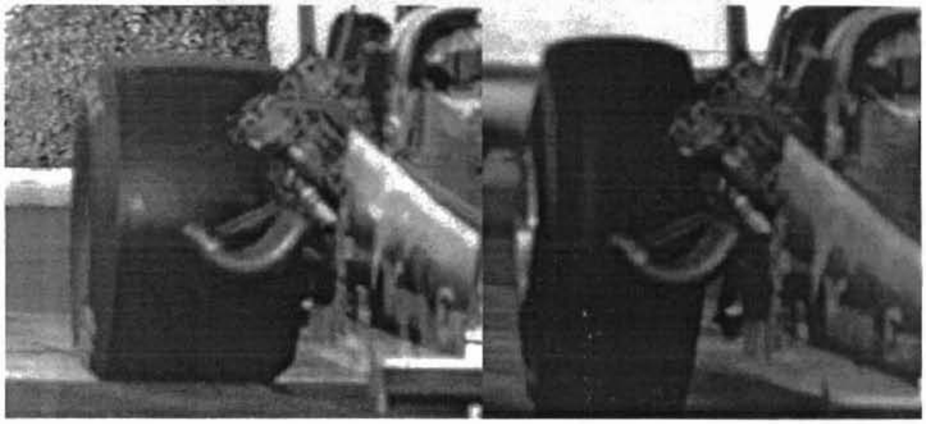

Figure 2-10: Tire Expansion on Top-Fuel Dragster Burnout

The tire footprint is over 250 square inches at the start of the run. With the wheels spinning at almost 8000 rpm the rotational inertia of the tire can deliver an enormous amount of down force to the car. When viewed in slow motion at the start of the run the tremendous torque is applied and the tire is balled up at the front of the contact patch as seen in Figure 2-11. The dragster squats and the weight transfers to the rear tires. The wheel rim spins at a faster rate than the rest of the tire causing the sidewalls to wrinkle up at the bottom. Once the tread reaches the rear part of the contact patch it speeds up to catch up with the rest of the wheel rim. This momentum causes great forces that are responsible for the incredible acceleration according to [Hallum, 1994].

Figure 2-11: Top-Fuel Dragster Tire at the Start of a Run

The deformation and wrinkling of the tire due to the large amount of torque applied can be seen above. At the bottom of the tire is the word "Goodyear" and due to the wrinkles in the sidewall it is not entirely visible.

The other perspective of the top-fuel dragster tire is the aerodynamics involved. The flow over the wheel has a great affect on the performance of the car because it results in a positive lift at the rear axle as mentioned before. The flow over a stationary semicircle can be used as an example for this lift effect. Starting out with the basic lift equation, the lift on a stationary semicircle shape was derived in [Munson, Young, Okiishi, 1994] to be the following:

$$L = \left(0.88 + \frac{1.96}{\sqrt{\mathrm{Rc}}}\right)\left(\frac{1}{2}\rho U^2 A\right) \qquad (2\text{-}5)$$

It can be seen that lift is created when there is flow over a semicircle. This is not what is used for determining the lift over that wheels because it is not accurate for a 3D cylinder that is rotating. This is just used to show that there is lift produced due to the flow over the rear wheels and that as the speed increases the lift force becomes greater.

2.3 Wing Design

To keep these rear wheels in contact with the race surface aerodynamic surfaces are used. There are two wings, the front and rear, on a top-fuel dragster car, which help the performance in different ways. The primary purpose of the front wing is to keep the vehicle from pitching up in the front and flipping over. Since the rear wing is mounted as far aft as possible, there is a tendency for the front wheels to be lifted off of the track. The counteracting balance comes from the negative lift produced by the front wing. The required down force of the front wing is enough to keep the overall vehicle from flipping over and provide enough pressure to the front wheels so that the driver has control over the steering. The rear wing is more of the focus of this research.

2.3.1 Multi-element Wings

Sometimes when designing a wing it is desired to produce more down force. Different methods used to obtain more down force are increasing the wing area, increase the camber of the airfoil, and delay flow separation by slotted flap design or multi-elements [Katz, 1995]. Since the wing area is fixed by the NHRA regulations, which will be presented in detail in the next section, then the alternative is to use wings with multi-elements.

Experimental studies on multi-element wings proved that larger lift coefficients could be obtained. These experiments were first performed by Handley Page and the results can be seen in Figure 2-12. This figure was provided by [Smith, 1975]. The airfoil was a RAF 19 and they are separated by a number of slots. The numbers represent the number of slots with a two-element airfoil having one slot, a three-element airfoil having two slots, and so on. It can be seen that higher angles of attacks can be reached and the coefficient of lift can reach as much as 4.

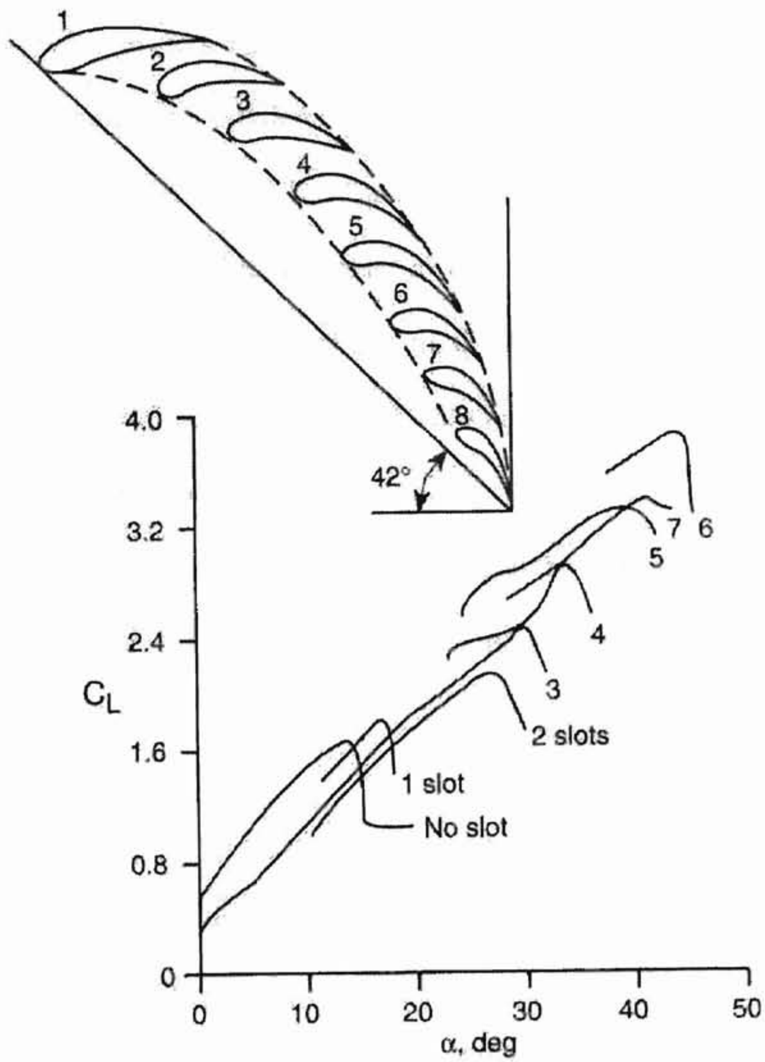

Figure 2-12: Effects of Multiple Elements on the Coefficient of Lift [Smith, 1975]

These slots allow high pressure air from the bottom side of the wing to exit through the gap and flow over the top of the next element. This will tend to reduce the separation while increasing lift and reducing drag.

2.3.2 Limitations on Rear Wing Design for Top-Fuel Dragsters

Since Top-Fuel Dragsters compete in sanctioned races, the governing body or the National Hot Rod Association (NHRA), has instilled rules and regulations that must be met. According to the NHRA 2000 Rulebook the rear wing is limited in type, size, and position. The wing must be locked into place as to prevent adjustment of any part of the wing during the run. The combined total area of all wings, canards, and airfoils mounted behind the front spindle can be no more than 1500 square inches. The position of the rear wing is limited by it height and aft placement. The trailing edge may not extend more than 50 inches behind the centerline of the rear axle and the height of any part of the wing may not exceed 90 inches measured vertically from the ground.

2.3.3 Typical Top-Fuel Dragster Wings

A typical rear wing design for a top-fuel dragster is a three-element wing with endplates. The material has been aluminum but with the advances in composites most are made of carbon fiber and Kevlar for the outer skins as well as the endplates.

Typical rear wings have an aspect ratio of around 2.4. The aspect ratio of a wing is defined by equation (2-6) as being the ratio of the span of the wing squared to the area of the wing.

$$AR = \frac{b^2}{S} \qquad (2\text{-}6)$$

The higher the aspect ratio the better the performance of the wing. When a wing is generating lift, it has a reduced pressure on the upper surface and an increased pressure on the lower surface. The air wants to get to the lower pressure and thus flows over the tip of the wing. This escaping air reduces the pressure difference near the tip of the wing and thus reduces the lift near the tip. For a wing with the same area this effect is greater for lower aspect ratio wings because the span of the wing is less than that of a high aspect ratio wing. For the high aspect ratio wing the pressure difference at the tip is less significant because it affects a smaller portion of the overall wing. This is why the higher the aspect ratio the better the performance characteristics.

To increase this aspect ratio means increasing the span of the wing or decrease the area of the wing. Increasing the span of the wing can only be done to a certain limit constrained by the width of the dragster. It can be extended past the width of the vehicle but during the race if any part of the dragster crosses the middle dividing line on the drag strip then that dragster is disqualified. This is the main reason that the span of the wing is kept at or below the width of the vehicle.

The effects of increasing this wing span were presented by [Winn, Kohlman, Kenner, 1999] which showed improvement as expected but increasing the span is not desirable as discussed earlier. They show increasing the span of the wing by 3 feet. This is great from an aerodynamic perspective but when it is looked at from the perspective of the race team or the driver it would add one more complication to the race. The driver would have to worry about staying that much further away from the center line.

In an attempt to increase the performance by decreasing this loss an addition to the wing called an endplate can be used. The endplate, seen in Figure 2-13 and provided by [Katz, 1995], maintains a pressure difference between the upper and lower portion of the wing that not only improves the performance of the wing at the tip and thus improves the overall wing performance. Therefore there is an effective aspect ratio calculation that can be made that is presented by [Raymer, 1992] and is shown in equation (2-7).

$$AR_{effective} = AR \cdot \left(1 + 1.9 \cdot \frac{h}{b}\right) \qquad (2\text{-}7)$$

Thus by increasing the height to span ratio of the endplate a greater effective aspect ratio can be obtained. The effects of changing the endplate design will be discussed later in another section.

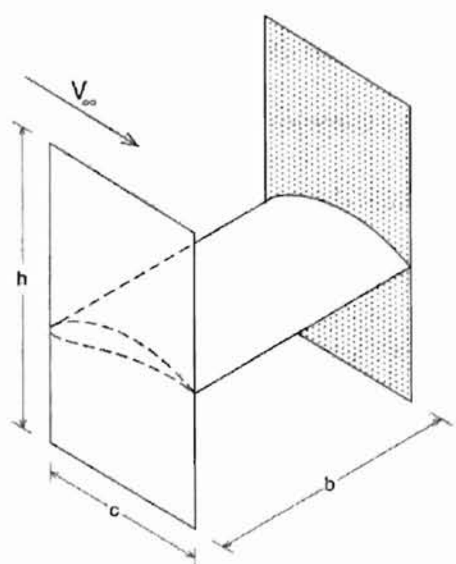

Figure 2-13: Endplate Size Dimensions

2.3.4 Endplate Design

As previously mention the effects of the endplates have proven to provide a more effective wing in the case of the low aspect ratio wing such as the rear wing of a dragster. The endplates on a typical dragster has been shaped based upon a "coolness" factor instead of on an aerodynamic performance factor. CFD analysis was performed on a three-element top-fuel dragster wing to study the aerodynamics involved. After careful analysis it was determined that due to the huge pressure difference between the top and bottom of the wing the flow was spilling over the top of the endplate and would disrupt the flow on the bottom surface of the wing. This reduced the amount of potential down force that the wing could generate. After determining this, adjustments were made to reduce this spillover effect and new endplates were designed and rerun in STARS. Vast improvements were made in the down force to drag ratio.

Although this improvement to the wing design was beneficial to the wings down force to drag ratio it has not been proven that the enormous amount of down force generated is necessary to the overall vehicle performance. This is where the study of the dynamics of the vehicle, which includes the aerodynamics, will be beneficial to the understanding of the overall effect of the dragster rear wing. It is also the intent of the author to show how much these improvements in wing design affects the performance of the vehicle such as the elapsed time and top speed for a quarter mile run.

CHAPTER 3

3. METHODOLOGY

This chapter is broken down into several sections that include the methodology behind the dragster model. The description of the STARS CFD code used and the implementation of a dragster wing into STARS. Also the setup to determine how the endplates effect the rear wing performance will be discussed followed by the development of a new type of dragster wing.

3.1 Modeling the Dragster

Several approaches were explored when trying to come up with a good dragster model. First the equations of motion for the dragster needed to be derived by studying all the forces acting on the vehicle. These included all of the lift and drag properties of the vehicle, the weight and weight transfer, the dimensions of certain parts of the dragster, and the performance of the engine and overall drive train. The lift and drag properties will be explored first building up to the full equations of motion.

3.1.1 Wheel Properties Used

The wheels were one of the more difficult components to get true data for because of the dynamics of these types of tires as discussed earlier. Lift and drag are generated by a number of different ways not just due to the flow around the tire but due to the rotation of the tires as well. In the previous chapter the aerodynamics of a rotating object was discussed. For the lift and drag characteristics of a rotating tire, research done by [Cogotti, 1983] will be used. Wind tunnel tests were done with the tires in direct contact with the balance and the wheel was powered.

C_d	0.579
C_l	0.18

Table 3-1: Lift and Drag Coefficients for the Tires from Cogotti's Research

Since the model was looking at general trends in aerodynamic effects on dragster performance a complicated tire model was not sought after. The data found on modeling tires was so detailed and was concerned with so many different aspects of the tires that it was decided that a simple tire model will be sufficient. Sure the tire can be analyzed and modeled in greater detail but the current research is concerned with finding general trends for the purpose of analyzing the rear wing and not concerned with advanced tire models.

3.1.2 Rear Wing Properties Used

The rear wing had two different sources of drag - induced drag and area drag. The first portion of drag, induced drag, is provided by the STARS code. This entails entering the dimensions of the object into a computer and using CFD to determine the aerodynamic properties of the object. STARS and implementing the wings into STARS is discussed later in this chapter.

The second type of drag used is area drag. The area drag is estimated by breaking the dragster wing into different components and estimating these different component drags.

The lift component for the wing is determined using STARS. The wetted area of the wing is provided by STARS and the plan form area of the wing is set by the NHRA rules.

3.1.3 Equations of Motion

After all the parameters are determined the next step is to determine the equations of motion for the dragster. The equations of motion are derived by summing the forces on the dragster. There are two regions that determine which equation is going to be used which can be seen in Figure 3-1. The first region is the traction limited acceleration portion of the track. This is where the acceleration power is so great that the wheels would slip if the throttle was held wide open. There is not enough down force to grip the wheels to the ground therefore the driver must ease on the throttle until they reach a point at which this is no longer a scenario where the wheels can spin. This point is called the critical velocity of the vehicle.

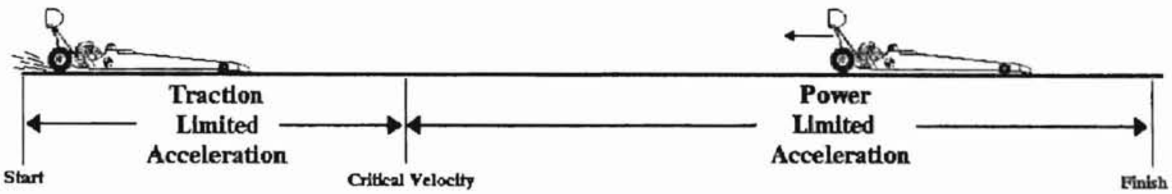

Figure 3-1: Dragster Run Schematic Showing Two Areas

This critical velocity point is the transition between the traction limited acceleration and the power limited acceleration. In the power limited acceleration region there is so much down force that the power used to accelerate the vehicle is not large enough to spin the wheels. In other words, the normal force from the wheels to the ground multiplied by the friction factor of the tires is greater than the force generated by the torque from the engine.

The two different equations of motion are shown below. The first equation of motion, Equation (3-1), is the traction limited acceleration which is valid below the critical velocity. After this critical velocity is reached the second equation of motion can be utilized which is the power limited acceleration shown in Equation (3-2).

For $\dot{x} < v_{cr}$

$$\ddot{x} + \left[\frac{1}{s_D} + \frac{\gamma\Lambda - \mu_{rr}}{s_L}\right]\dot{x}^2 - [\gamma\lambda - \mu_{rr}]g = 0 \qquad (3\text{-}1)$$

For
$\dot{x} > v_{cr}$

$$\ddot{x} - \frac{\mathrm{P}}{m\dot{x}} + \left[\frac{1}{s_D} - \frac{\mu_{rr}}{s_L}\right]\dot{x}^2 + \mu_{rr} g = 0 \qquad (3\text{-}2)$$

where

$$\lambda = \frac{a}{1 - h\gamma}$$

$$\Lambda = \frac{a - d}{1 - h\gamma}$$

The idea of this model is to use the lift and drag coefficient data along with the other vehicle properties such as the effective input engine power and vehicle dimensions to find the critical velocity of the vehicle. Since the critical speed is the speed at which the traction-limited driving force equals the power-limited driving force it can be found by equating (3-1) and. (3-2). The resulting equation is a cubic equation in critical speed where the critical speed is the smaller positive root of equation (3-3).

$$\dot{s}^3 - \frac{\lambda g}{\Lambda} s_L \dot{s} + \frac{\mathrm{P} s_L}{m \Lambda \gamma} = 0 \qquad (3\text{-}3)$$

where s_L is the aerodynamic radius and is given by

$$s_L = \frac{m}{\frac{1}{2}\rho A C_L}$$

After the critical velocity is found the corresponding position and time are calculated using the acceleration from equation (3-1) and simple dynamics. From this point the differential equation for velocity less than the critical velocity can be solved.

Using the critical velocity and position as inputs and the corresponding time as the starting time the second differential equation (3-2) for velocity greater than critical velocity can be solved.

Plotting can be done of position, velocity, and acceleration for the given vehicle data. In the results section this model will be implemented using dragster characteristics and this will be compared to position, velocity, and acceleration from and actual dragster run.

Once the model is established and validated it can be used in a number of ways. First of all trends can be found to see how aerodynamic characteristics will affect the performance of a dragster. Once this is know the second approach will be to use if to come up with a new wing design that will allow the performance of the dragster to improve either by elapsed time, by top speed, or maybe both.

3.2 Validation of the Dragster Model

In order to validate the model it was necessary to match the position, velocity, and acceleration data from an actual dragster run. Speed versus distance and position versus time data was found [Winn and Kohlman, 1999] and used for the validation. In order to get the speed versus time curves the position versus time data had to be differentiated. Double differentiation of the position versus time data was used to compare the acceleration data of the model.

The first validation plot is position versus time which is shown below in Figure 3-2. In this plot the two different regions of analysis, both below and above the critical velocity, can be seen. The circles are the actual data and the lines are from the model. The model matches the actual data very well.

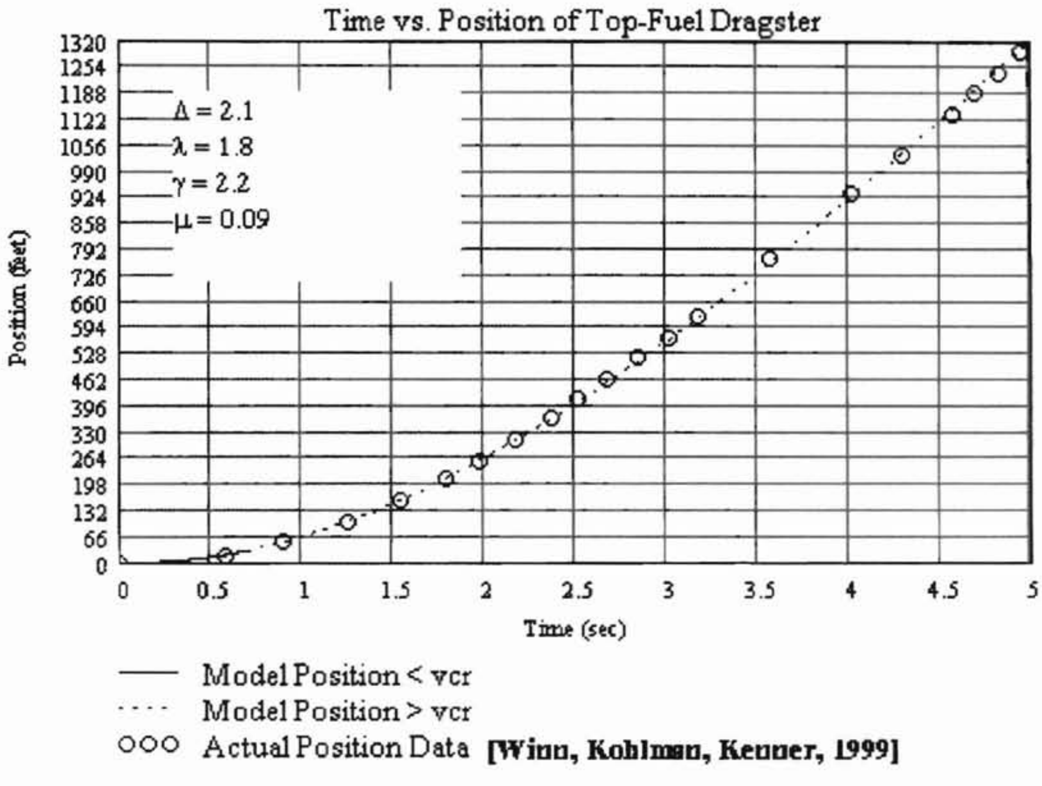

Figure 3-2: Validation of Position vs Time for a Top-Fuel Dragster (1/4 Mile)

In order to get speed versus time data the data from Figure 3-2 had to be differentiated. This data is represented by the circles in Figure 3-3, below, along with the model data depicted by the lines. Once again the model shows the regions where the two different equations of motion were used by plotting a solid line and a dashed line. The speed where these two lines meet is the critical velocity. This data matches up fairly well but a small error can be seen which is due to the differentiation of the data. Once differentiated the error that was there in the position versus time plot is enlarged.

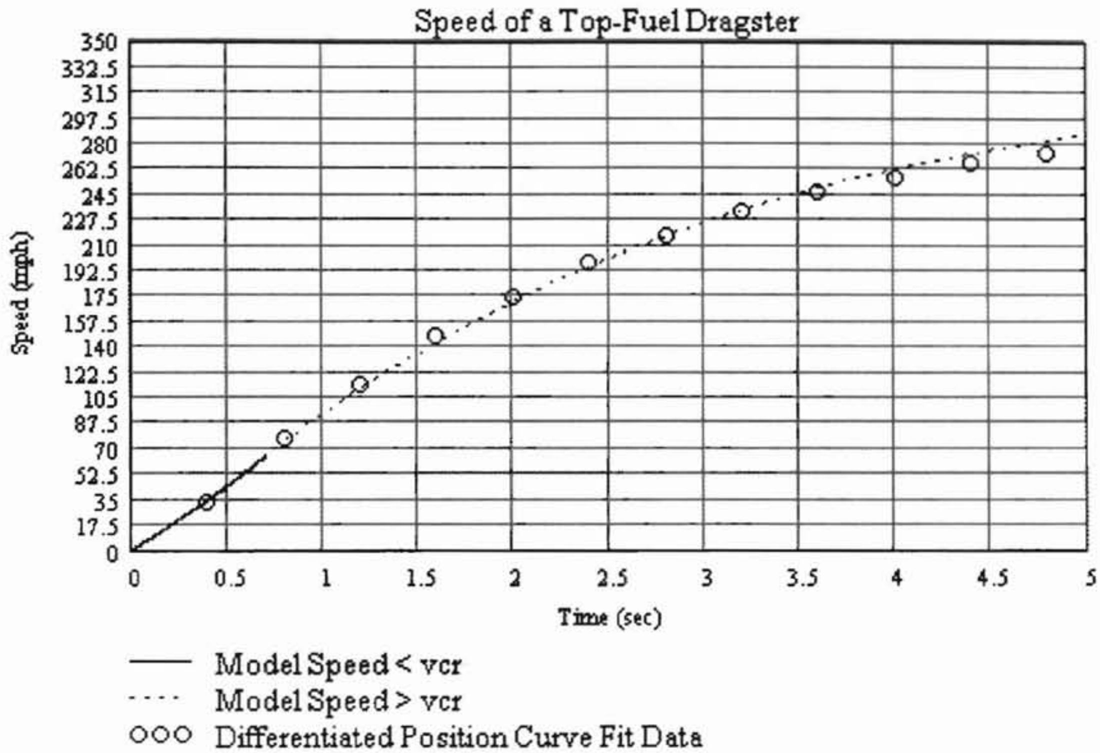

Figure 3-3: Validation of Speed vs Time for a Top-Fuel Dragster (1/4 Mile)

Acceleration data versus time was not readily available and therefore the position versus time data was double differentiated to get the actual data in Figure 3-4 below. The model still matches the trend of the actual data.

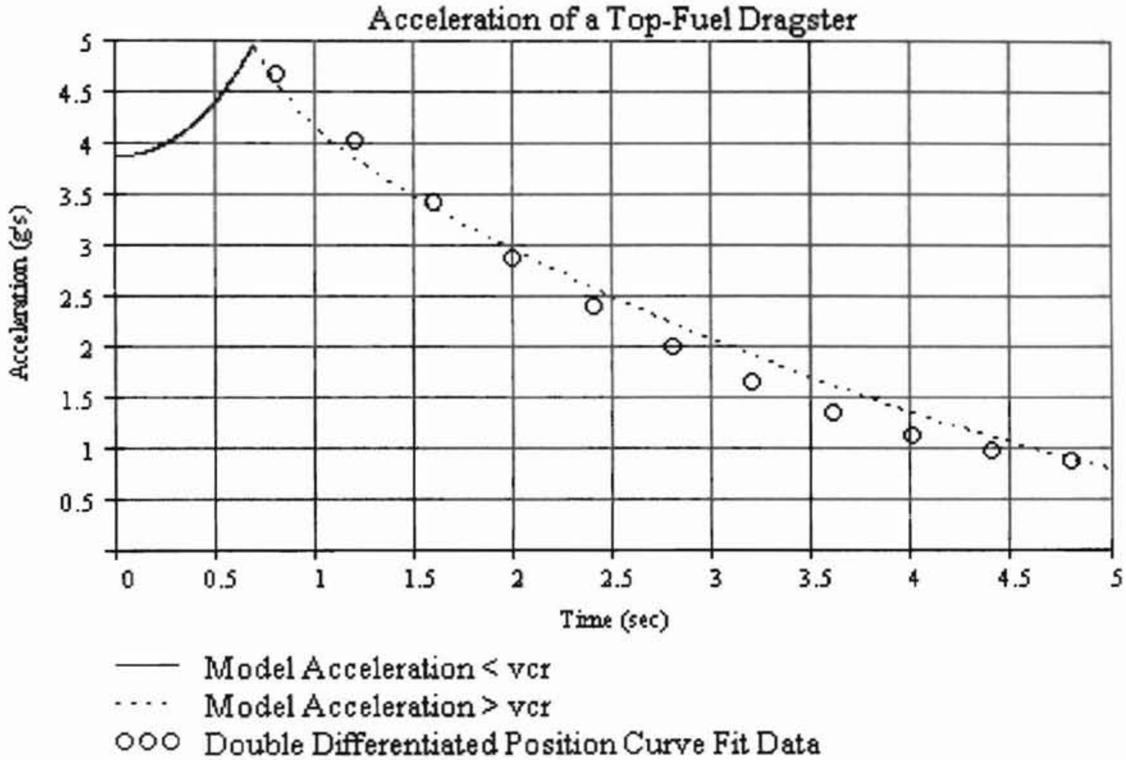

Figure 3-4: Validation of Acceleration vs Time for a Top-Fuel Dragster (1/4 Mile)

There was also actual speed versus position data that was used to validate the model. This data is shown in Figure 3-5 with the actual data depicted by circles. Once again the model matches the data very well.

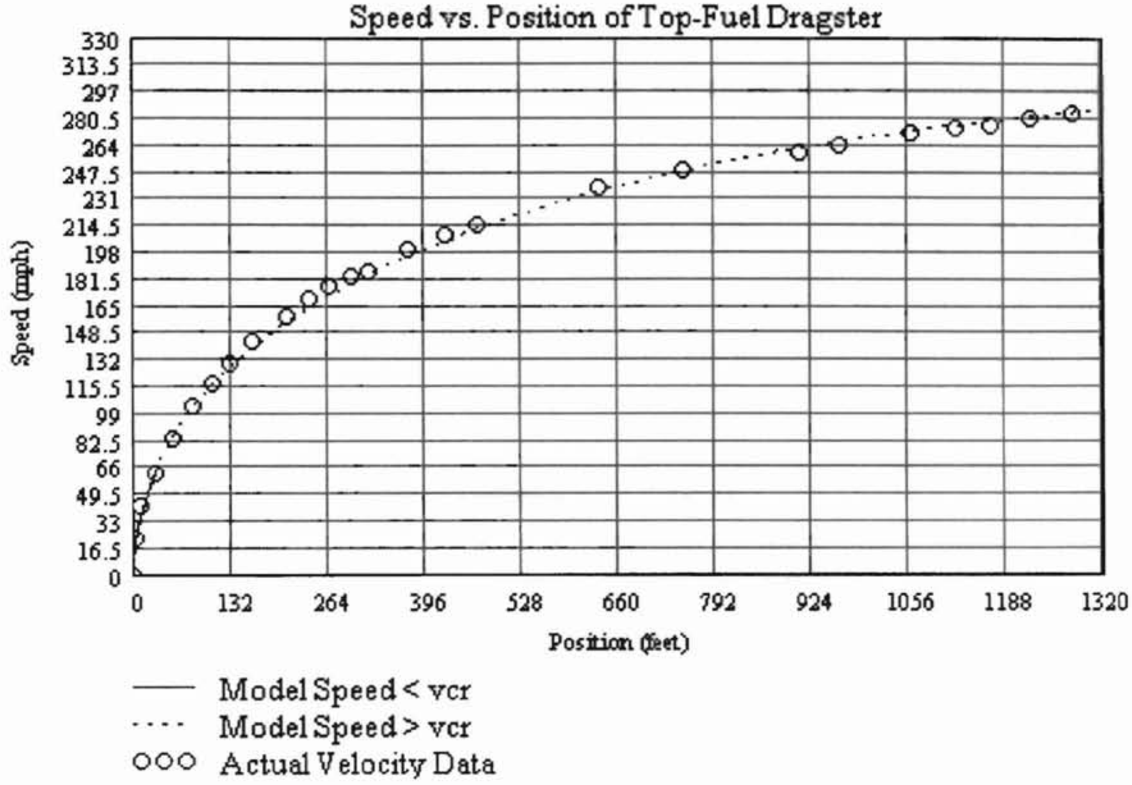

Figure 3-5: Validation of Speed vs Position for a Top-Fuel Dragster (1/4 Mile)

3.3 STARS CFD Module

One of the research tools used for this project is portion of a set of codes developed at NASA Dryden Flight Research Center known as STARS. STARS stands for STructural Analysis RoutineS, which is a highly integrated computer program for multidisciplinary analysis of flight vehicles including static and dynamic structural analysis, CFD, heat transfer, and aeroservoelasticity [Gupta, 1997]. For the current effort, only the CFD module of the code will be utilized for analyzing the aerodynamic characteristics of the wings.

The CFD module is an Euler based code that applies finite element CFD on an unstructured grid. The mesh generation uses the advancing front technique to generate the unstructured mesh, which had been proven to be effective in complex structures. When implementing the CFD module it is pertinent to follow a set of steps. This module consists of the following four major parts and should be run in the order that they are listed:

- SURFACE - generates a surface triangulation
- VOLUME - generates a three-dimensional computational domain
- SETBND - defines the boundary conditions in the domain
- EULER - steady or unsteady Euler flow solver

The easiest way to explain these different modules is to implement an actual problem into STARS step-by-step. The steps used and the data file structures and contents will be discussed in more detail in the next section. The problem that is being used is the rear dragster wing that has a style 3 endplate. The differences in the wings and endplates will be discussed later.

3.4 Implementing the Dragster Wing into STARS

As mentioned before there are four main modules or steps to follow, in order, before the user gets the solution. The first step in order to analyze the dragster wing in STARS is to setup the geometry data into the format so that STARS can read it. After the geometry is entered a mesh generation is enacted and a refinement in the density of the grid is performed until a suitable mesh is found. The last step before running the flow solver is to specify the boundary conditions for the geometry and flow domain. The aforementioned modules are discussed in more detail in the following subsections.

3.4.1 Geometry Specifications in STARS

The geometry is made up of curves and surfaces that define the geometry of the dragster wing and the geometry of the flow domain. The geometry data file is a formatted data file that will be referred to as *case.sur*, were *case* can be any name that the user specifies. The dragster rear wing geometry file can be found in Appendix A-1.

The lines are oriented in a specific direction, defined in the direction of the arrows in Figure 3-6, according to the way STARS reads in the geometry. The lines are defined by means of an ordered set of points. The curve component is a continuous cubic spline, which is interpolated through these points. The model is a half span model with a symmetry plane. Using this symmetry plane cuts down on the computational time of the job without sacrificing the accuracy of the solution.

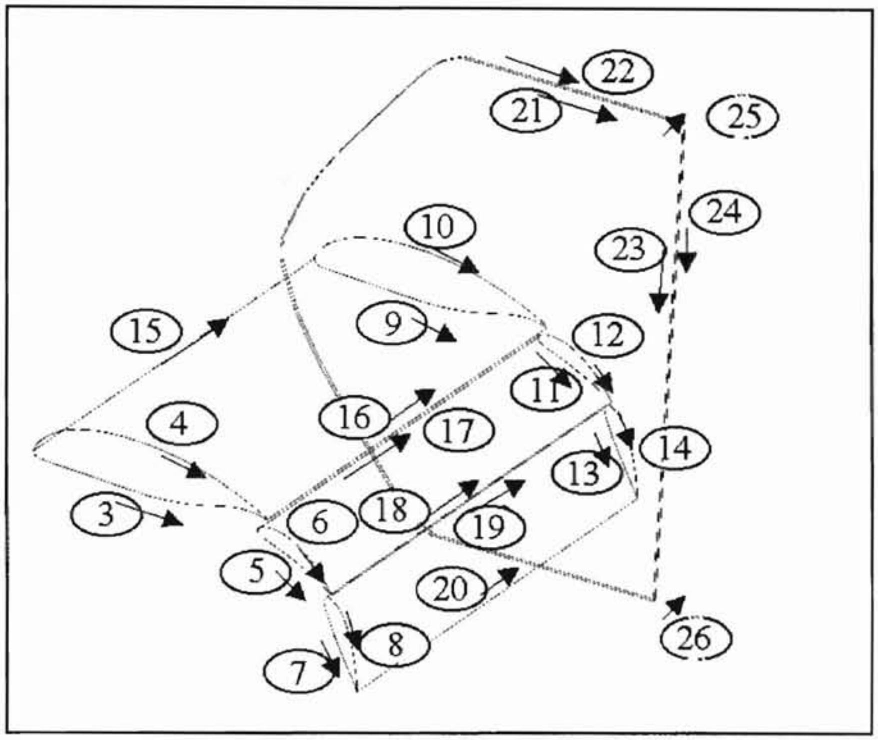

Figure 3-6: Wing Geometry Specification

It might be noticed that the numbering in Figure 3-6 starts out at three. The first two numbered lines define the flow domain that surrounds the geometry. The flow domain is a large hemisphere. There are ten chord lengths between the wing geometry and the outer surface of the hemisphere. The flat side of the hemisphere is the symmetry plane and is where the half span model of the rear dragster wing is attached.

After the curves are defined the next step in STARS is to specify the surfaces of the geometry. This is done by specifying each line that makes up the surface in a specific order. There are two possibilities that STARS will see depending on the order that the lines are specified - either a surface or a whole in a surface. When defining the surface the right hand rule must be used. The direction of the lines are important to this step and when using the right hand rule the fingers curl in the direction of the specified lines and the thumb has to point into the flow. If the thumb points into the geometry then the surface was not specified correctly.

When this is completed the wing looks like Figure 3-7. For the dragster wing that was analyzed, the largest and main element is based upon a set of data points. The chord length of this element is 14.1 inches long. This main element is set at zero angle of attack. The second element is an NACA 9400 type airfoil with a chord length of 5.25 inches. It is set at a 28-degree angle of attack with respect to the chord line of the main element. The third and final element is an NACA 4300 type airfoil with a chord length of 5.25 inches. It is set at a 65-degree angle of attack with respect to the main element chord line.

The configuration of the wing analyzed was 0°-28°-65°. The configuration, 0°-28°-65°, refers to the angle of attack of each of the three individual elements. The wing was adjustable to different configurations but this configuration was the one most commonly used and therefore was the configuration that was used in the analysis.

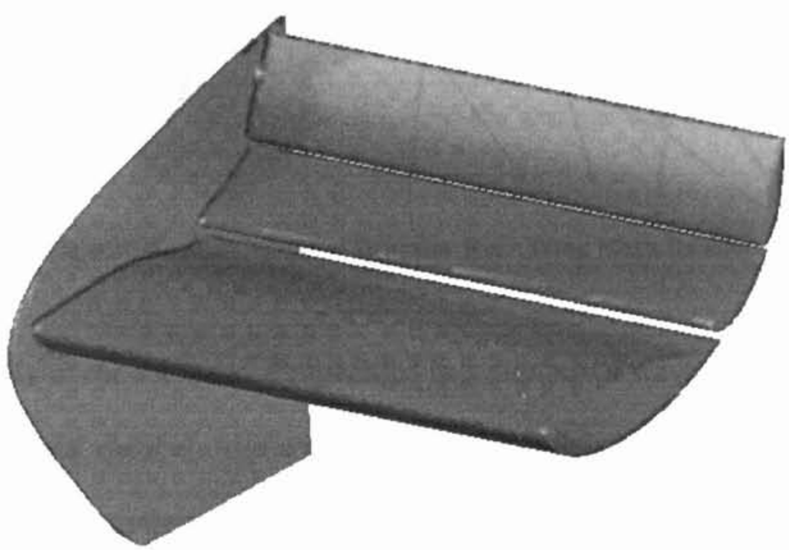

Figure 3-7: Rendered View of a Half-Span model with a Style 3 Endplate

3.4.2 Grid Specifications in STARS

Once the geometry is defined a mesh density must be specified in the (*.bac*) file, which is listed in Appendix A-2. The mesh density must be small enough on the geometry in order for the solution to be accurate. The half model of the wing can be seen in Figure 3-8. The symmetry plane, where the half span model is attached, has a larger triangular mesh than the wing surface. This allows the solution to converge faster because the amount of calculations that the code has to go through is greatly reduced.

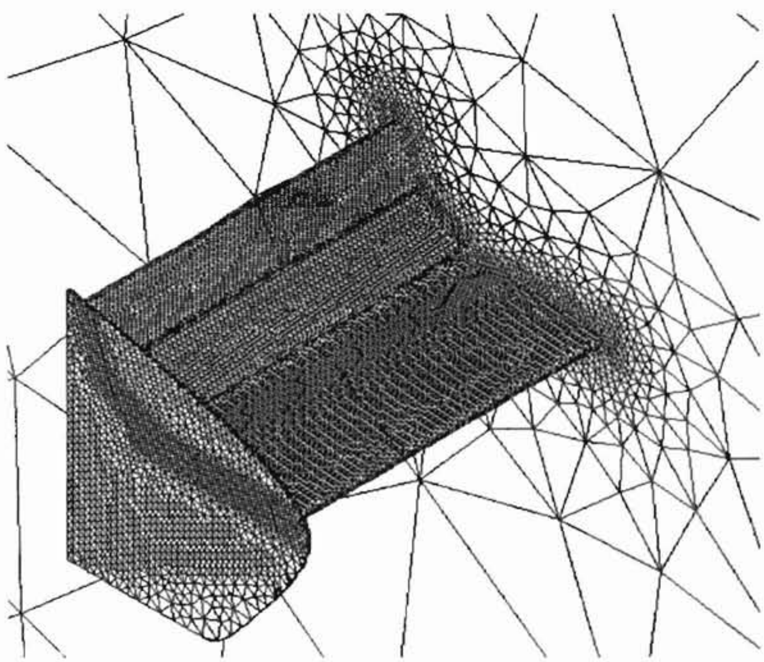

Figure 3-8: Half Model of Dragster Rear Wing Mesh Density

The density of the mesh can be specified in a number of ways. In the (*.bac*) file the user can specify any number of sources in order to get the specified mesh density. The user can chose from three types of sources being a point source, a line source, or a triangle source.

A point source allows for a sphere like mesh density that can change the size of mesh to start out with, how large of a sphere, and how far out until the mesh size is double of the original starting size. Point sources can be used on the front of an airplane body, such as the nose of the X-29 experimental aircraft, in order to make the geometry mesh tighter.

The line source differs from a point source in that it is cylinder like and there is a specified length instead of a sphere. The line sources are typically used in the leading and trailing edges of a wing because of the sharp transition in geometry.

The triangle source is a mesh density in the shape of a three dimensional triangle. They can be used in a number of ways for a number of different situations. In the dragster wing case two triangle sources are used per wing in a way as to make a rectangle running thru the chord of the wing to refine the mesh on the surface of the wings. They are also used on the endplates since the endplate is so thin it allowed for a refined mesh so that the solution around the endplate is accurate.

3.4.2.1 SURFACE Module

After generating the geometry data file and the background mesh data file the first step is to run the SURFACE module. The SURFACE module generates a couple of data files. The first is a (*.RST*) file, where the *.RST* is just the suffix that is added to the problem name, e.g. *fin.RST* or *wing.RST*. This file is an auxiliary file in which all of the information about the generation processed is dumped. This allows the user to re-start the SURFACE module if the program is stopped before completion.

The second file generated is a (*.fro*) file that stores the information about the triangulation of the surface in the three-dimensional and the parametric space. This file is used for input to the VOLUME and SETBND modules, which will be discussed later. The (*.fro*) file is not listed in the appendix because it takes up 1060 pages of numbers in 10 point font and the information is not pertinent to developing a model in STARS.

3.4.2.2 VOLUME Module

The VOLUME module only requires two files to run - the background mesh file (*.bac*) and the surface triangulation file (*.fro*), that was generated from the SURFACE module. The Volume module outputs a restart file (*.RVT*) and a tetrahedral mesh file (*.gri*). The restart file (*.RVT*) can be read by the VOLUME module in case the program was interrupted or unable to finish. It is similar to the restart file of the SURFACE module. The (*.gri*) file holds the description of the tetrahedral mesh. This is one of the input files to the SETBND module. The (*.gri*) file is extremely large, over 7200 pages of numbers in 10 point font, and therefore is not listed in the appendix.

3.4.3 Boundary Condition Specification in STARS

After running the SURFACE and VOLUME modules, it is now time to look at the boundary conditions. The boundary condition specifications, (*.bco*) in STARS, is pretty straightforward and can be found in Appendix A-3. The user is required to flag the curve segments and surface regions in a formatted data form. The surface region flags define the type of boundary conditions to be applied to a certain surface and are defined in Table

3-2. If the surface was a symmetry plane then that surface would be flagged with a 2 as indicated in the table.

Flag	Surface Type
1	Wall
2	Symmetry
3-4	Far Field
5-6	Engine Inlet
7-8	Engine Outlet

Table 3-2: Surface Region Flags

The user must also specify the curve segment flags. These identify points in the triangulation, which lie on the surface regions, where the normal to the surface is not defined. These are singular points in the geometry and at these points there is no wall boundary corrections applied. Such points include the trailing edges of wings or any similar geometry. The flags for the curve segments can be found in Table 3-3.

Flag	Singularity
0	No Singularity
1	All are Singular
2	Singular Point at First and Last
3	Singular Point at First Only
4	Singular Point at Last Only

Table 3-3: Curve Segment Flags

3.4.3.1 SETBND Module

After the boundary conditions are specified, the third module can be run. This is the SETBND module, which is the flow solver preprocessor. It transforms the element-based description of the tetrahedral mesh into the side-based data structure employed by the EULER module. The SETBND module requires the surface triangulation file (*.fro*), the tetrahedral mesh file (*.gri*), and the boundary conditions file (*.bco*).

The output to the SETBND module is a file that contains the combination of both the surface triangulation file (*.fro*) and the tetrahedral mesh file (*.gri*) into a single file referred to as the (*.plt*) file. This file can then be used for another module that is sometimes used, which is the REMESH module. The (*.plt*) file is a binary file and is not listed in the appendix.

The REMESH file is not discussed as one of the main modules because it is not necessary to run this module in order to obtain a solution. The REMESH module looks at the concentration of flow activity and can refine the mesh density in this area in order to acquire a more accurate solution.

The other output file from the SETBND module is the solver data file (*.geo*). This file contains the side-based data structure representing the computational mesh and all the information required by the flow solver. The (*.geo*) file is another large data file that is binary and is not listed in the appendix.

3.4.4 Solver Control Specifications

This solver control file (*.cons*) contains a set of flow conditions and algorithmic constants for the Euler flow solver and a sample can be found in Appendix A-4. The flow solver contains built-in defaults that can be overwritten by the user if another value is specified in the solver control file. This is where the the free-stream Mach number, the angle of attack, side slip angle, as well as fluid properties must be specified. Other algorithmic properties include the number of timesteps, dissipation coefficients, CFL number, and residual smoothing parameters to name a few.

3.4.4.1 EULER Module

Now that the control specification file is generated and all three previous modules had be run then the last module can be started. The solver module or the EULER module is the unstructured Euler flow solver which performs numerical computation of the steady-state solutions of the transient form of the Euler equations of compressible inviscid flow.

The SOLVE module needs both the solver data file (*.geo*) and the solver control file (*.cons*) in order to run. The module outputs nodal values of flow variables (density, velocity, and pressure) in a (*.unk*) file. The EULER module also outputs another file that contains the history of the convergence of the L-2 norm of the residuals of the conserved variables in a (*.rsd*) file. This can be used as a convergence criterion that will be discussed in a later chapter. Once the EULER module has run and the solution has converged, the CFD portion of the STARS code has been completed.

The final step would be to view the solution with a postprocessor where a variation of figures and graphs both two- and three-dimensional can be generated. Several of these figures are shown in the results section of this paper.

3.5 The Effects that Endplates have on Rear Wing Performance

CFD was used to analyze the flow over an existing top-fuel dragster wing both with and without an endplate. This wing geometry, that was discussed in the previous section was used for each of the three test cases analyzed. Therefore, the three wings vary only in the endplate design as can be seen in Figure 3-9 below. The first case was to study of the dragster wing without an endplate. The second case used one endplate design that was currently being used on a dragster wing built by Advanced Racing Composites (ARC). This will be referred to as a style 3 endplate. The third and final wing used an endplate that tried to improve the performance characteristics of the wing by changing just the geometry of the endplate. This endplate is referred to as the new endplate.

Figure 3-9: Three Different Endplate Geometry Analyzed

The CFD analysis was run to depict a race at the top design speed at the highest racing altitude. This meant using a Mach number of 0.434, which corresponded to a design velocity of 325 mph at an altitude of 5500 feet (Denver, CO).

The CFD solver starts out at the given free-stream Mach number and after converging gives a resulting flow-field on the wing. Therefore, it is necessary to determine when the solution converges. STARS can output flow parameter residuals (*.rsd*) file and maximum Mach numbers for every time step. The steady-state solution convergence criteria for maximum Mach number was used instead of the residuals of flow parameters. It was determined that the maximum Mach number is a much better convergence indicator than the flow parameter residuals [Stephens, 1998].

Since the input files for the STARS modules can be long and detailed, when changing geometry, a spreadsheet was used to create the geometry and background mesh data files. The spreadsheet was set up to allow many different parameters to be changed. Changes could be made to the span of the wing, the angle of attack of each of the airfoils, the gap spacing in between each of the wing elements, the position of the wing inside the flow domain, as well as the type of endplate to be use. This spread sheet saved a lot of time in the generation of the input data files.

3.6 Box Wing Design

After analyzing the dragster model and looking at the trends to improve performance some thought went into a different rear wing design. A simpler design that was made of less components would be a plus but most important improved dragster performance was sought.

Previous work had been done with a high-lift low Reynolds number airfoil that showed some potential for this type of project. The airfoil is a Selig 1223 that was found at the University of Illinois at Urbana-Champaign airfoil data website. It was decided that the approach would be to use this airfoil with a boxwing type design instead of the typical three-element design that is seen today on top-fuel dragsters. The boxwing type design will be talked about later on in this section.

The Selig 1223 airfoil, as seen in Figure 3-10, has a large coefficient of lift. This airfoil was designed to be a heavy lifting airfoil. The airfoil data points can be found in Appendix C-1.

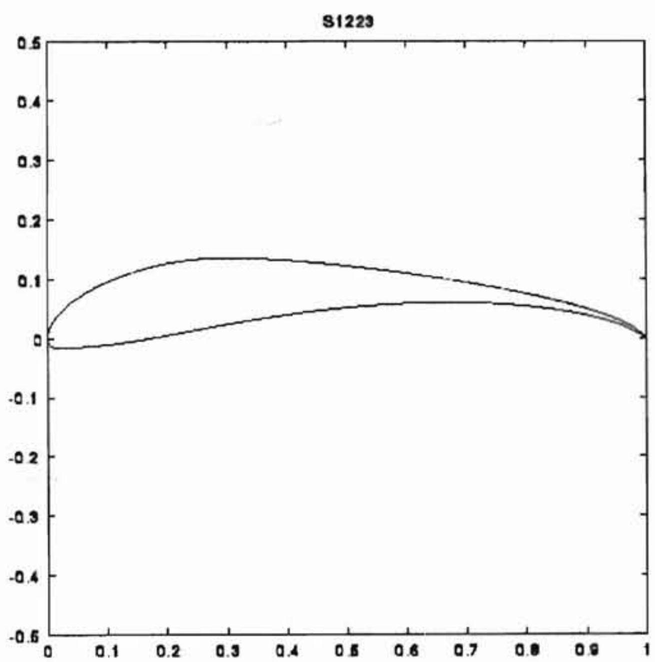

Figure 3-10: Selig 1223 Airfoil

This airfoil has a very thin trailing edge as can be seen in the figure above. This requires some knowledge of manufacturing as well as the materials that will be used to built the wing. With materials like carbon fiber, which is one of the currently used materials for dragster wings, this airfoil is not a problem. Because the wing's thin trailing edge you need a material that is strong so that it would not break off. Carbon fiber could be used to make this trailing edge strong enough.

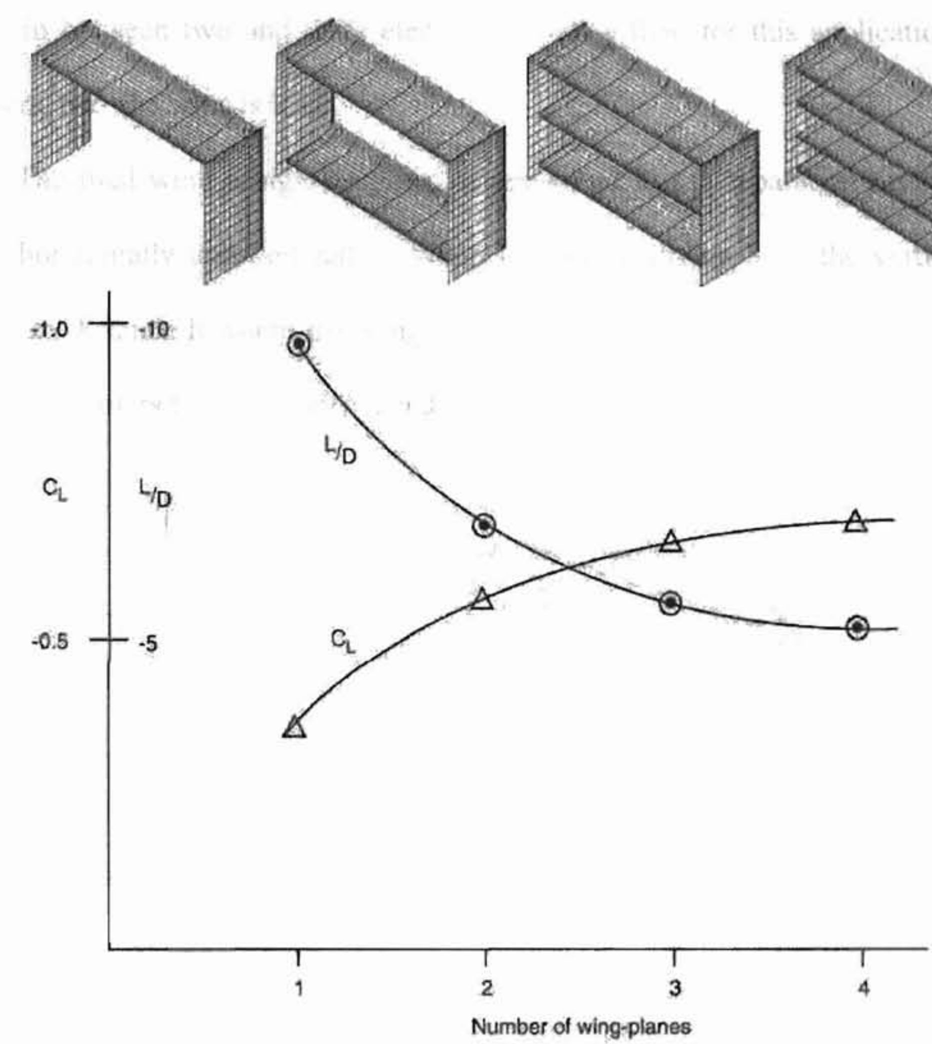

Figure 3-11: Effect of the Number of Elements on an F-1 Type Wing [Katz, 1995]

Next the effect of the wing was considered using simple back of the envelope calculations. It was thought that a single wing with the Selig 1223 airfoil did not produce adequate lift. Therefore a boxwing design seemed more appropriate. Looking at Figure 3-11, provided by [Katz, 1995], it can be shown that the number of elements should not exceed 2. The figure shows that as the number of elements increase so does the coefficient of lift or down force. The other plot in the figure is the ratio of down force to drag and as the number of elements increases this down force to drag ratio decreases. This means that with more elements the wing is producing more drag. These two curves meet in between two and three elements showing that, for this application where drag matters, two elements is ideal.

The final wing design consisted of one chord length separation between the wings both horizontally and vertically. When looking at Figure 3-12 the vertical separation refers to distance h where the wing would be moved one chord length. The horizontal separation refers to the distance x and is one chord length as well.

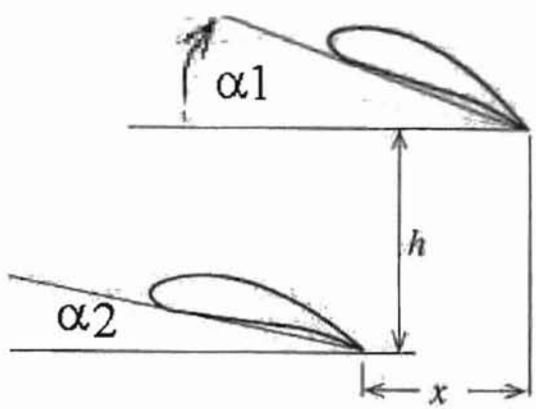

Figure 3-12: Decalage Angle

The two wings are identical in chord and span which would cut down building time because only one type of wing would be needed. This would eliminate the production of three different types of wings as is the case for the currently used multi-element wings. The wings are set at a different angle of attack which changes the performance characteristics of the wings. The difference in the angle of attach between the top wing and the bottom wing is known as decalage angle. When looking at Figure 3-12 above, the decalage angle will be the difference between $\alpha 1$ and $\alpha 2$. If the bottom airfoil was set at 5° angle of attack and the top airfoil was set at 15° then the decalage angle would be the difference in the two or 10°.

A study was done to look at the effect that decalage angle has on the performance characteristics of the wing. Therefore three decalage angles were tested computationally, using STARS, and the angles were set at 0°, 8°, and 12°. Further computation was done by varying the overall angle of attack of the whole boxwing starting at 0° and ranging up to, in some instances, 25°. A half model of the boxwing design is pictured below in Figure 3-13.

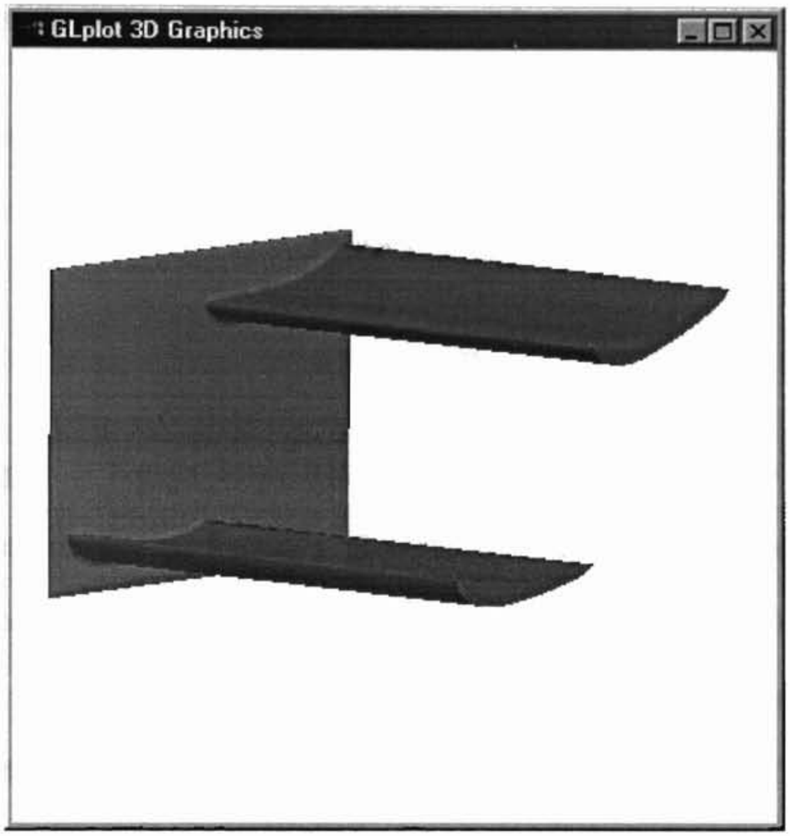

Figure 3-13: Rendered View of half model Boxwing with a 12° Decalage Angle

No studies were done on the shape of the boxwing endplates. Therefore a simple square endplate was used for the computational analysis. This will be talked about further in the results section.

Since a lot of variations to the wing were going to be performed it was beneficial to make a spreadsheet that would produce the STARS input data file after the wing parameters were changed. The spreadsheet allowed for each angle of attack of the two wings, the endplate dimensions both vertically and horizontally, the chord of the airfoil, the length of the wing, as well as the position of the wing in the flow domain all to be changed. This saved a lot of time between data runs.

CHAPTER 4

4. RESULTS

This chapter is broken down into several sections including the results of the endplate effects on the performance characteristics of the wing, the gap spacing comparisons for a multi-element wing, and angle of attach comparisons between wings. The results of the boxwing design will also be addressed. Finally the dynamic model comparisons of a dragster run with be shown and discussed. This section will look at various wings used and show how each affected the performance of the dragster.

4.1 Effects of Endplate on Three-Element Dragster Wings

The effects of endplates section explores several ways that endplates can effect wing performance by studying a three-element wing without an endplate as well as two different endplate designs. This section is broken down into several subsections including pressure contours, cross flow velocities, velocities at the tip of the wings, down force to drag ratio, and Mach number and coefficient of pressure distribution over the wing.

4.1.1 Pressure Contours

When looking at the three-dimensional pressure contours generated by STARS the effects of the endplates can be easily seen. The wing without the endplate, Figure 4-1, shows how three-dimensional the airflow can be without the endplate. In these pressure plots the tip of the wing is the closest to the reader and the symmetry plane is the farthest. On the main element the suction pressure along the tip of the wing is dramatically decreased due to the spillover caused by the large pressure gradient present towards the tip of the wing. This can be seen by looking at the various color differences that are represented in the pressure bar on the right hand side of the figure.

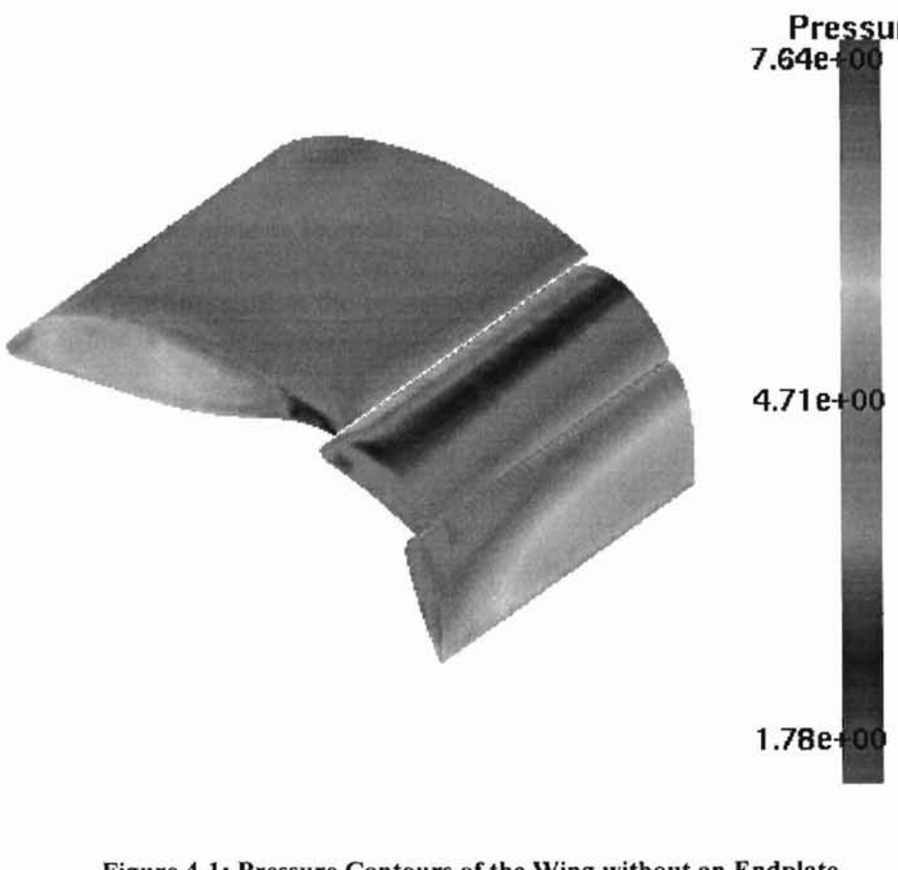

Figure 4-1: Pressure Contours of the Wing without an Endplate

This effect is not only visible on the main element but can also be seen on the second and third elements as well. In Figure 4-1, only towards the tip of the wing the pressure contours tend to dissipate as compared to the pressure contour at the mid-span of the model. The wings with the endplates have a more uniformly distributed suction pressure strip along the entire length of the second element.

As for the last element on the three-element wing, the advantage of the endplate can once again be easily seen. The non-uniform pressure gradient appears to be in the shape of a quarter of an ellipse. Towards the tip of the third element in Figure 4-1, the wing without the endplate, a very distinct non-uniform pressure gradient can be seen. Although the pressure on wings with the endplates is not entirely uniform it is relatively more so than the wing without the endplate. This does not appear on the two wings with endplates as seen in Figure 4-2 with the style 3 endplate and Figure 4-3 with the new endplate design. For the two figures with endplates, the edge that appears closest to the reader is where the endplate is located. However, the endplate has been removed during the post-process plotting so that the pressure on the elements at the tip of the wing can be viewed.

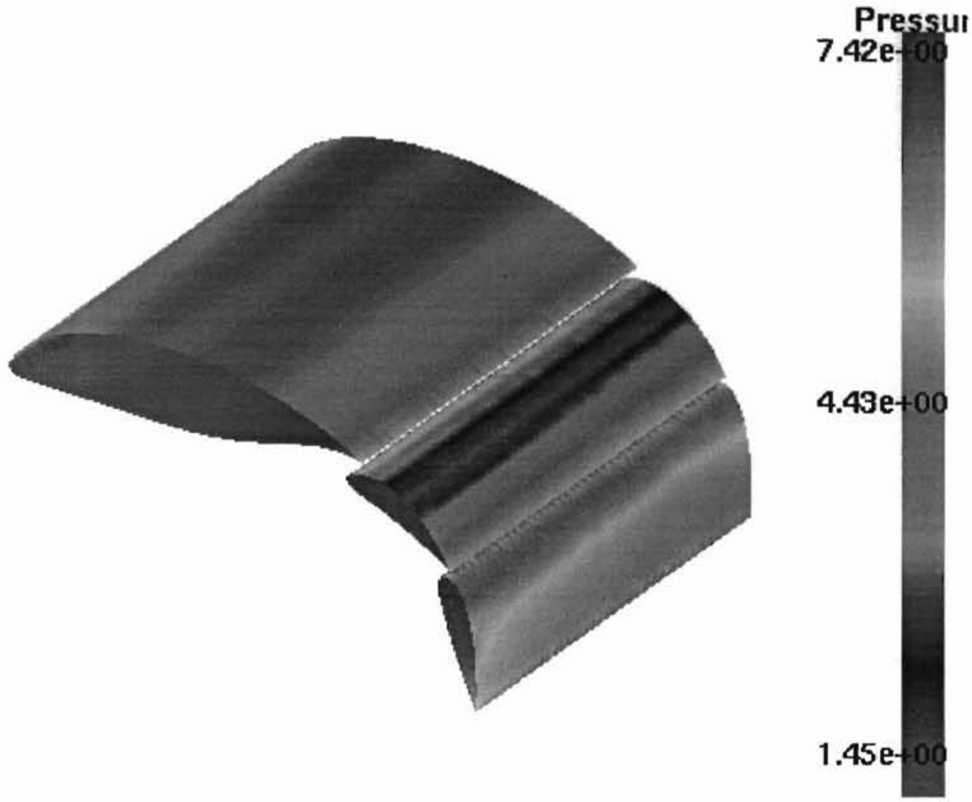

Figure 4-2: Pressure Contour of Wing with Style 3 Endplate

On the wing with the style 3 endplate, Figure 4-2, the main element has evenly distributed pressure sections as we move from the leading edge of the main element and move back. The second element has a very uniform pressure distribution which is recognized when comparing the tip sections of Figure 4-1 and Figure 4-2. It is not until the third element that we see the tip pressure start to dissipate. The flow here is extremely high, over Mach 1, and the angle of this third element is at 65° to the free stream. When the conditions are remembered it is hard to believe that the pressure distribution at this section of the wing is as uniform as it appears.

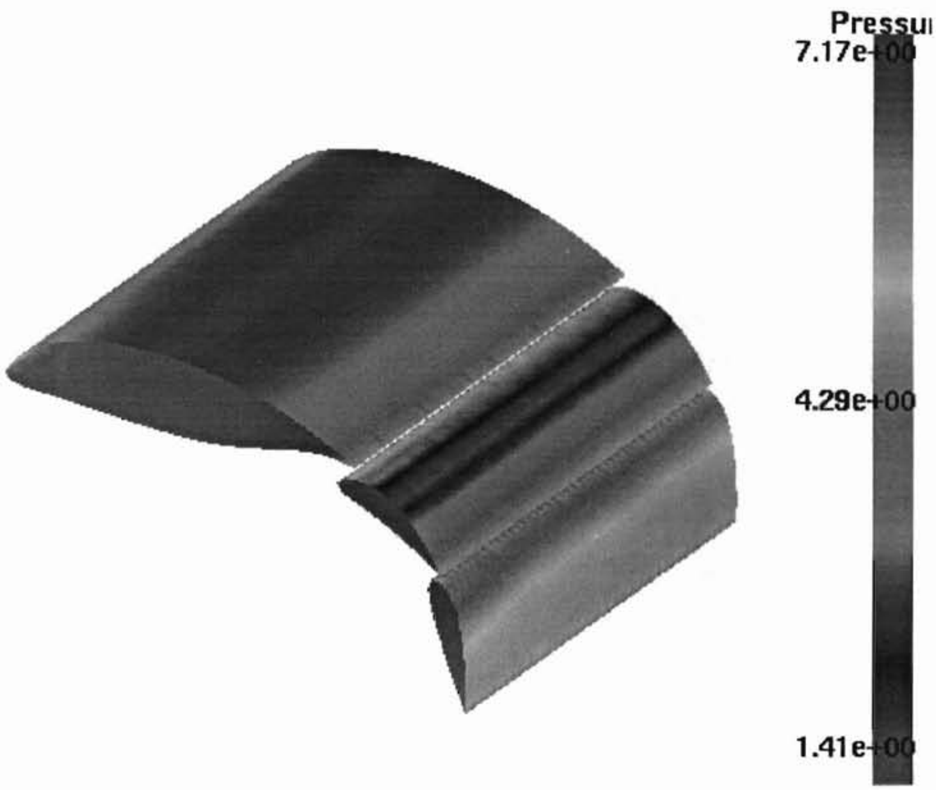

Figure 4-3: Pressure Contour of Wing with New Style Endplate

The first and second elements of the wing with the new style of endplate in Figure 4-3 appear as uniform as they were in Figure 4-2 with the style 3 endplate. The third element for the new endplate design however appears to be more uniform then that of the third element of the style 3 endplate. This larger new endplate controls the flow better by reducing this spillover effect.

From another perspective, Figure 4-4 shows a side view of the endplate with the symmetry plane in the background. This then can be somewhat viewed as the gradient pressure that the endplate sees and thus shows once again why the airflow favors to spillover the top edge of the endplate. The bottom does not seem to be as great of a pressure gradient and thus only moderate spillover affects occur. This figure helped in deciding how the new endplate geometry should be manipulated in order to reduce this pressure gradient.

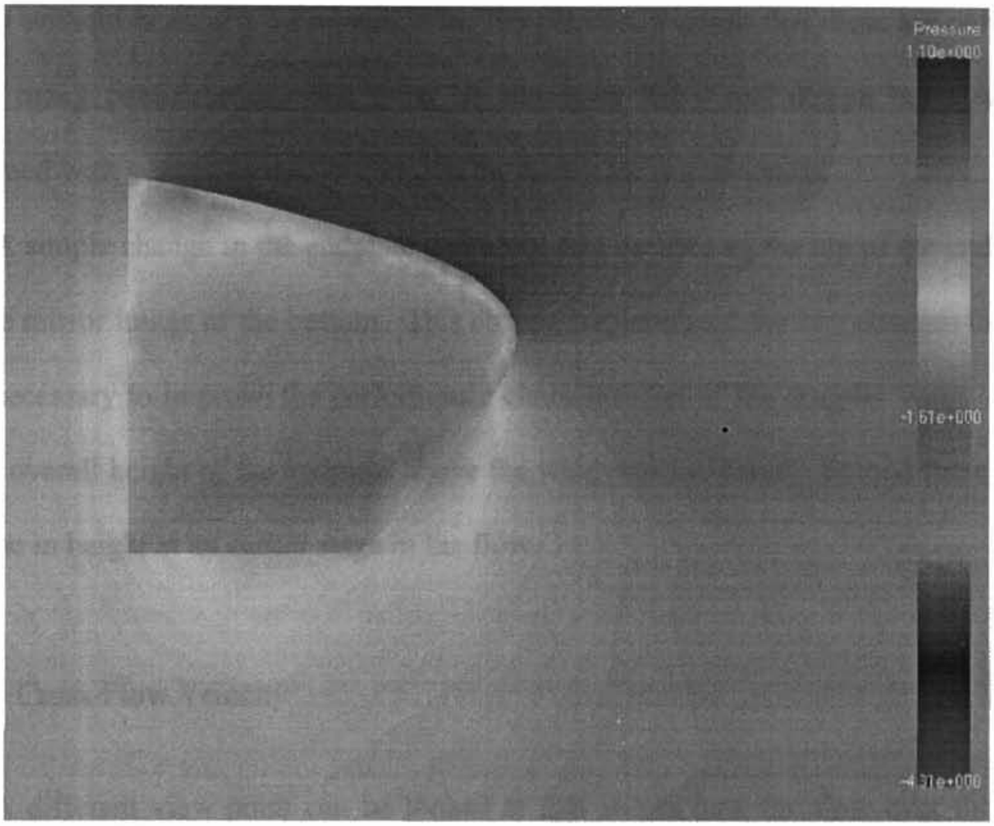

Figure 4-4: Pressure Gradient for Style 3 Endplate

The figure above was produced during the initial studies of the flow around the three-element wing with the style 3 endplate and led into an investigation of the effects that endplates have on wing performance as well as my development of the new endplate design.

It can be seen the high-pressure on top, represented by the darker area in the figure, extends way above the wing as well as above the top of the endplate. Ideally, from the pressure gradient standpoint, it would be best to extend the endplate up until the pressure in the far field is the same as the pressure on the endplate. There are two reasons why this is not done. First there is a point by which the overall drag will outweigh the benefit of extending the endplate. The second factor could be to make the structural strong enough without bearing a lot of weight on the vehicle. I admit that these are only a few of the many considerations that must be addressed for a real design but I was just concerned with minor changes to endplate geometry for improvement.

A simple change in the endplate geometry was decided so the top of the endplate is just the mirror image of the bottom. This change implemented the two changes that I felt were necessary to improve the performance characteristics of the dragster wing. First of all the overall height of the endplate above the wing was increased. Second there was an increase in height at an earlier stage in the flow.

4.1.2 Cross-Flow Velocity

A different view point can be looked at that shows how the flow over this three-element wing is effected by endplate geometry. This different perspective is cross flow velocity cuts that show the flow on a cut plane at user specified locations on the wing. Cross-flow velocity cuts were taken at three different positions parallel to the flow velocity axis.

The first position was at a distance 7 inches back from the leading edge of the main airfoil as depicted in the far left picture of Figure 4-5. This was chosen to look at early spill over effects generated by the main element. The second cross-flow cut was at 14 inches back from the leading edge of the main element and can be seen in Figure 4-5 as well. This position cuts through the trailing edge of the main element and the leading edge of the second element. The other picture in Figure 4-5 is the last cross-flow cut was located 20 inches back from the main element's leading edge. This is at the trailing edge of the last element where the most sever circulation can be seen. Each of these cut planes will be looked at separately although they each show similar results.

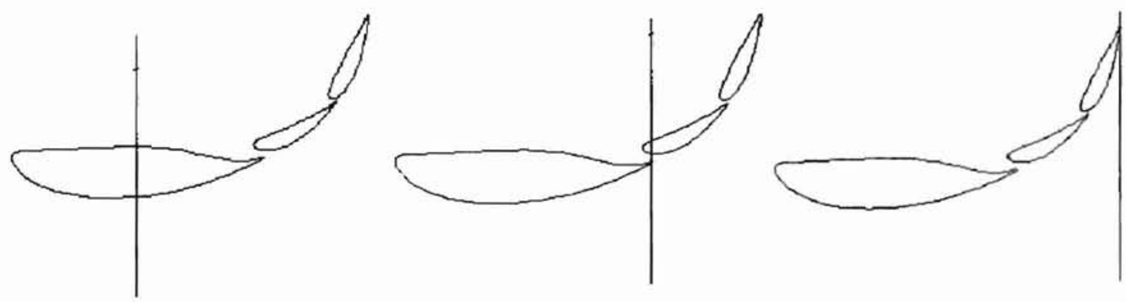

Figure 4-5: Cross Flow Velocity Cuts Represented by Vertical Lines

For the first cut plane at 7 inches back from the leading edge of the main element the spillover effect is minimal but the effects are very distinct. In Figure 4-6, without the endplate present, a circulation can be seen coming from the top of the wing around the tips of the wing to the suction side as discussed earlier. The figure shows a number of different size and oriented lines. The length of the line is proportional to the speed of the air around the dragster wing. The longer the line the faster the air is traveling. The orientation of the line is the direction of the air at that instance for the steady-state solution. The mid span of the half model is at the readers left hand side of these figures and the tip of the wing is on the right hand side. There is no endplate present to deflect this flow from circulating to the lower pressure side of the wing. From Figure 4-1 the three dimensional effects of can been seen from a different perspective from that discussed and shown earlier.

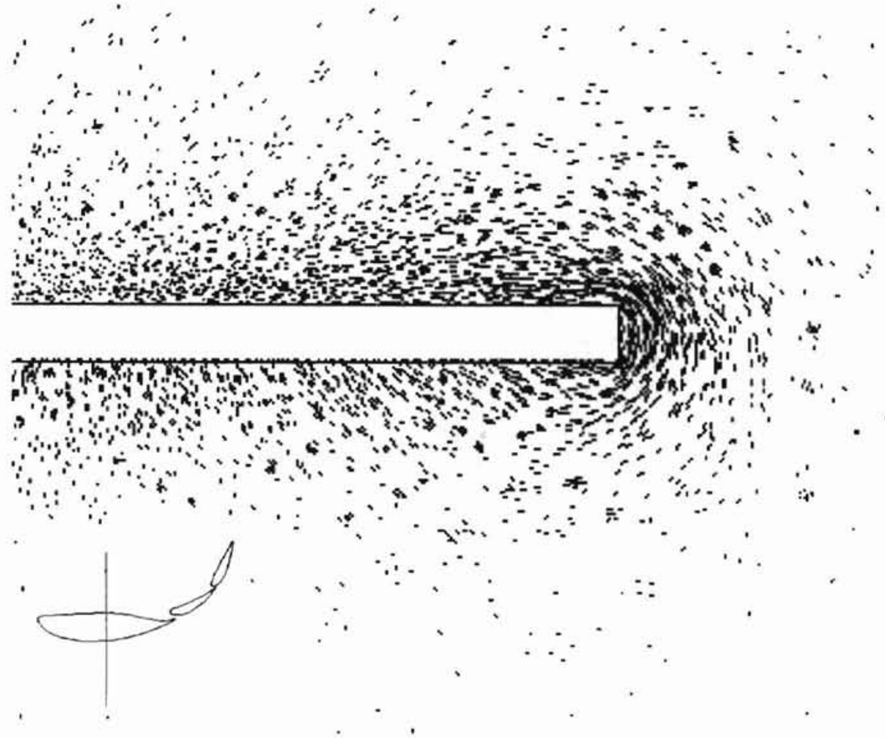

Figure 4-6: Cross-Flow Velocity 7 in. back from L.E. w/o an Endplate

If we now look at the second cross-flow plane cut, 14 inches back from the leading edge of the main element, the circulation strength is increased. Figure 4-7 shows the increased velocity of the flow coming around the tip of the wing.

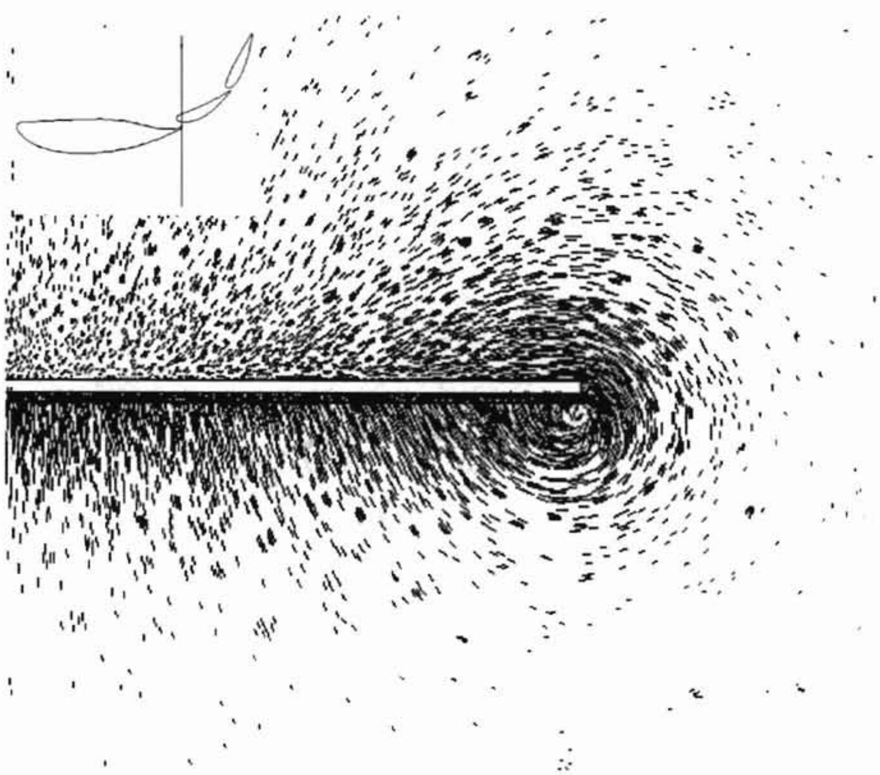

Figure 4-7: Cross-Flow Velocity 14 in. back from L.E. w/o an Endplate

The same effects can once again be seen in the cross-flow velocity plane cut towards the trailing edge of the third element.

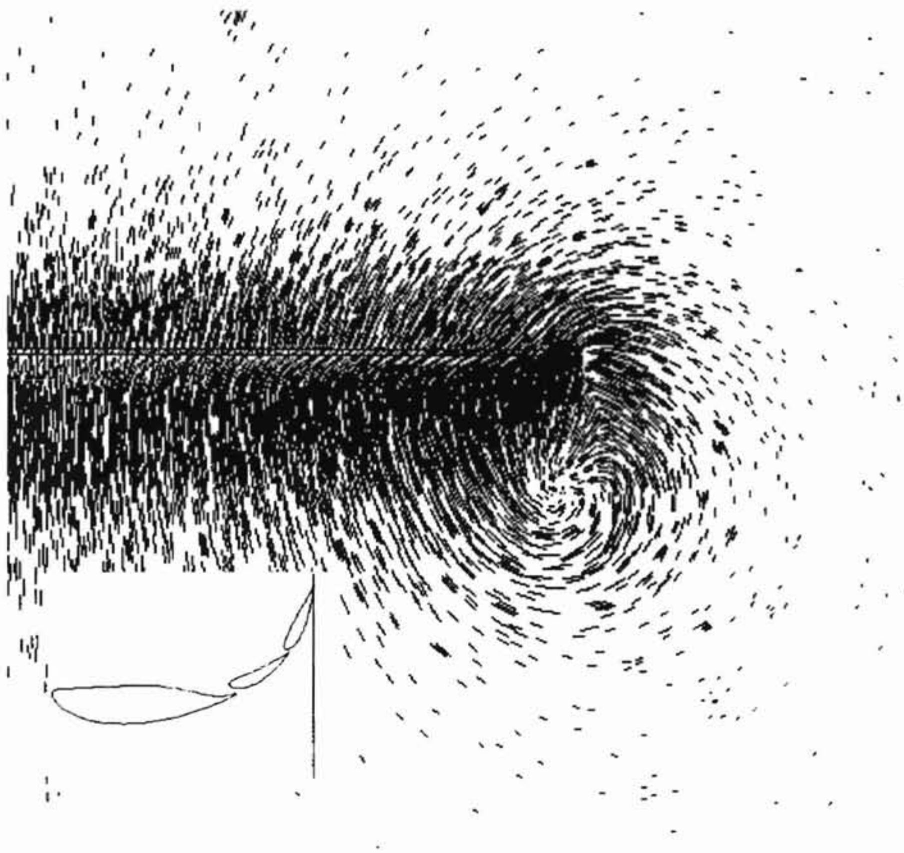

Figure 4-8: Cross-Flow Velocity 20 in. back from L.E. w/o an Endplate

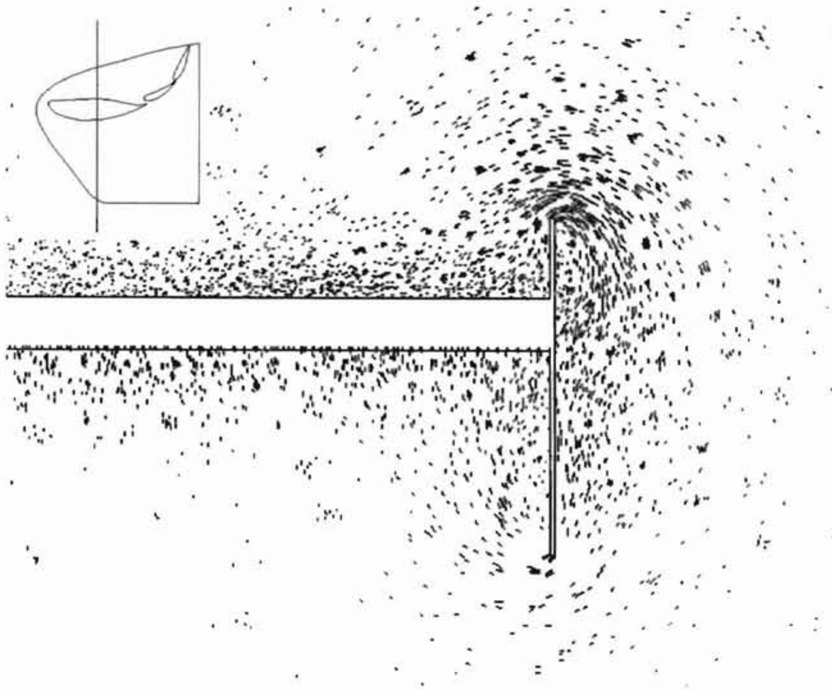

Figure 4-9: Cross-Flow Velocity 7 in. back from L.E. with Style 3 Endplate

Comparing that to the wing with the style 3 endplate, Figure 4-9, it can be seen that the airflow hits the inside of the endplate and is forced to flow up and over the endplate. At the top of the endplate the circulation is still present but it is less noticeable and certainly less sever. This circulation is disruptive to the suction side of the wing causing a decrease in suction as was shown in Figure 4-1 where the pressure is very noticeable changed. This is why endplates are so important to a low aspect ratio wing such as this rear dragster wing. Now since this circulation arose this early on in the flow it was decided that the height of the new endplate design needed to be increased at this location. This was also seen previously from the pressure gradient in Figure 4-4.

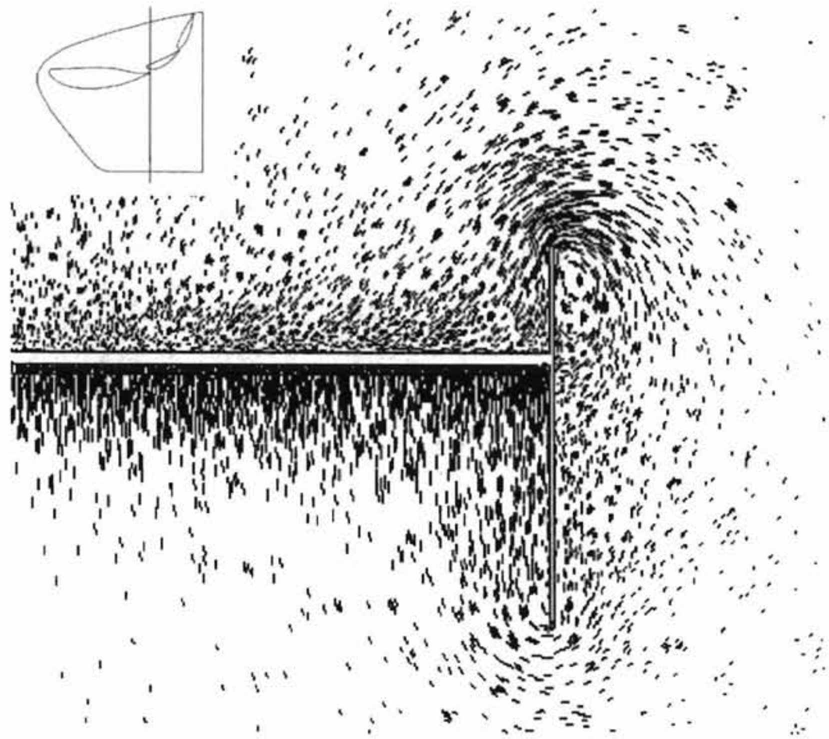

Figure 4-10: Cross-Flow Velocity 14 in. back from L.E. with Style 3 Endplate

The spillover effects are increased as seen in Figure 4-10. Again the high pressure gradients that are present matched with the shortness of the endplate above the airfoil section allow this flow to spill over and disrupt the flow.

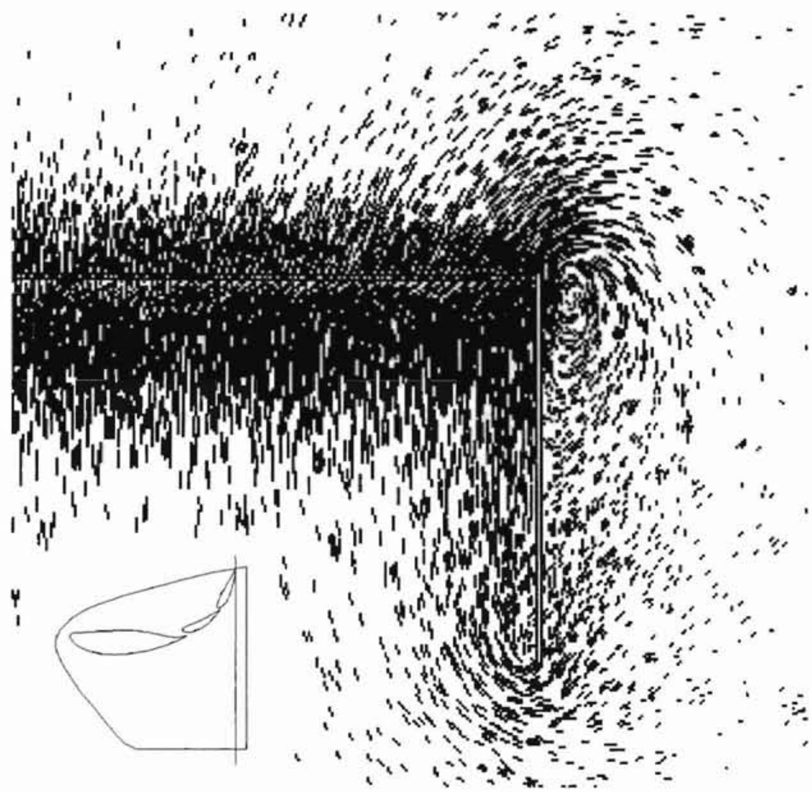

Figure 4-11: Cross-Flow Velocity 20 in. back from L.E. with Style 3 Endplate

The style 3 endplate has hardly any height above the trailing edge of the third element so the effects of the endplate are very minimal. The lower portion of the style 3 endplate is beneficial to reducing the circulation around the suction side of the wing.

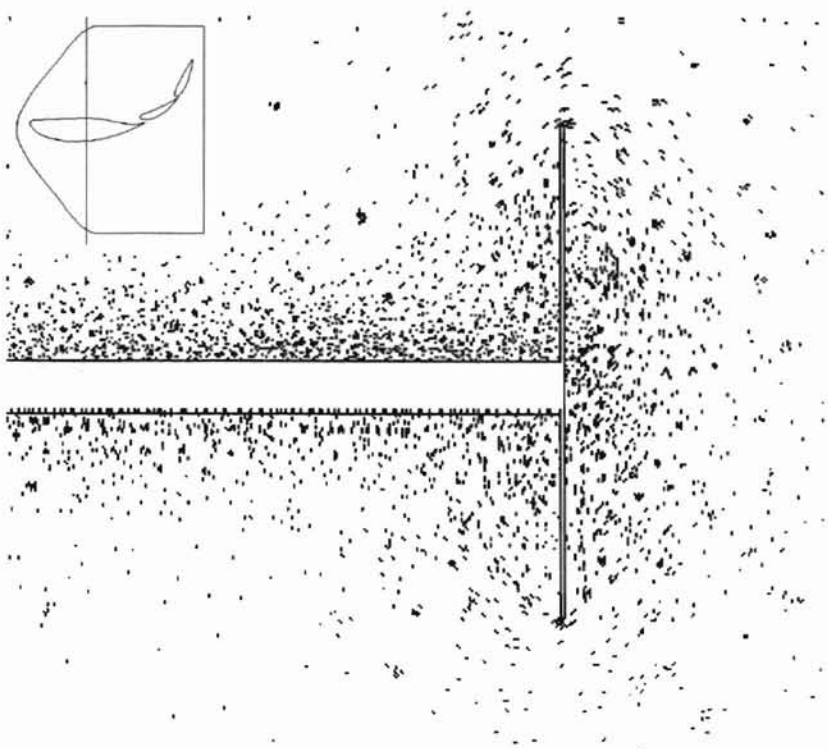

Figure 4-12: Cross-Flow Velocity 7 in. back from L.E. with New Endplate

Now looking at the new endplate design in Figure 4-13 the effects of the increased height still shows an improvement in the reduction of the spillover effect. The airflow has to travel a longer distance up over the endplate while decreasing its pressure gradient to the airflow on the outside of the endplate. Thus there is a decrease in the spillover.

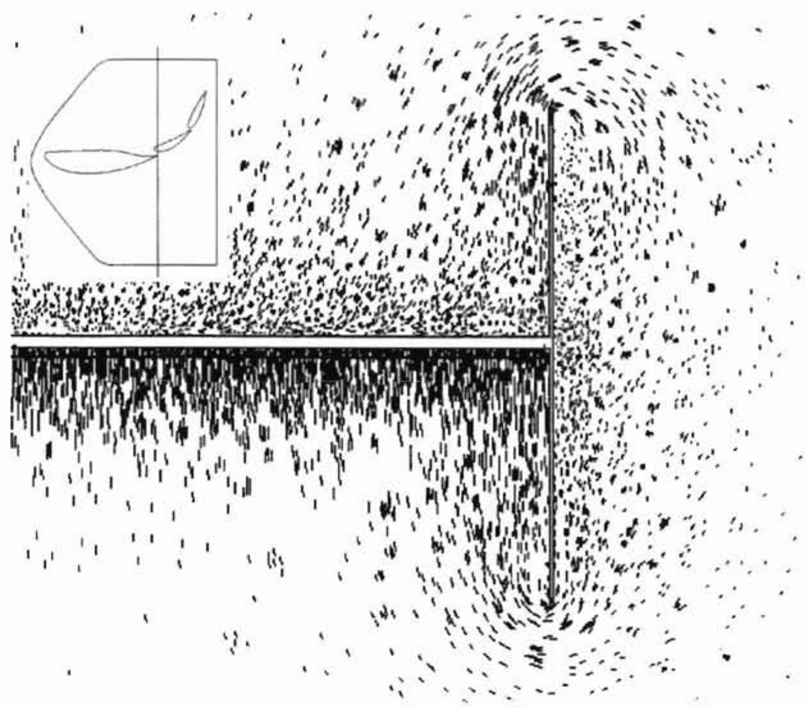

Figure 4-13: Cross-Flow Velocity 14 in. back from L.E. with New Endplate

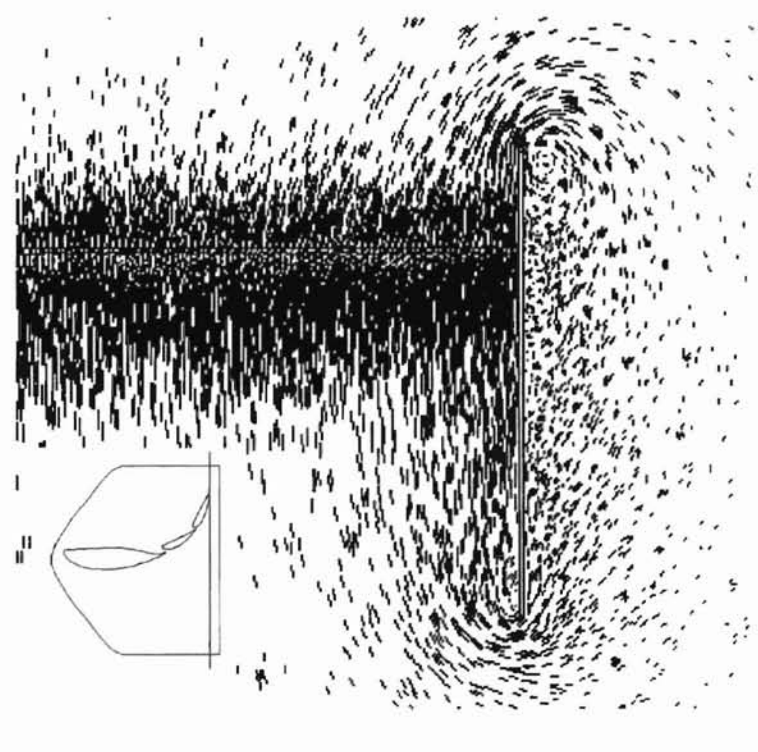

Figure 4-14: Cross-Flow Velocity 20 in. back from L.E. with New Endplate

Once again it was necessary on the new endplate design to increase the height above the third element in an attempt to reduce this circulation over the top of the endplate. It was once again very beneficial to incorporate this height change as can be seen in the reduced circulation in Figure 4-14.

This cross-flow velocity is only one view of what is going on as far as the flow velocity on and around the endplate. Therefore, it is necessary to look at a cut plane velocity profile parallel to the endplate.

4.1.3 Velocity at the Tip of the Wing

The velocity around the tip of the wing can give even more insight to the benefits of the endplates. In Figure 4-15, a cut plane at the tip of the wing, shows the circulation generated by the wing and how disruptive and almost how chaotic the airflow is behind the three-elemental wings due to the lack of an endplate.

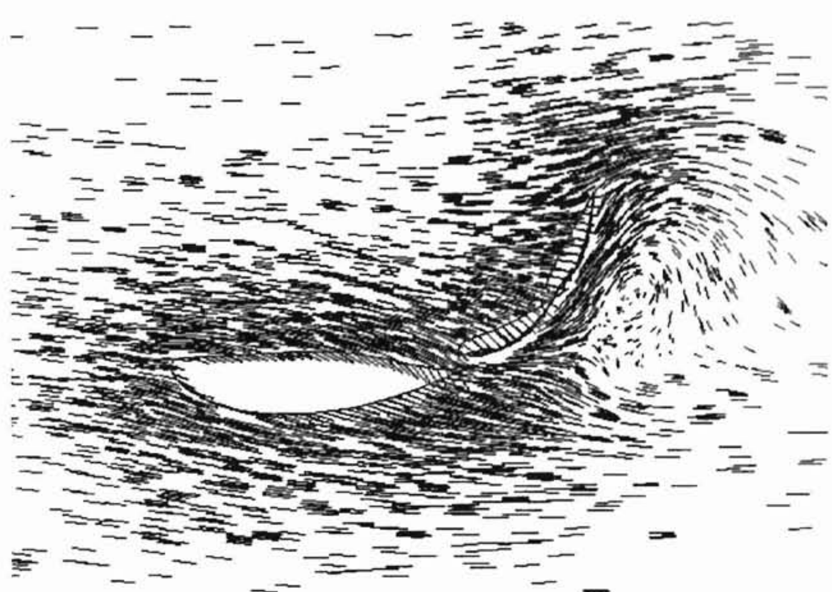

Figure 4-15: Velocity at the Wingtip without an Endplate

If there were an endplate attached the spillover flow would be reduced making for a less disruptive flow on the bottom of the wing. This is shown by looking at the flow on top and on bottom of the wing with an endplate present as in Figure 4-16. There are no distinct disruptive flows coming around the wingtips because the flow as you can see has to travel over the endplate. Figure 4-16 is a good example to show that the flow moves up the inside of the endplate which would then spillover and mix with the existing flow on the outside of the endplate. Once again it should be noted that the idea is to reduce the amount of flow spilling over.

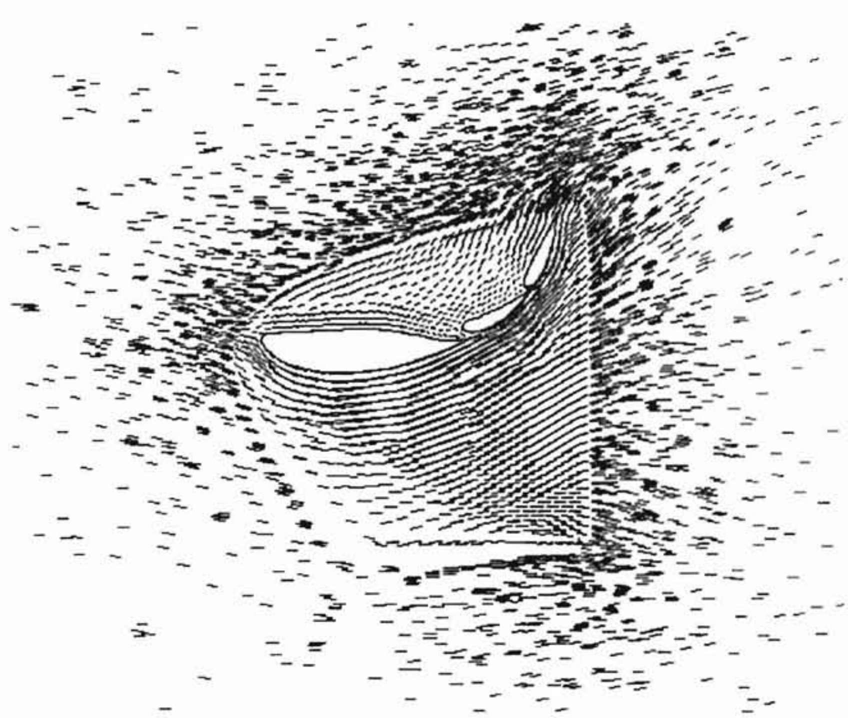

Figure 4-16: Velocity just inside Style 3 Endplate

Compare the velocity just inside the endplate of Figure 4-16 with the style 3 endplate to Figure 4-17 with the new endplate design. It can be seen that the flow at the top of the new endplate design, Figure 4-17, is not as vertical as the flow at the top of the style 3 endplate. This indicates that there is less severity to the disruptive nature of the flow as airflow spills over. The angle of the velocity at the top of the new endplate design becomes very similar to that of the style 3 endplate towards the tail end of the endplate. This is due to the last wing element being at such a high angle, 65°, causing the flow to accelerate in the direction of its projected chord line.

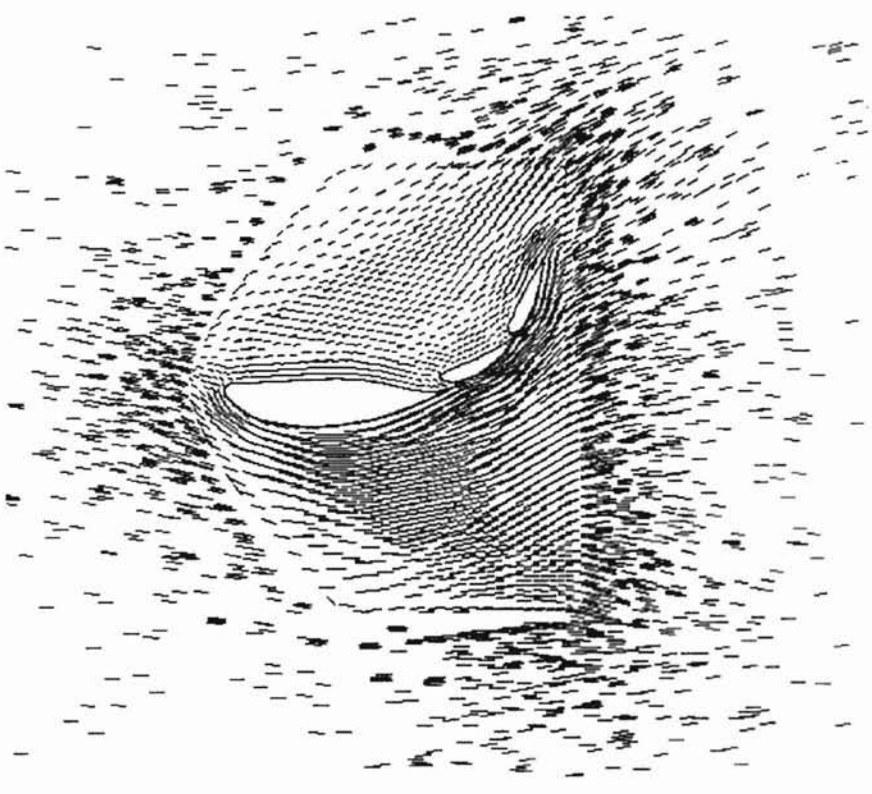

Figure 4-17: Velocity just inside New Endplate

4.1.4 Down Force to Drag Ratio

Another important parameter to look at the effects that endplate geometry have on the ratio of down force to drag. This parameter allows easy comparison between the different geometry. The idea is to maximize the ratio of down force to drag. It should be noted that it is not being said that we want to maximize the amount of down force but we want to maximize the ratio, ie get the most down force with the least amount of drag.

The forces that are calculated using STARS are not the actual down force and drag forces directly. They are in fact non-dimensional lift and drag coefficients. However they are not non-dimensional in the true sense but the coefficient of pressure is divided by a factor of two. We can utilize these coefficients without further manipulation since the ratio of the down force to drag is being calculated.

If we look at Table 4-1 at the wing without the endplate and compare it to the either of the wings with an endplate. There is a large difference in the amount of down force created by the wing with endplates. The drag however for the wing without the endplate is smaller but this is not important because we are concerned with the ratio of the two parameters.

	Down Force	Drag	L/D Ratio
No Endplate	741.9	232.4	3.19
Style 3 Endplate	960.7	258.5	3.72
New Endplate	967.6	242.6	4.0

Table 4-1: Down Force and Drag for the Three Test Cases Analyzed

If we look at the actual increase in the down force to drag ratio we can get a better feel for how much of an improvement changing the endplate can have. As shown in Table 4-2 there is a 16.6% increase in the ratio when we attach the style 3 endplate to the basic wing. This ratio is further increased by 25.4% when we look at adding the new endplate design. This data shows that the new endplate design is effective because it increases the down force to drag ratio by 7.2% over the style 3 endplate while only adding a minimal amount of area to the overall wing.

Geometry being Compared	Percent Increase of Lift to Drag Ratio
No Endplate to Style 3	16.6
No Endplate to New Design	25.4
Style 3 to New Design	7.2

Table 4-2: Increase of Lift to Drag Ratio for the Three Test Cases Analyzed

4.1.5 Mach Number and Coefficient of Pressure Distribution

The Mach number and coefficient of pressure distribution at the tip of the wing can be useful in showing where the maximum amount of flow velocity and suction is occurring, respectively. This gives the analysis a more physical comparison than just looking at the three-dimensional color pressure plots as was shown in the beginning of the section.

The pressure distribution in Figure 4-18 shows the coefficient of pressure for each of the three test cases analyzed. The first case where there was not an endplate, the coefficient of pressure on the suction side is about –2.5 on the first element as compared to –3 for the wings with the endplates. For the second wing element the difference in pressure on the suction side between the wing with an endplate and the wing without an endplate is about 1.5. The suction side of the third element and the positive pressure sides of all three-elements do not show a dramatic difference but there is still a moderate change.

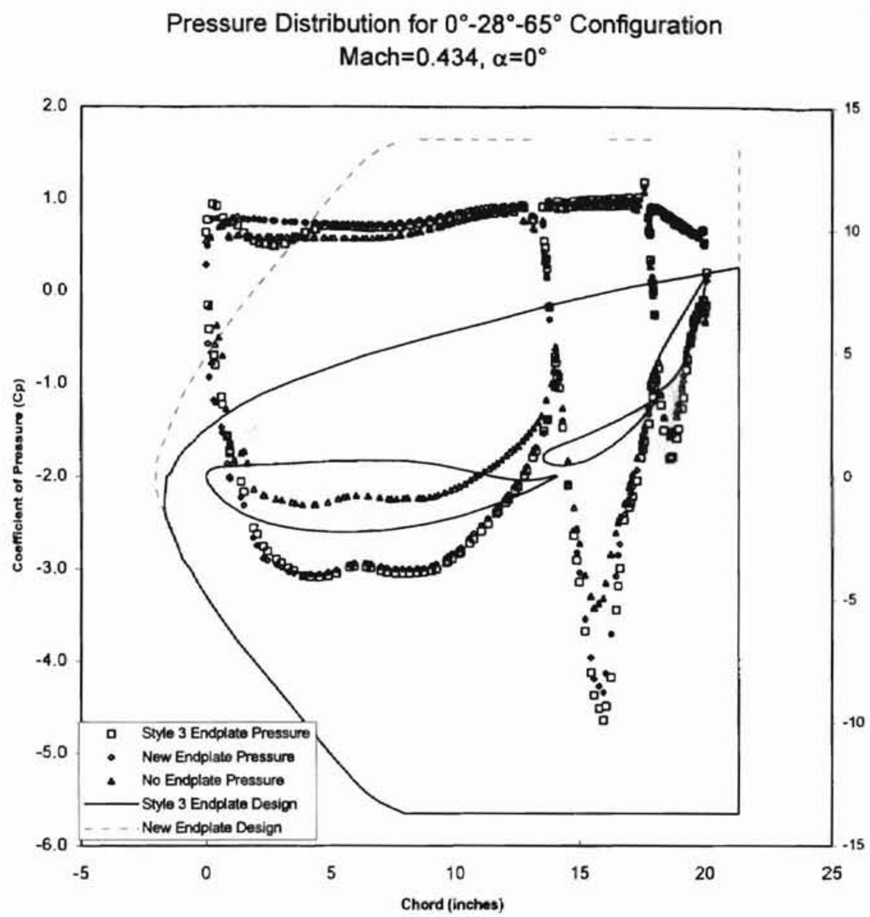

Figure 4-18: Pressure Distribution at the Tip of the Wing for Three Configurations

For the difference between the coefficient of pressure on the two endplates it is very difficult to tell from this data which is better. Although if you look closely at the positive pressure side of the wing, or top of the wing, you will notice that the new endplate design gives a little bit higher pressure.

As for the Mach number distribution in Figure 4-19 it can be seen that the Mach number for the wings with the endplates allowed for a larger amount of data points to become supersonic. The maximum Mach number for the wing without the endplate only reaches about eight-tenths the speed of sound on the first element. Comparing this to the first element for the wings with endplates, the Mach numbers almost reaches the speed of sound. For the second wing element the effect of the endplate is about the same. On the third wing element there is not a noticeable difference.

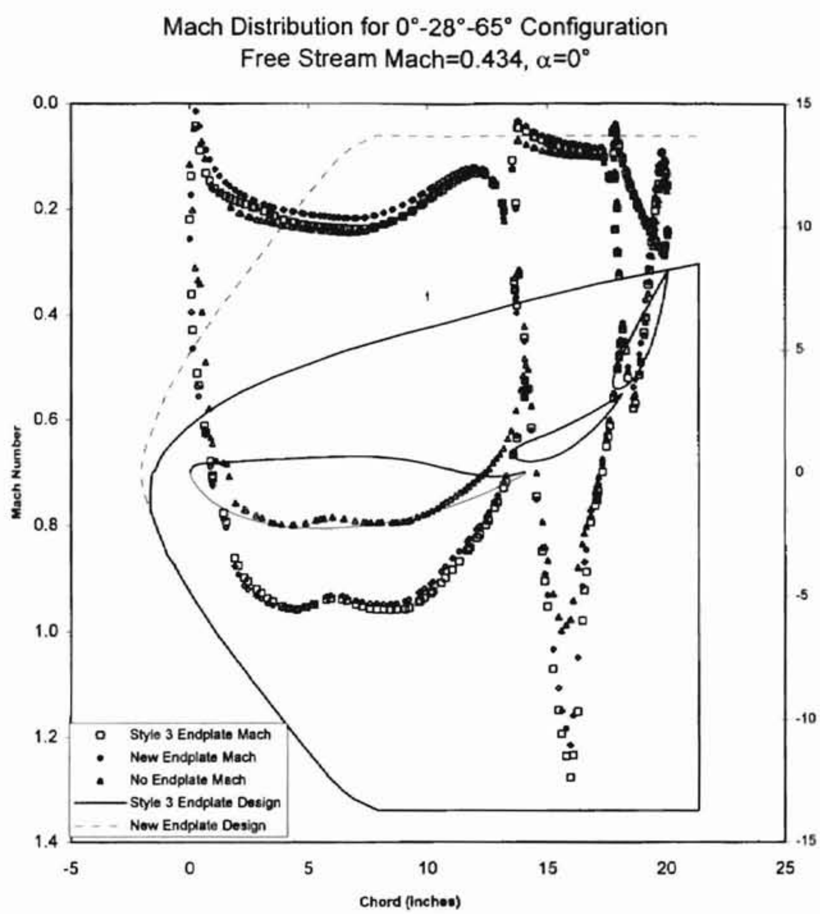

Figure 4-19: Mach Distribution at the Tip of the Wing for the Three Configurations

The topside of the wing shows a pretty uniform Mach number distribution between the three test cases analyzed. There is a slight increase in Mach number for the new endplate design over the style 3 endplate. It is believed that this can be linked to the reduced spillover affect seen on the top of the endplate.

4.2 Gap Spacing Comparisons for a Three-Element Dragster Wing

Gap spacing can affect the performance characteristics of these wings as well. Therefore the effects of gap spacing between the elements of a multi-element wing will be studied This gap spacing is critical because it allows a certain amount of flow to pass between the elements and this amount of flow is very sensitive when looking at the performance of a multi-element wing.

The best way to look at this is a velocity cut plane at the mid span of the half model as seen in Figure 4-20. The multi-element wing has a 0°-28°-65° configuration at a Mach umber of 0.434 for an overall angle of attack of 0°. As a reminder the configuration, 0°-28°-65°, refers to the angle of attack of each of the three individual elements.

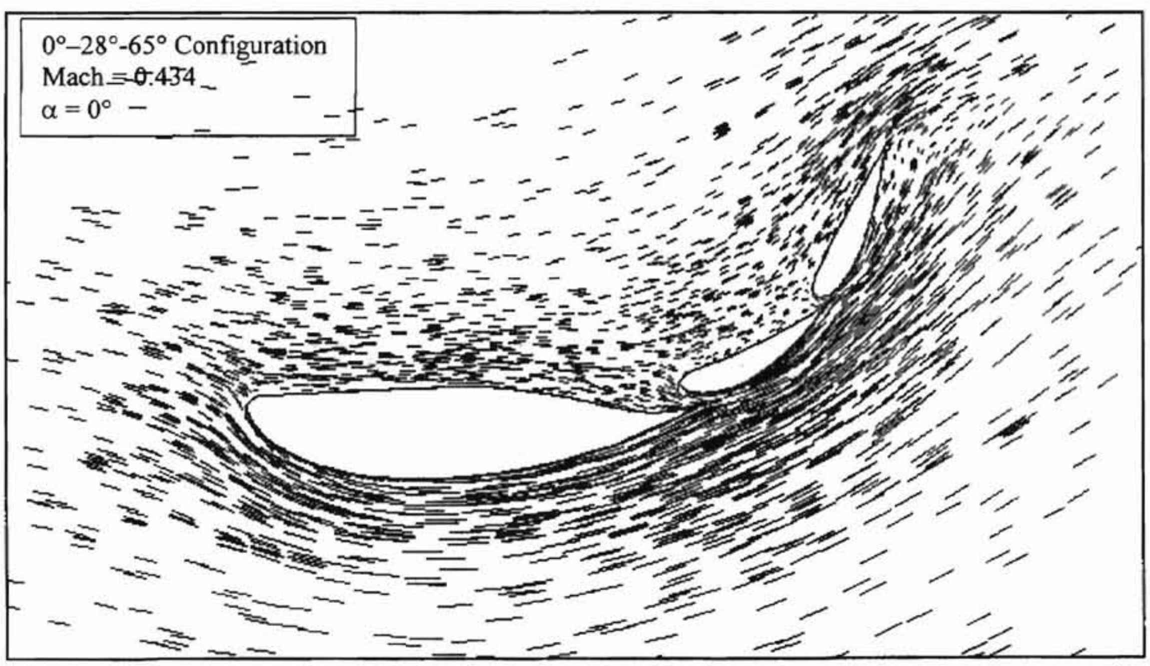

Figure 4-20: Velocity Profile of Wing with Original Gap Spacing

Pay attention to the gap size in between the elements as well as the flow field around and in between the gaps when looking at Figure 4-20 and Figure 4-21. It can be seen in Figure 4-20 that the flow around the second element, particularly the flow right in front of the second element, is more smooth looking than the flow around the second element in Figure 4-21. In the latter mentioned figure the gap size is too large and allows too much air to flow to pass. This causes a Ventura affect before the second element letting a massive amount of air through the gap which disrupts the flow. The same effects can be seen in the flow around the third element.

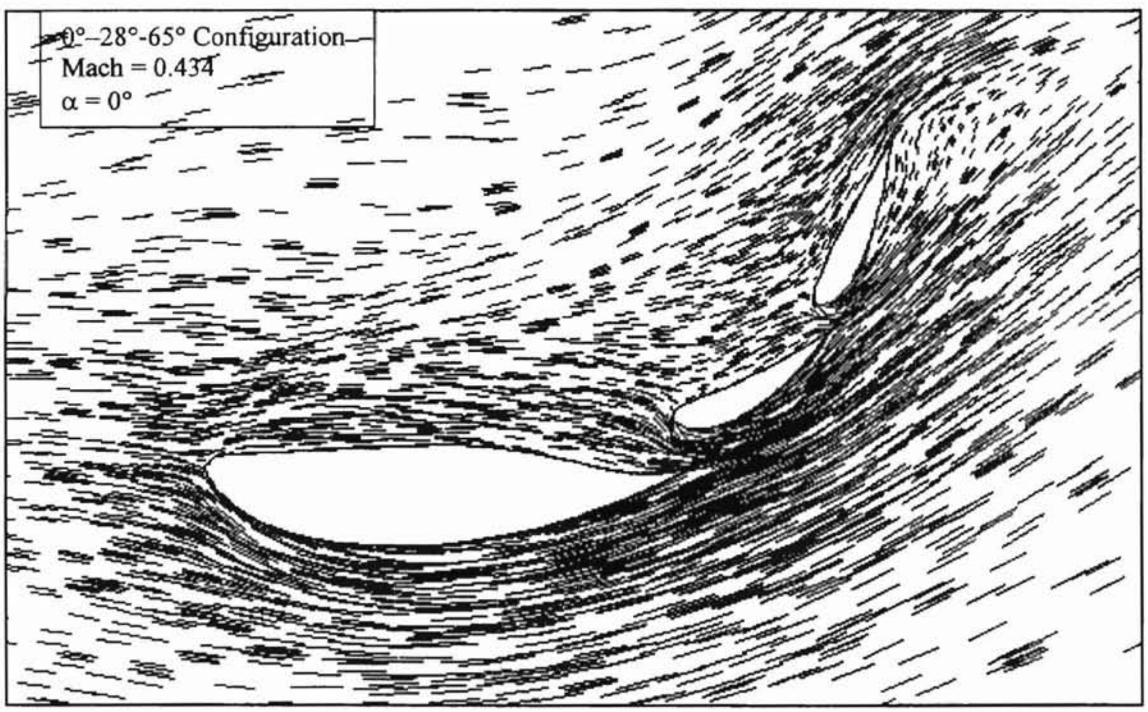

Figure 4-21: Velocity Profile of Wing with Modified Gap Spacing

When looking at the flow at the trailing edge of the third element another effect can be seen. With the increase in gap spacing the appears to be a flow separation. An Euler flow solver is unable to predict flow separation but the chaotic flow just aft of the trailing edge of the third element shows signs of flow separation. It almost appears to have a circulation around this area and is very disruptive to the flow.

When the gap size was increased there was a decrease in the amount of down force generated. The decrease in down force was 6.8% under the amount of down force generated by the original gap spacing. The increased gap spacing also resulted in an increased the down force to drag ratio by 15.7%.

4.3 Angle of Attach Comparisons of Three-Element Dragster Wings

The effects of angle of attack on dragster wing with the style 3 endplate was studied to see how it affected the performance of the wing. The configuration was a 0°-28°-65° wing that was varied at two different angles of attack being 0° and 5°. The reason for this analysis is due to the top-fuel dragster teams wanting to vary the angle of attack on the rear wing to change the performance characteristics. These comparisons were looked at both through pressure cut plane data as well as down force and drag data, which was generated using STARS.

The pressure distribution data, as seen in Figure 4-22, is a pressure cut plane at mid span of the half model. As seen in the figure below there is little differences for the last two elements in the coefficient of pressure between each of the two angles of attack. However, the main difference appear on the first element and are mainly present toward the leading edge of that element. When the whole wing is rotated 5°, tilted forward, the suction pressure has a greater distribution than the wing at 0° angle of attack. When looking from three quarters of the way back from the leading edge of the first element all the way back to the trailing edge of the third element there is little difference.

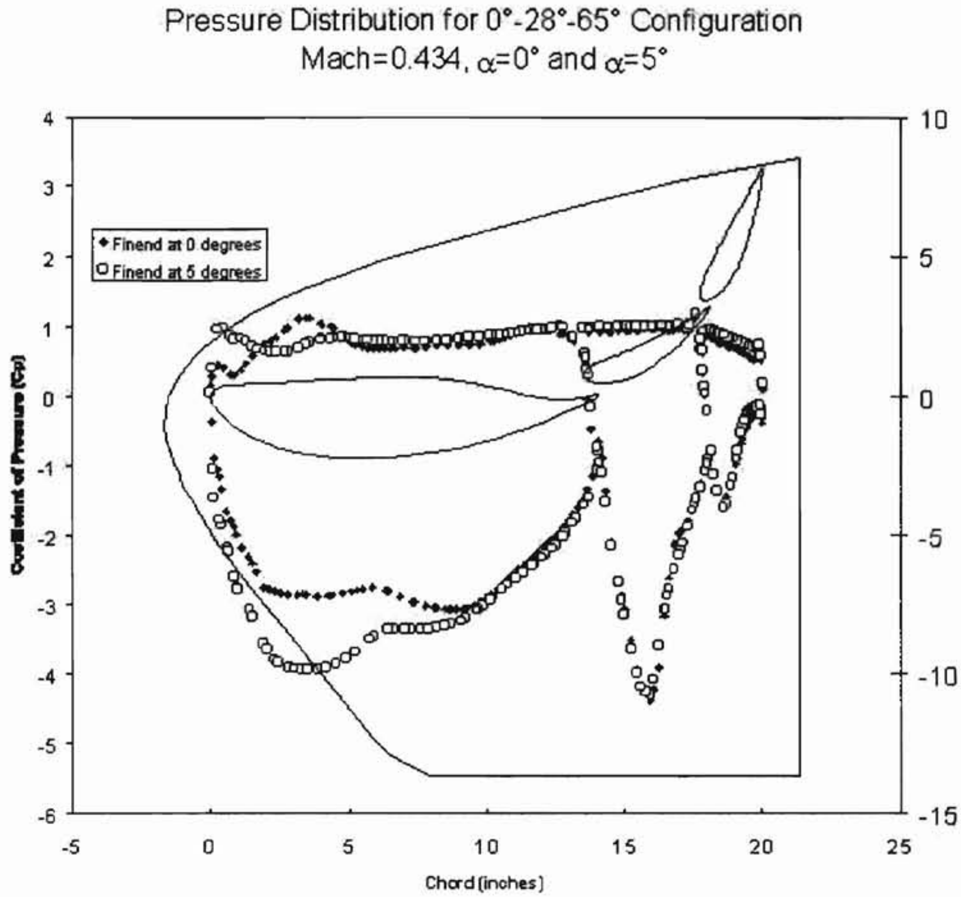

Figure 4-22: Pressure Plots for Angle of Attack Comparisons

For a feel on how much it affects the performance of the wing it is necessary to look at the down force and drag of the wing. An increase in angle of attack to $\alpha = 5°$ increases the down force by 8.9%. This might be considered good if all we were interested in was down force the drag must be considered in our case. The drag also increased but increased by 20.4%. This is greater than the increase in down force and therefore it decreases the down force to drag ratio by 9.7%. Based upon wing performance alone this increase in angle of attack would be a mistake.

4.4 World Record Performances

It should be noted that the improvement to the endplate design over the previously used style 3 endplate helped two top-fuel dragster teams break two different world records. Two weeks after the introduction of this new endplate Larry Dixon piloted a dragster owned by Don Prudhomme to the quickest elapse time record in the quarter mile history. At Houston Park Raceway in April of 1999 he posted a 4.486 second run beating the previous record by 0.03 seconds. Weeks later, with the same new endplate design, Tony Schumacher at the Checker-Schuck's Kragen Nationals downed the top-fuel dragster speed record reaching 330.23 mph in the quarter mile.

Granted the wing was not the only factor involved in the record-breaking runs but given the vast improvements they can be considered to be somewhat responsible. These wings can require close to 2000 hp to drag them through the air. The new endplate design reduced the drag and thus reduced the needed horsepower to drag the wing through the air. This additional horsepower can then go to acceleration and thus potentially allowing the vehicle to reduce the elapsed time or increase the top speed.

4.5 Using the Dragster Model to Analyze the Problem

Since the model matched the actual data well it is now the objective to see what affects the aerodynamics has on the performance of the dragster.

The first figure below, Figure 4-23, shows the actual input power to a dragster. This is used for the input power to the dragster for the validation analysis in the previous section. Along with this input power is the power left over to accelerate the dragster and is labeled acceleration power. This is the power after the drag and various friction components are taken away from the trust component. This acceleration power is an output from the model. There is a point on the plot that is labeled critical horsepower and this is the point where the vehicle hits critical velocity. At any time below this the model is assuming that it is on the verge of slipping which was discussed in earlier sections.

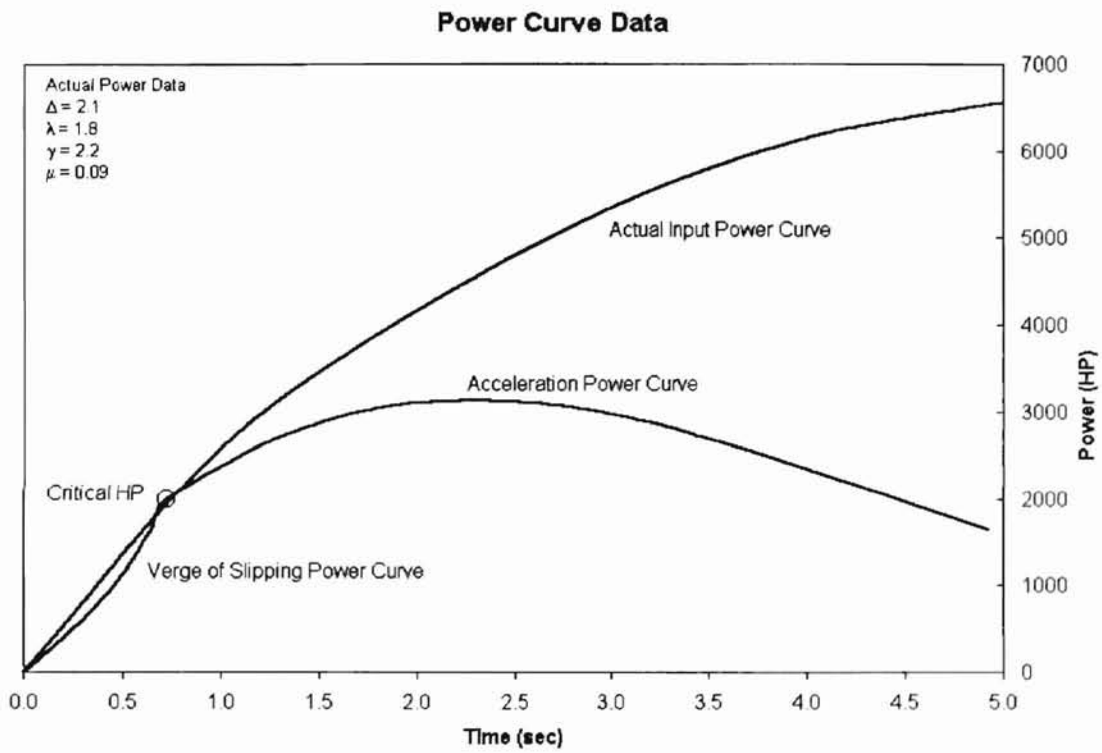

Figure 4-23: Input Power Curve and Acceleration Power Curve versus Time

Looking at difference in power between the two curves is an indication into how much power is being lost. The acceleration power is critical because this is the power being used to accelerate the vehicle. Therefore it is necessary to determine where these loses are coming from.

In the next figure, Figure 4-24, there are two additional lines. One is the amount of power that the car absorbs due to drag and friction. Looking at the drag coefficient of the wing in comparison, Table 4-3, with the rest of the components under consideration showed that it was a major factor in this power loss.

Coefficient of Drag Scaled to Wing Area

Wheels	Cl	-0.14142	Cogotti for Rotating Wheels
	Cd	0.45489	Cogotti for Rotating Wheels
Wing Induced	Cl	-2.47700	STARS
	Cd	0.60100	STARS
Wing Area Top	Cd	0.00963	Estimated
Wing Area Endplate	Cd	0.00380	Estimated
Body	Cd	0.01733	Estimated by 3D Wedge

Table 4-3: Lift and Drag Coefficients for the Dragster Model

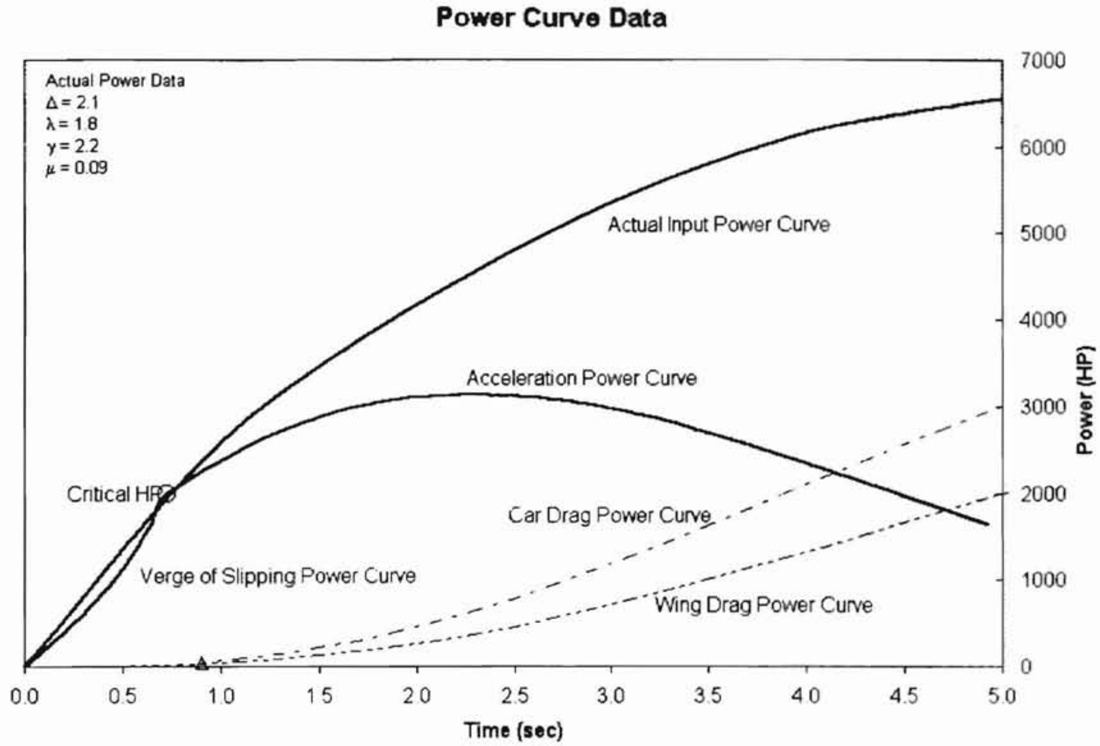

Figure 4-24: Power Curves along with Drag Power versus Time

At the end of the race the wing is making up almost two thirds of the total loss of power of the dragster. It is necessary to find out how changing this drag would affect the performance of the dragster. In order to do this the model was run with different drag coefficients while keeping constant the lift to drag ratio. This was done for four drag coefficients and six different lift to drag ratios and the results can be seen in Figure 4-25.

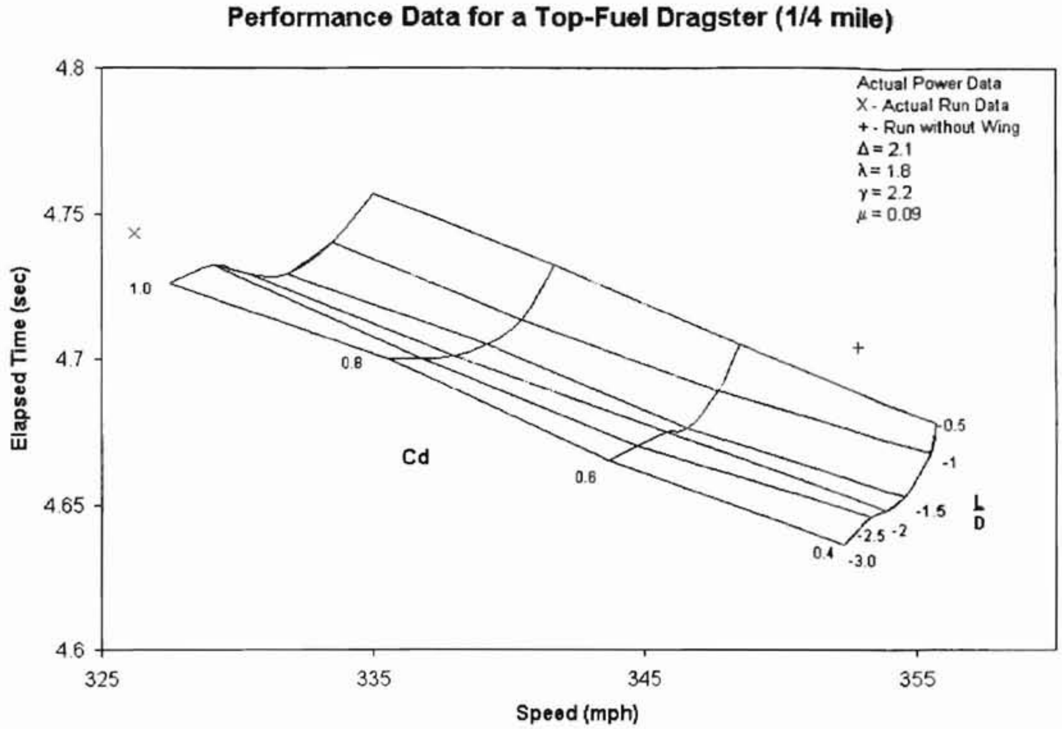

Figure 4-25: Elapsed Time and Speed Data for Varying Drag Coefficient

This figure shows how much reducing the drag coefficient can improve the elapsed time of the dragster as well as how much it can increase the top speed. The X on the figure shows a dragster whose lift and drag characteristics were estimated and the wing data was generated from STARS for the finnew wing design. The finnew design is a wing that is currently being used by several dragster teams. The elapsed times and top speed are not current with the times and top speeds of today's dragsters but it must be understood that the input power used was from actual data that might not meet the siput power data of a dragster now. The idea of this is to not look at the times and speeds that were achieved but to look at the trends of changing the parameters.

Another point on the graph to look at is the + mark. This run is the same dragster but the wing is taken off so that is produces not down force or drag force. It has a lower elapsed time because the reduction in drag but the catch is that the driving style would have to change. This can better be seen below in Figure 4-26.

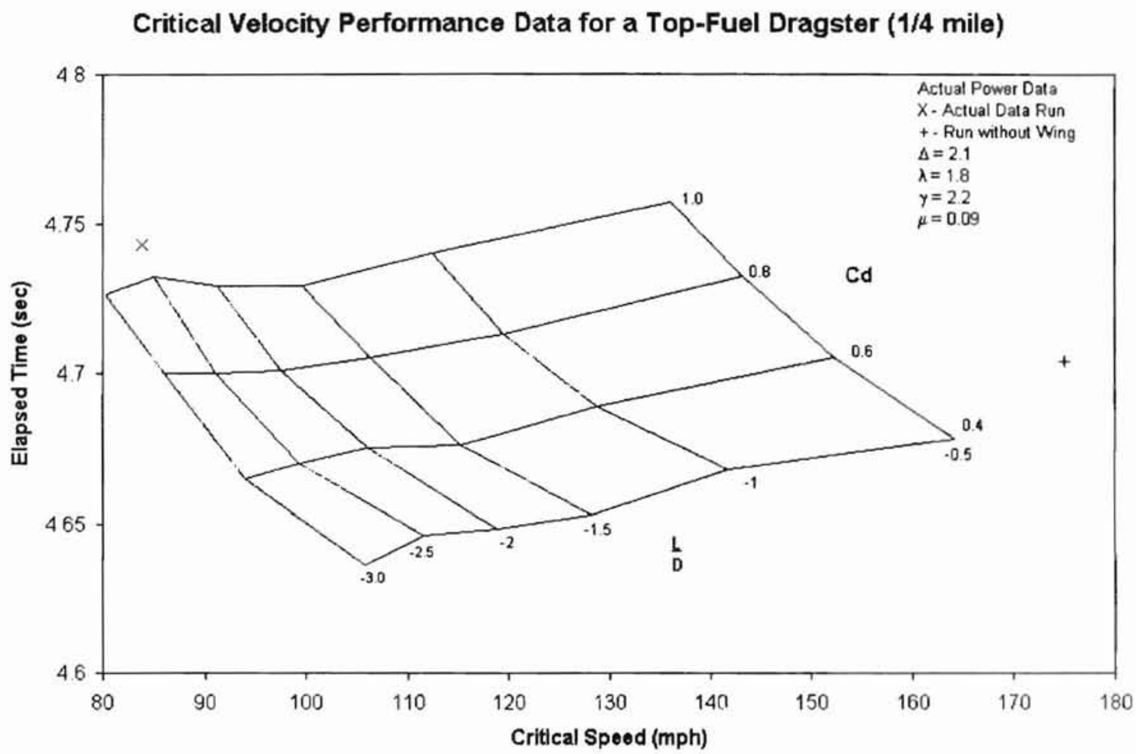

Figure 4-26: Elapsed Time and Critical Speed Data for Varying Drag Coefficient

The critical speed is over twice that of the dragster with the wing. This means that there is not enough down force early on and with the given input power curve it is not able to give full power until it reaches this speed. If it had more power earlier than this point than the tires would slip and loose traction. This means that the driver must be less aggressive during the race in the dragster without the wing. This shows how important reducing this drag can be as far as performance is concerned.

The question then is whether running a dragster without a wing is the best or is there some other way that is better. It is still not know how the lift coefficient affects the performance of the dragster. The question must be answered then how much lift does the dragster need and at what point on the track is the lift needed? The best way to figure this out is to vary the lift coefficient for a fixed lift to drag ratio. This data is plotted below in Figure 4-27.

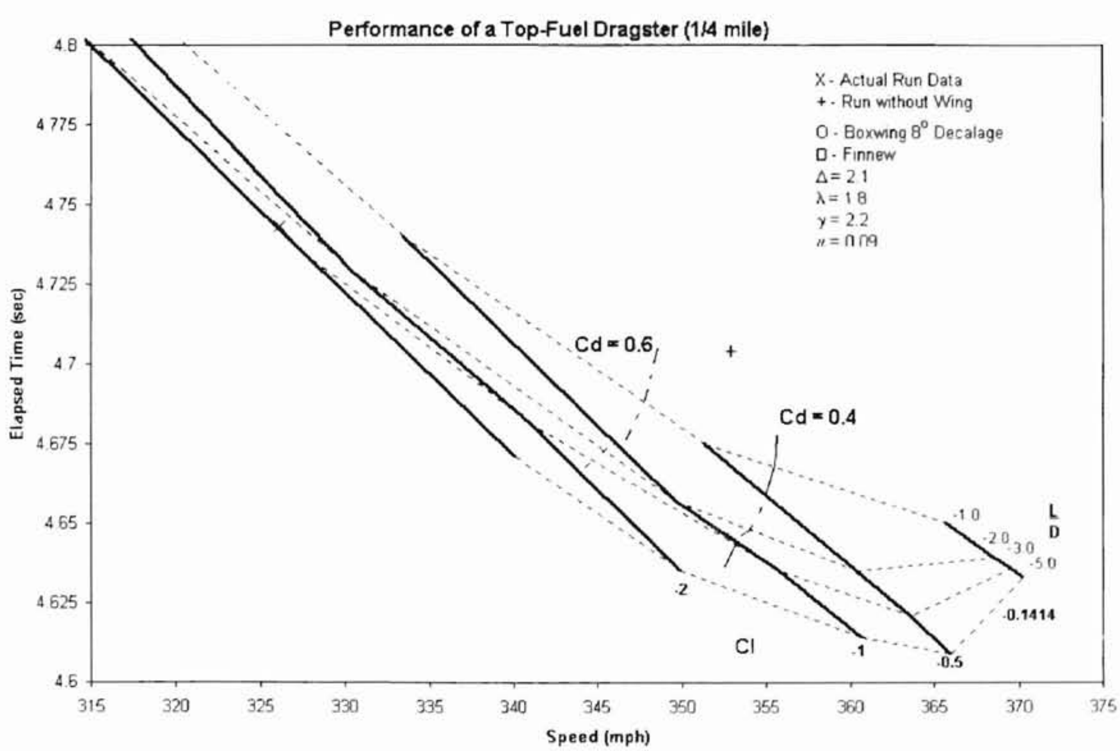

Figure 4-27: Elapsed Time and Speed Data for Varying Lift Coefficient

Looking at the constant drag coefficient lines (C_d=0.6 and C_d=0.4) backs up the theory from before that to get a better elapsed time it is necessary to reduce the drag coefficient. The lift coefficient can be looked at as well showing that for a constant lift to drag ratio reducing the lift coefficient from -3 to -0.5 will reduce the elapsed time and increase the top speed of the dragster. Once the dragster gets below a lift coefficient of around -0.5 the elapsed time increases. This starts to show that reducing the lift coefficient down to zero does not help the performance of the dragster.

In this region where there is a low lift coefficient and a high lift to drag ratio the performance of the dragster suffers because of the critical speed is too great for the car to have its best run. This can better be seen in Figure 4-28. The elapsed time is around 175 mph. This is somewhat misleading because the drag coefficient for the dragster cannot be this low unless significant modifications to the aerodynamics of the overall car is made. Looking at the run of the dragster without the wing it has a drag coefficient between 0.4 and 0.6. The drag from the large open wheels and the body of the dragster are to blame for this drag.

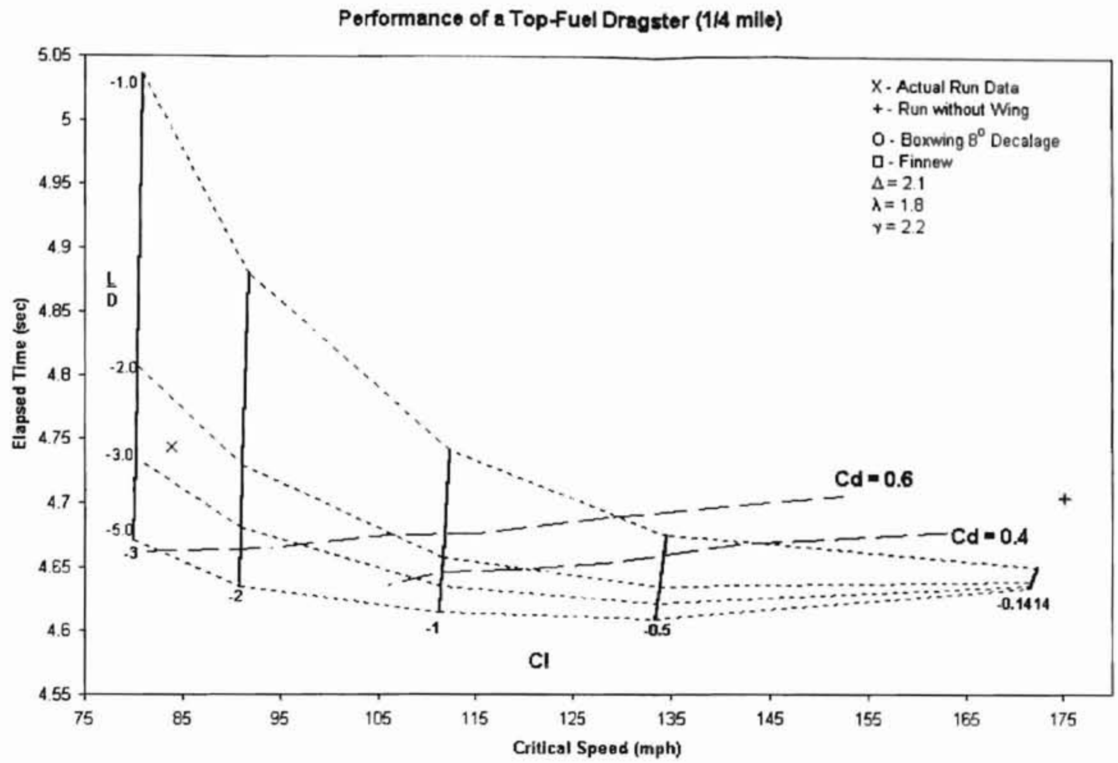

Figure 4-28: Elapsed Time and Critical Speed Data for Varying Lift Coefficient

These figures are somewhat misleading because if we are looking at changing the wing on the car then it is not simply looking at just changing the lift coefficient. Lets say for instance that you were looking at changing the angle of attack of a wing and you were able to increase the lift coefficient from -1 to -2. It is clear at to where the lift coefficient lines are and how they affect elapsed time but what now happens is that when the angle of attack changed not only did the lift coefficient change but the lift to drag ratio changed as well. So it is not as easy to see how it is affected because the lift to drag ratio is not constant and the user of the figures must determine the new lift to drag ratio.

Wing configurations will be plotted later in this paper but what I want to do is to talk about designing a new wing. From looking at the previous plots a wing that has a lower lift coefficient with the highest lift to drag ratio will get us into a lower elapsed time. As was mentioned earlier the design of a boxwing was considered for many reasons and the results from STARS will be discussed in the next section.

4.6 Steady Results of Boxwing Design

The new boxwing design was analyzed computationally using STARS. The performance characteristics of this wing compared to the old style three-element wings will be looked at in this section. Various plots and figures are provided to show a variety of different comparisons between the wings including pressure plots, mach plots, coefficient of lift versus angle of attack, coefficient of drag versus angle of attack, coefficient of lift versus coefficient of drag, and several others.

4.6.1 Decalage Angle Comparisons

STARS simulations were performed for various boxwing configurations. The decalage angle was varied for three different angles. For every decalage angle the angle of attack was then varied over a wide range to find the characteristics of this particular type of wing. This data was used to analyze the performance of this wing and then use it also to compare this boxwing to existing wings.

4.6.1.1 Pressure Plots

The pressure plots are for three different decalage angles for a wide range of overall wing angle of attacks. The side view of the wing at zero angle of attack is also plotted on the graphs in order to clarify the two distinct sections of pressure distribution on the plots.

The two regions of pressure distribution clearly show the difference in loading of the two wings. The front wing is loaded too much while the back wing is not loaded enough. The reason that this happens is because the influence of the wings on each other. The front lower wing reduces the effective angle of attack of the back upper wing and the back upper wing increases the effective angle of attack that the lower front wing sees. This is why we change the decalage angle as to try to evenly load these wings to account for the influences of the wings on each other.

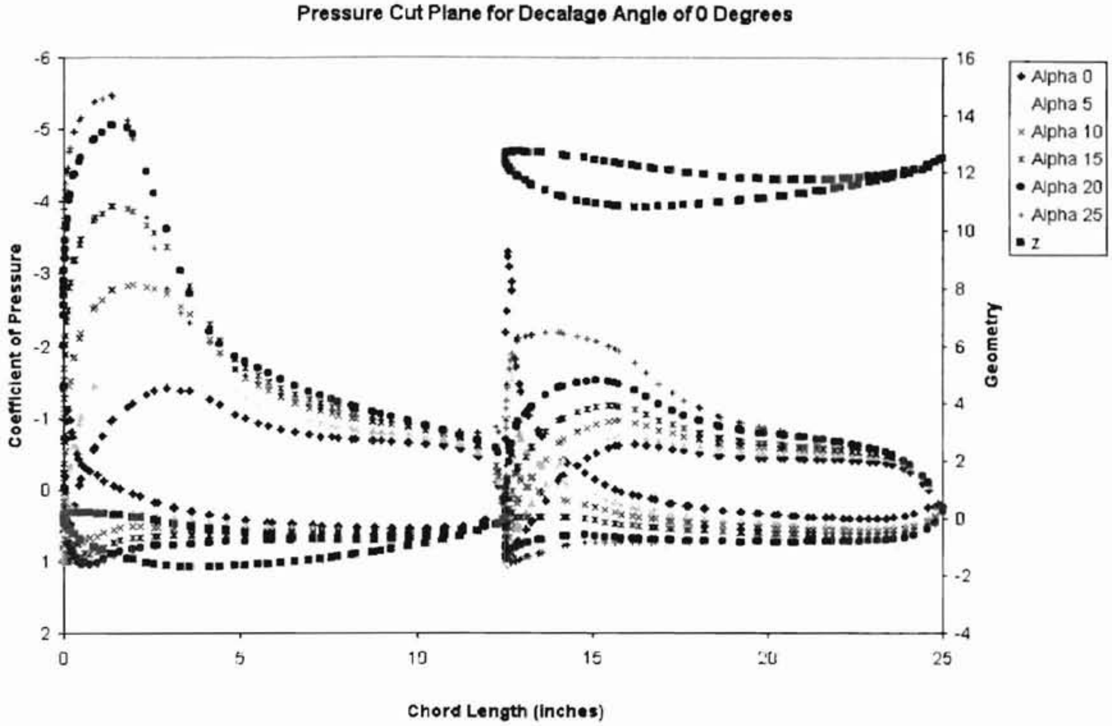

Figure 4-29: Pressure Plot for Boxwing at 0 Degree Decalage Angle

As can be seen in Figure 4-30 the pressure distribution is starting to level out and provide a more efficient wing. In this figure the decalage angle is 8°. As mentioned earlier the difference in angles between the two wings is the decalage angle. When the lower front wing is parallel to the ground, at a zero angle of attack, the upper back wing is turned at an 8° angle, where the tail of the wing is up.

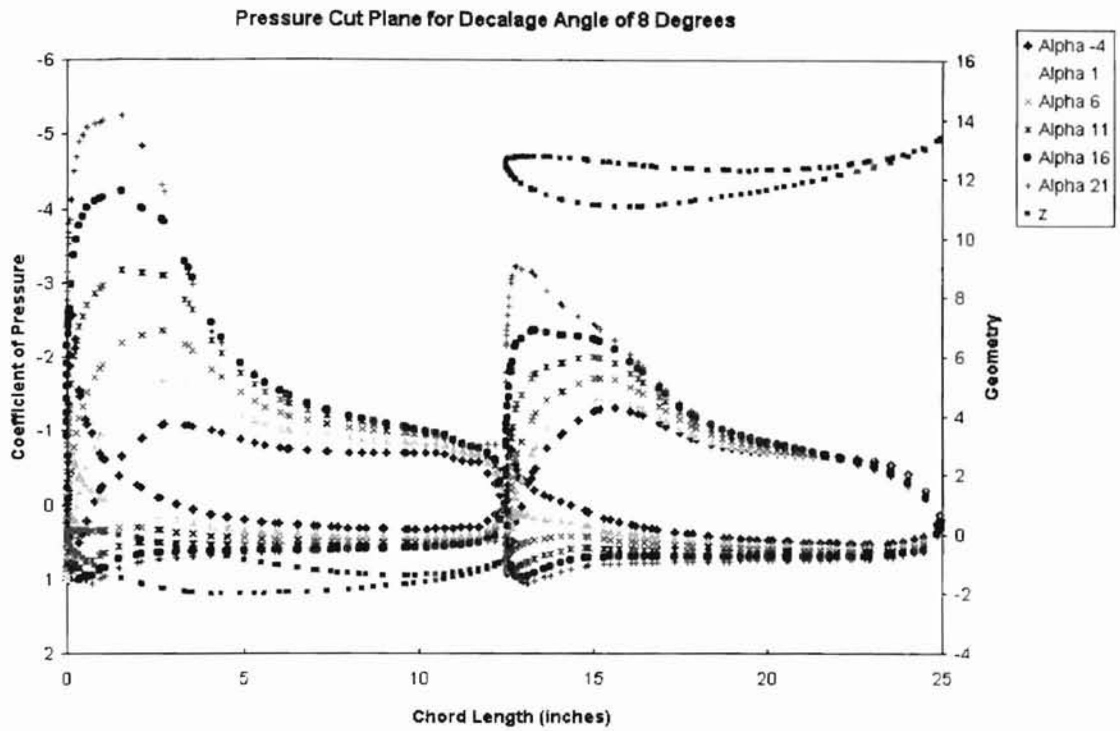

Figure 4-30: Pressure Plot for Boxwing at 8 Degree Decalage Angle

Since the distribution is still quite a bit off another decalage angle is studied. The pressure distribution of a 12° decalage angle boxwing is shown in Figure 4-31. There are only two overall angles of attacks that were run using STARS but the patterns for the more evenly distributed pressure contours can be seen. In these plots the side view of the boxwing is also plotted and in this figure the decalage angle is more noticeable.

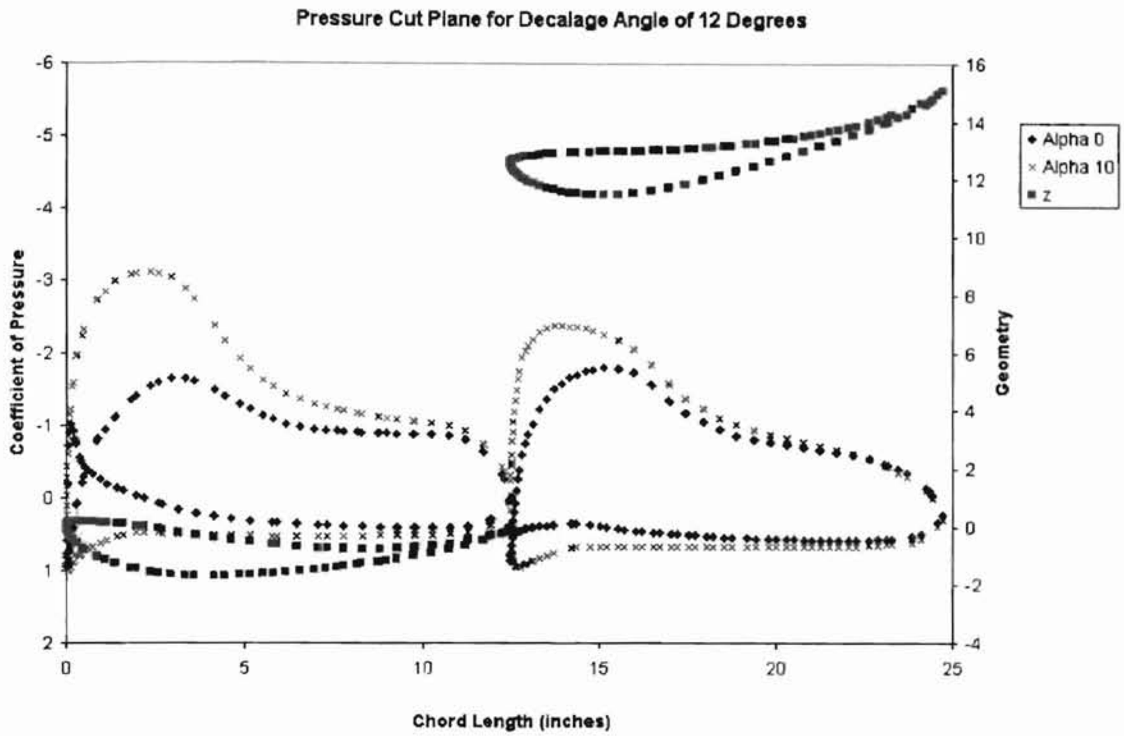

Figure 4-31: Pressure Plot for Boxwing at 12 Degree Decalage Angle

4.6.1.2 Mach Plots

Similarly to the pressure plots, the Mach plots are shown for three different decalage angles for a wide range of overall wing angle of attacks. The side view of the wing at zero angle of attack is also plotted on the graphs in order to clarify the two distinct sections of Mach distribution on the plots

The first plot, Figure 4-32, the decalage angle is 0° and once again the distribution of Mach number is distributed unevenly between the two wings. The Mach number on the lower front wing for high overall angles of attack has points where it is above Mach 1 but the upper back wing only sees subsonic flow no matter how high the overall angle of attack.

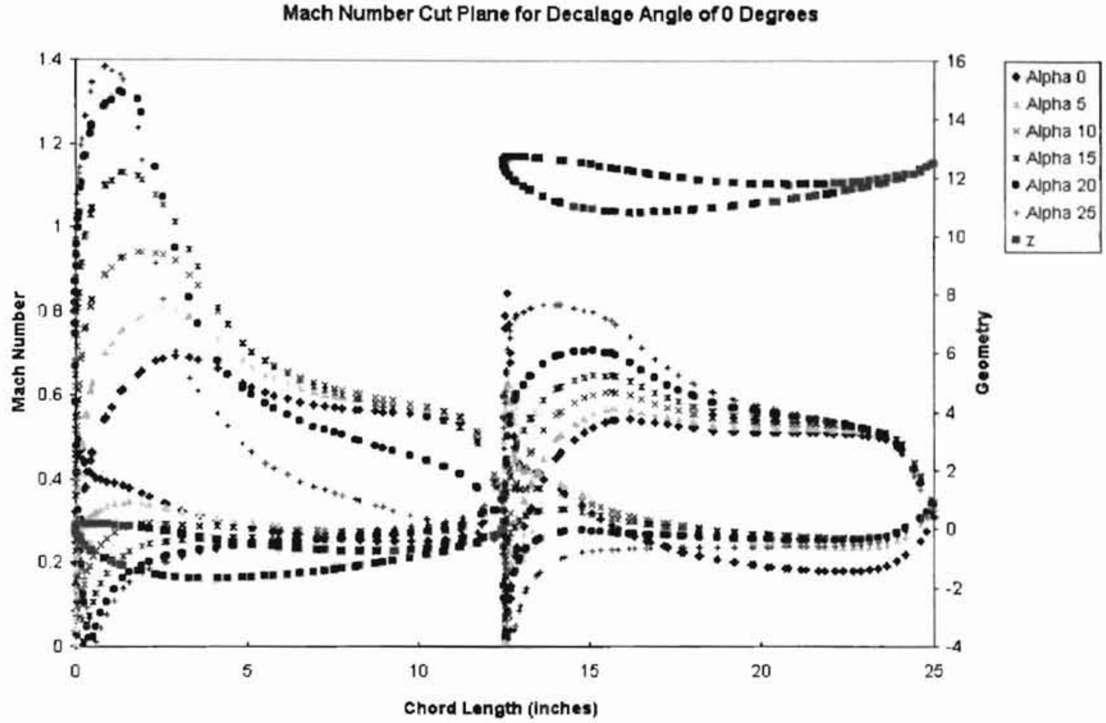

Figure 4-32: Mach Number Plot for Boxwing with 0 Degree Decalage Angle

The same patterns for the pressure plot for the 8° decalage angle occur for the Mach plot as well. In Figure 4-33 the distribution of Mach starts to even out. For the 21° angle of attack the upper back wing almost sees Mach 1 while the lower front wing sees Mach numbers to almost Mach 1.4.

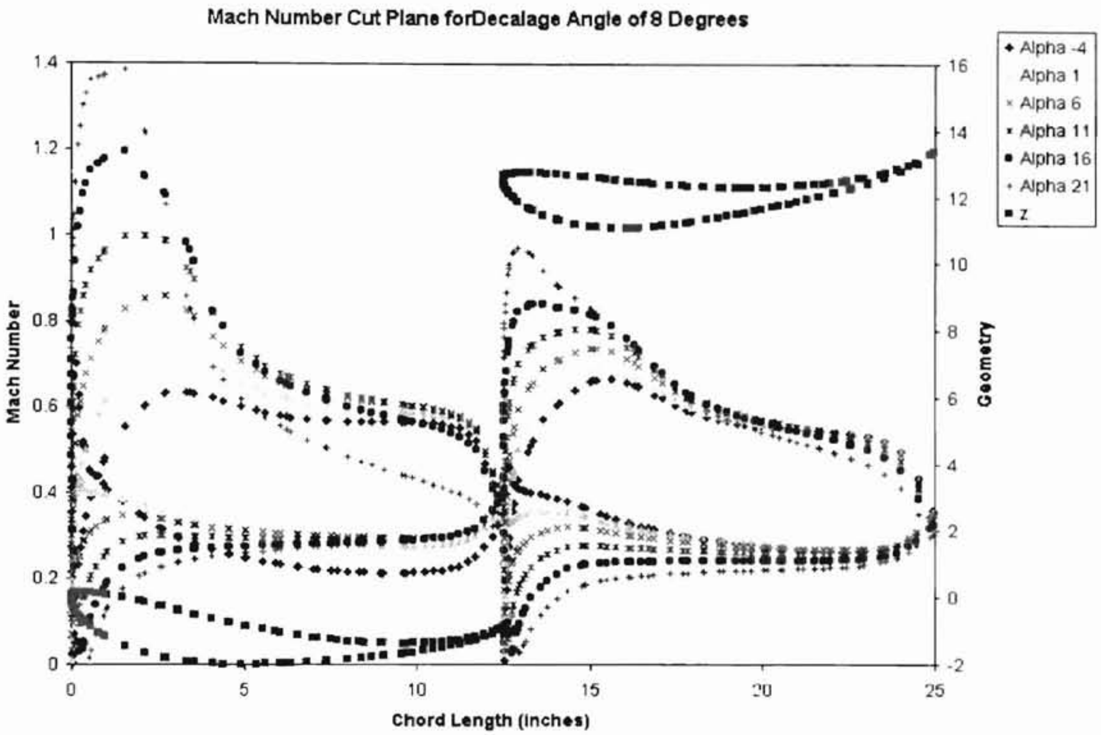

Figure 4-33: Mach Numbar Plot for Boxwing at 8 Degree Declage Angle

The 12° decalage angle shown in Figure 4-34 once again looks like that of the pressure plot for the 12° decalage angle as expected. The angles of attack larger than 10° were not run but the patterns can be seen as the Mach distribution evens out even more. More decalage angles could have been run but the idea is not to get this wing to its optimal design but to look at a whole new approach to dragster wings to see if a better performance can be achieved which will be talked about in the next section.

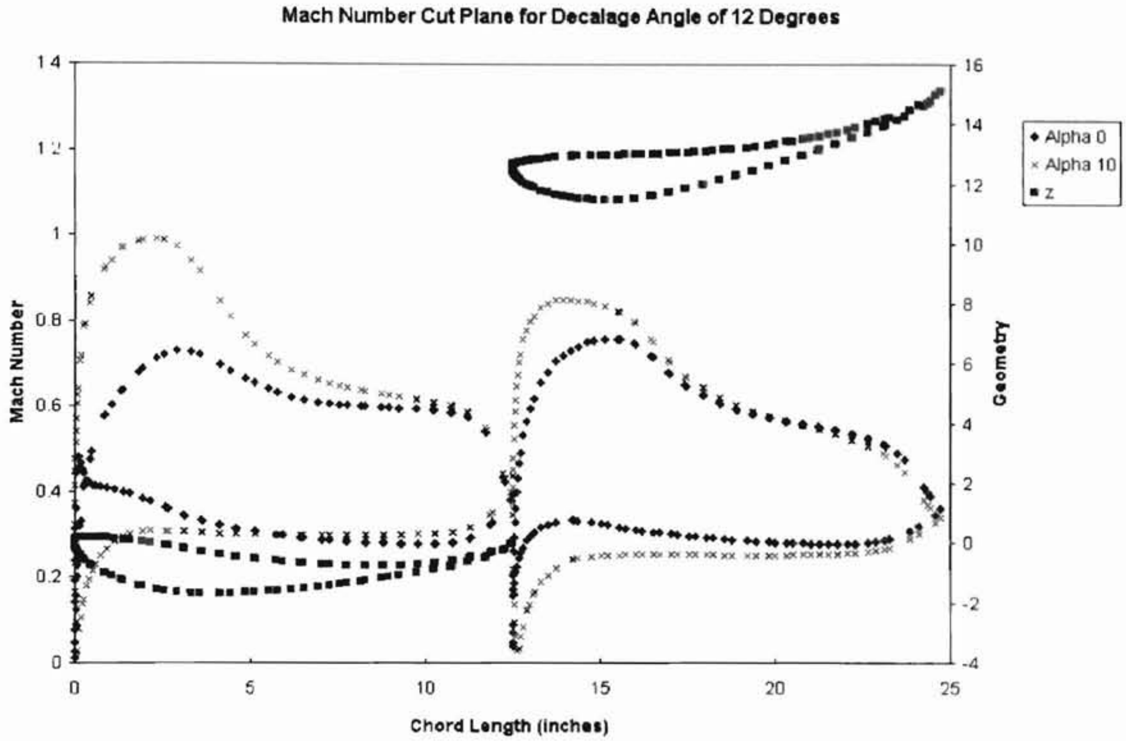

Figure 4-34: Mach Number Plot for Boxwing at 12 Degree Decalage Angle

4.6.2 Boxwing and Three-Element Wing Comparisons

In an attempt to compare these different wing types certain wing performance characteristics were studied and plotted. Some of these include coefficient of lift versus angle of attack, coefficient of drag versus angle of attack, coefficient of lift to coefficient of drag, and coefficient of lift to drag versus angle of attack.

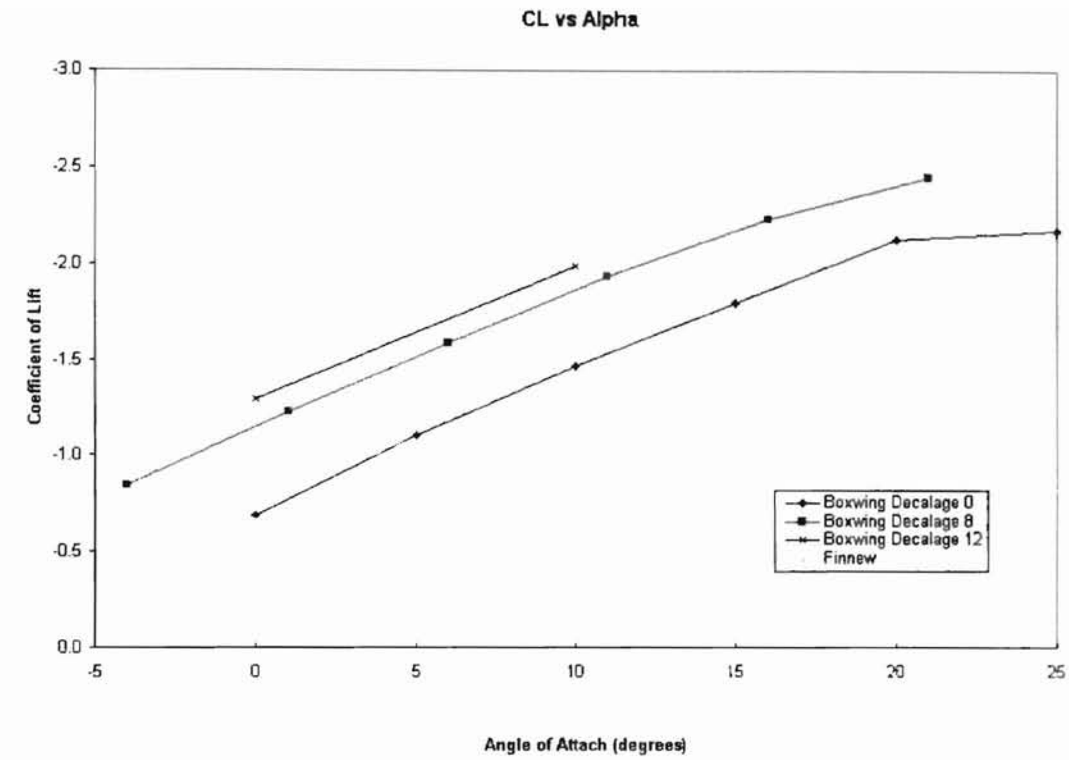

Figure 4-35: Coefficient of Lift vs Angle of Attack

The coefficient of lift versus angle of attack plot in Figure 4-35 shows how the lift coefficient a particular wing has when it is adjusted to a certain angle of attack. It can be seen that the wing labeled finnew, which is the three-element wing at a 0°-28°-65° configuration with the new endplate, has quite a bit higher $C_{L\alpha}$ than the other boxwing designs. The boxwing design with a decalage angle of 12 degrees has the potential of reaching the same coefficient of lift as the finnew wing if the boxwing is set to an overall angle of attack of 20°.

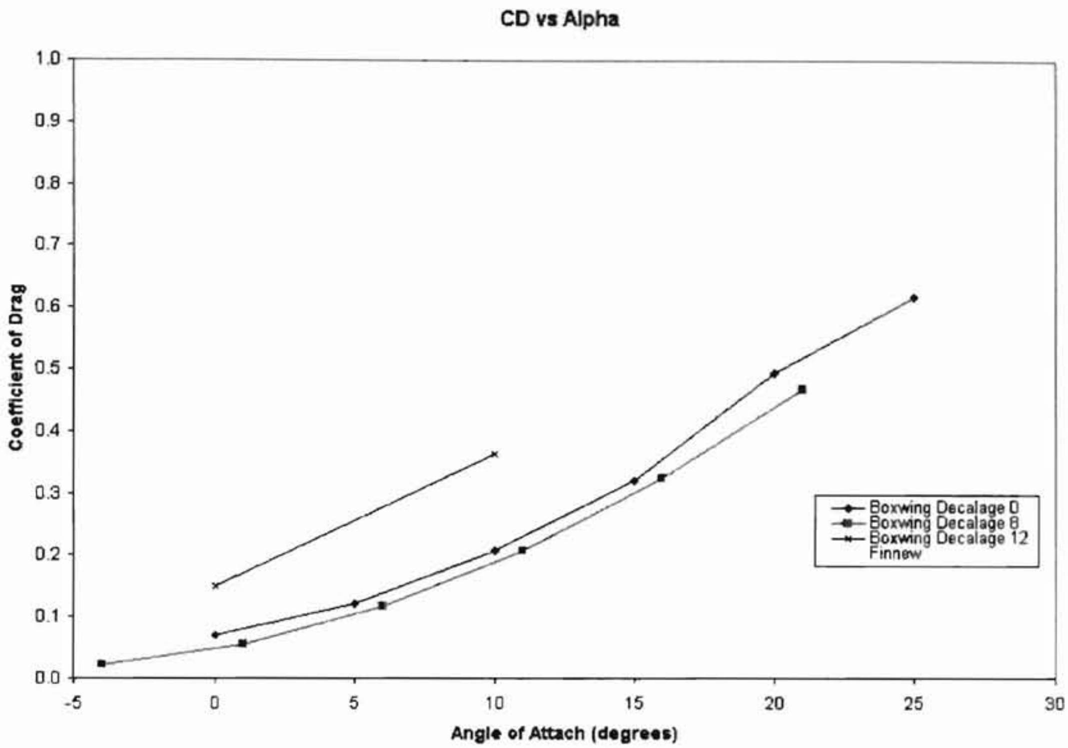

Figure 4-36: Coefficient of Drag vs Angle of Attack

The next plot above, Figure 4-36, is a plot of the coefficient of drag versus angle of attack.

This figure is deceiving at first because it looks like the boxwing design has a lot lower drag coefficient than the three-element design. This is not necessary true because the boxwing at these lower angles of attack does not produce the same lift as the three-element wing at the same angles of attack. It might be better to look at the coefficient of drag to the coefficient of lift to see a better comparison.

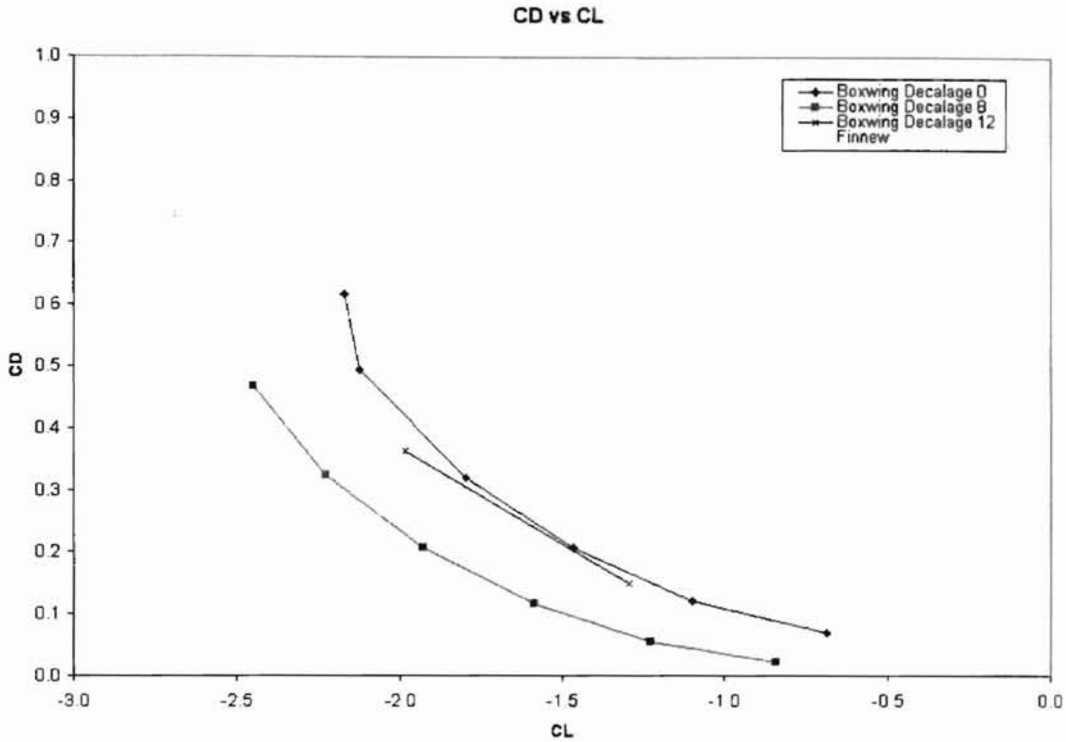

Figure 4-37: Coefficient of Drag vs Coefficient of Lift

Figure 4-37 above represents the coefficient of drag versus the coefficient of lift plot. This allows for the comparison of how efficient the wings can be if you will. This tells us how much lift we can get out of a wing with the punishment of the amount of drag that the wing had by nature.

It is hard to compare the boxwing to the three-element wing in this plot because they do not have the same lift coefficient. Therefore it is better to look at a plot that compares the ratio of the coefficients of lift to drag versus the coefficient of lift. This gives a better comparison of the wings.

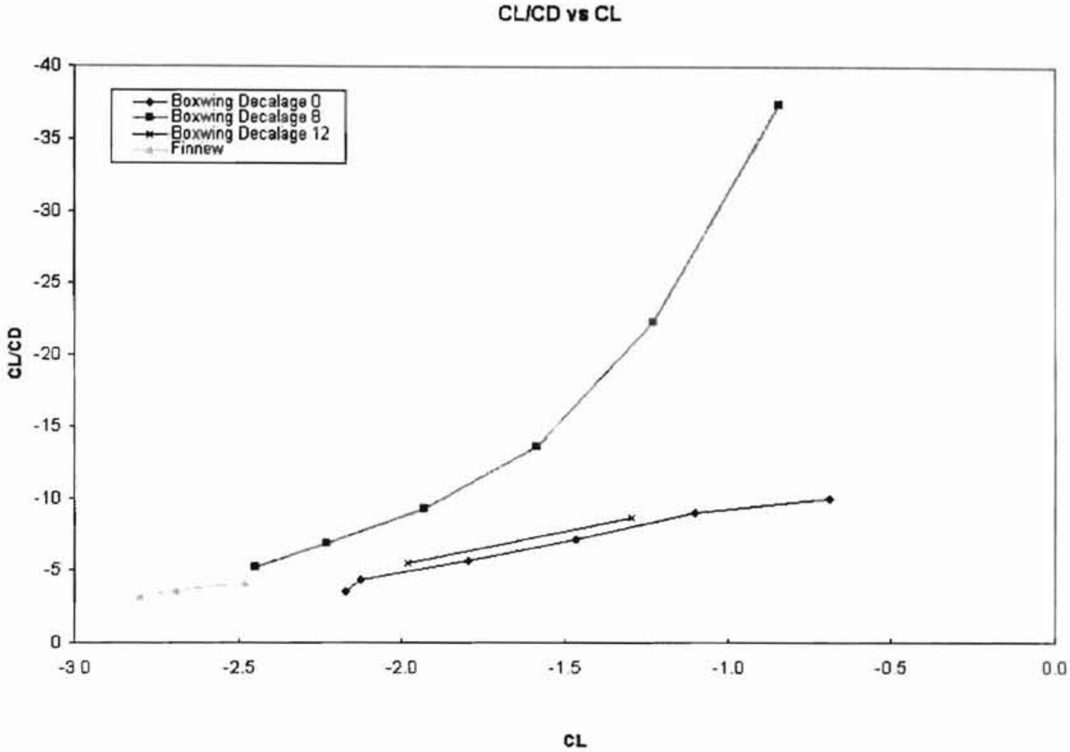

Figure 4-38: Coefficient of Lift to Drag vs Coefficient of Lift

This plot of the coefficients of lift to drag versus the coefficient of lift, shown in Figure 4-38, allows us to see the efficiency of the wings in a way. For a given coefficient of lift that is desired, a wing can be picked based upon its lift to drag ratio. A wing that has a better lift to drag ratio is punished less, in terms of drag, when there is an increase in the amount of lift produced. It is ideal to have a higher lift to drag ratio.

4.7 Dragster Performance Comparisons using the Dynamic Model

This portion of the results is what is the most important. Even though all the previous comparisons on wing performance was done the individual wing characteristics was not what this research was about fully. The true results is how these different wings and how the changes to these wings truly effected the overall performance of the dragster. The improvements to the performance of the individual components is needed but the improvements should not be recognized without knowing how they will improve the performance of the dragster. Large improvements to a component might not necessarily provide large improvements to the performance of the dragster and vise versa.

A true test is to input these component changes into a dynamic model for the dragster and see how they affect the quarter mile time and speed. Since the dragster teams are concerned with the finishing times and top speeds of the dragsters then it is important to be able to give the teams a figure on how certain changes will affect the time and speed of their vehicles.

4.7.1 Performance Data for Various Rear Wings

Wing data from an actual dragster as well as the new boxwing design was used when running the model to determine how the aerodynamic changes would affect the performance. The wings were varied at different angles of attack since most dragster teams tamper with this feature. The data was plotted on the charts that were generated earlier and the results are shown in Figure 4-39.

The figure shows two wings with the first being the finnew design. This is a current wing that is being used on dragsters. It is varied for three different angles of attack from 0° to 10°. As the angle of attack increases so does the elapsed time while the top speed of the vehicle decreases.

The second wing that is analyzed is the boxwing configuration with an 8° decalage angle. This to was varied for several angles of attack. The angles range from -4° to 21° and are in increments of 5°. When the chord of the lower wing is parallel to ground then the angle of attack is set to be at 0°. As the angle of attack is lowered from 21° the elapses time decreases and the top speed increases up until the wing is set to 1°. When the wing is set to a lower angle of attack the performance of elapsed time decreases but the top speed increases.

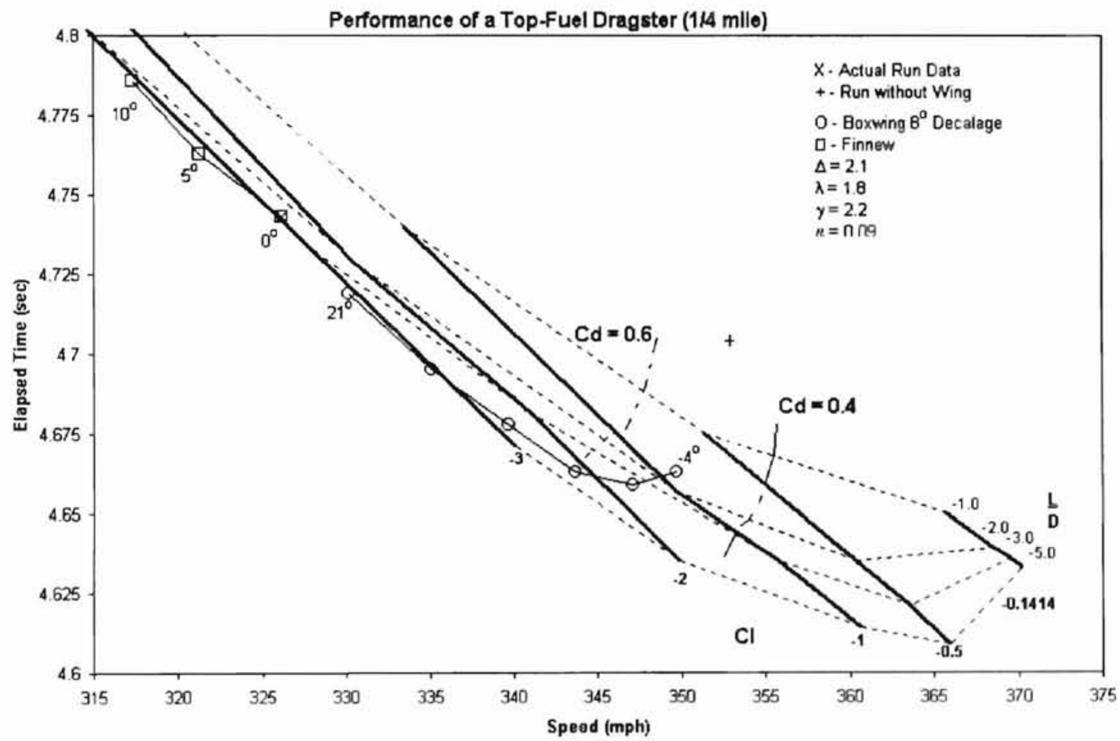

Figure 4-39: Elapsed Time and Speed Data with Different Wing Configurations

The next figure shows how this data affects the elapsed time and the critical speed of the dragster.

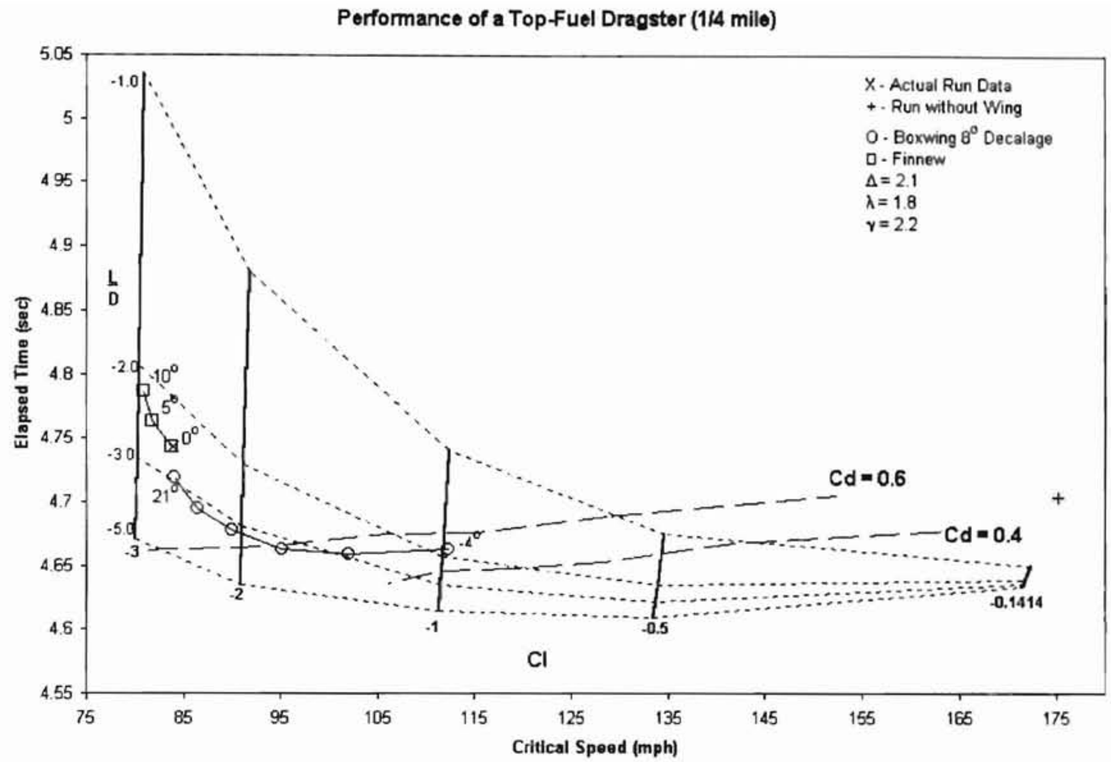

Figure 4-40: Elapsed Time and Speed Data with Different Wing Configurations

4.7.2 Performance Data for Various Input Power Curves

More data was studied looking at how the power input curve distribution effects the performance of the dragster. The wing and car properties were held constant and the input horsepower curve was varied. There are three power curves that were studied as can be seen in Figure 4-41.

The actual power curve depicted on the figure is a curve fit from an actual run of a top-fuel dragster. This is the power curve used as an input to the model to generate all the other model data. Two other power curves were generated to look at how and in what way would the horsepower curve effect the performance of the dragster.

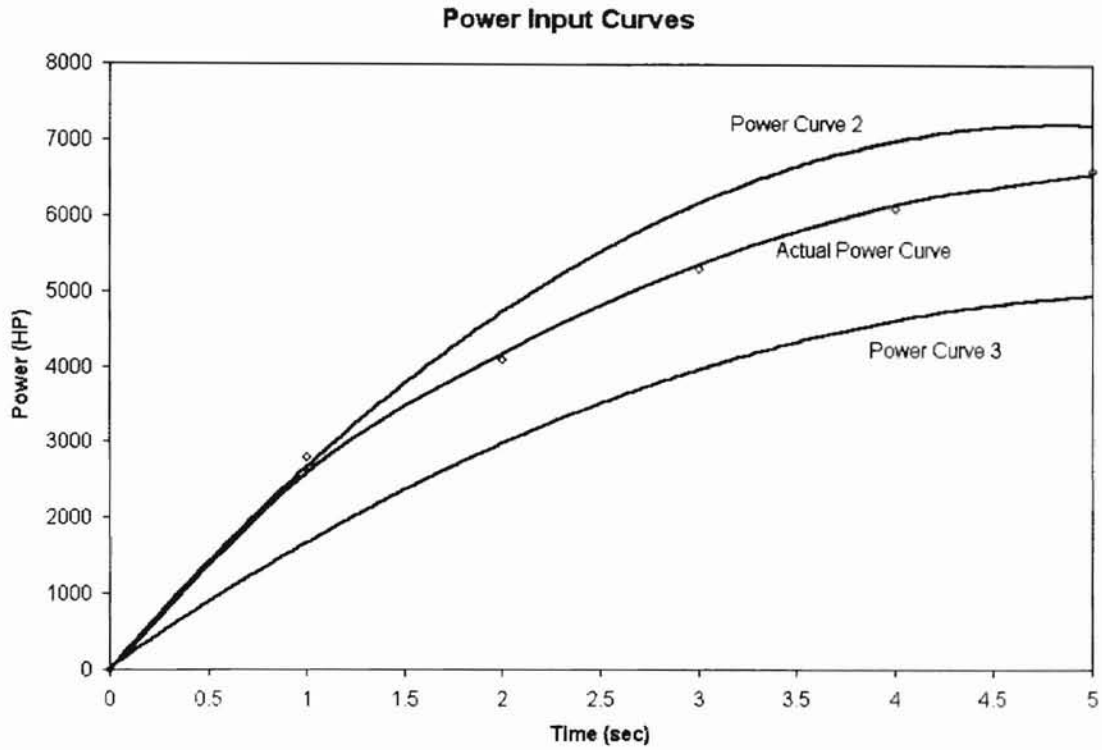

Figure 4-41: Model Power Input Curves to look at Horsepower Effects

This data was used for certain coefficients of lift and a constant drag coefficient of 1.0 to generate Figure 4-42, below. As can be seen the actual power curve is in the middle of the figure. When a lower power curve is used, simulating a dragster that has a reduced amount of power or maybe a slower start than usual, depicted by power curve three in Figure 4-41, the elapsed times increase and the top speed decrease considerably. For this power curve data the coefficients of lift can be looked at in more detail. For a higher lift coefficient like -3 the elapsed time is higher than that with a lower coefficient of lift such as -0.5. This is a different trend for larger power curves where the elapsed time improves as the coefficient of lift is increased as can be seen for the actual power curve as well as power curve two.

Power curve two as seen in Figure 4-41 increases the top speed and decreases the elapsed time of the dragster. The power curve has a higher horsepower curve than that of the actual power curve. There is an improvement in the performance of the dragster. Even having this higher power curve with a coefficient of lift of -0.5 compared to the actual power curve with a higher coefficient of lift, such as -3, produces a lower elapsed time.

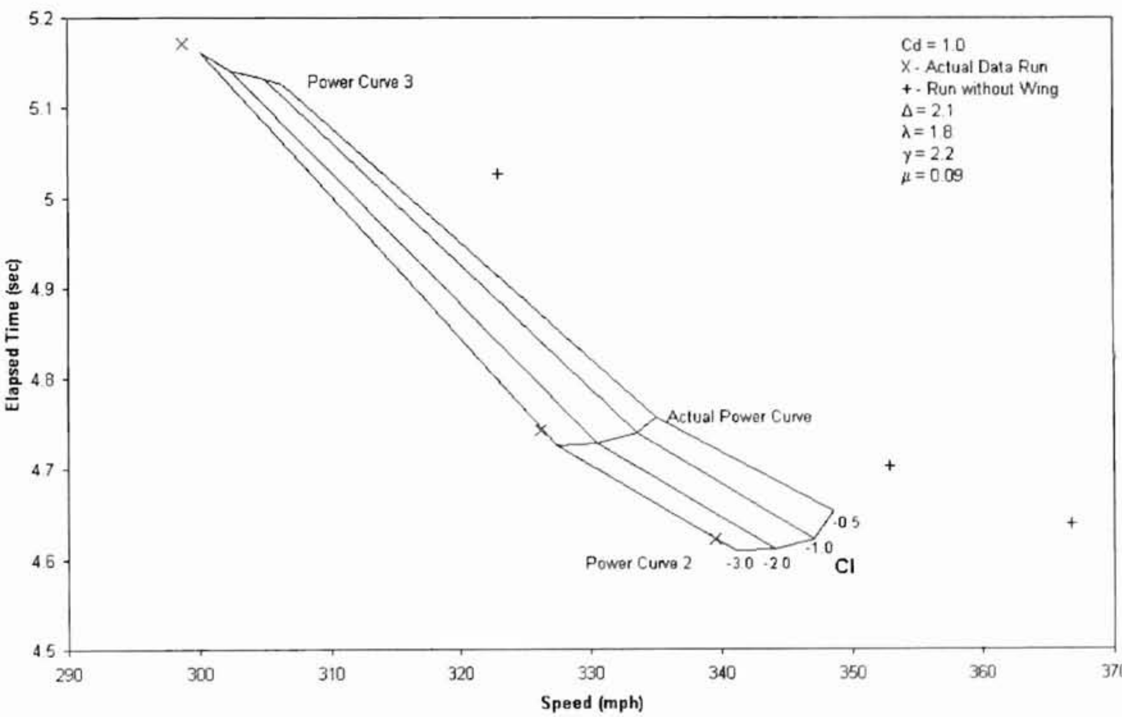

Figure 4-42: Power Curve Input Effects on Elapsed Time and Top Speed

This tells us that more power is important when it can be generated but whether more that power curve two is better has not been studied. Lower power curves, such as power curve three, start to show that if the dragster has a reduction in power that it is better to have a lower lift coefficient. These three power curves were the only ones studied but a lot can be learned from them as far as performance effects are concerned.

What also should be noted in Figure 4-42 is the performance effects of the dragsters with and without the rear wing. The dragsters with the wings are represented by the "X" marks in the figure and the dragster without the wing is represented by the "+" marks. For the lower power curves the dragster without the wing out performs the dragster with the rear wing. For a dragster with greater power as in the actual power curve data, the dragster without the rear wing still has an advantage, elapsed time wise, over the dragster with the wing. When the highest power curve is looked at, power curve 2, the dragster with the wing has a lower elapsed time that the dragster without a rear wing.

This tells us that for lower powered dragsters, keeping all other parameters the same, it is better to take the rear wing off. If a dragster were to increase the power used today then the team would be more advantageous to put the wing on if having a rear wing or not were their only choices. I do want to reinstate the fact that these are not the only choices. As was shown previously, for the current dragsters today, using a lower drag wing with higher lift to drag ratios is better than no wing but using no rear wing right now is better that using the wings that the dragsters are currently using.

CHAPTER 5

5. CONCLUSIONS AND RECOMMENDATIONS

5.1 Conclusions

By modeling the performance of a dragster and looking at the effects that aerodynamics has of the performance of a dragster has proven very beneficial. It gives us an insight into the questions of how much down force is needed and how changing these aerodynamic characteristics will truly effect the performance of the dragster. It was always said that these dragsters want as much down force as possible but from this model it is not necessarily true. What was shown to be the most beneficial is the reduction of the drag and the reduction of the coefficient of lift up to a certain point. The improvement to the lift to drag ratio is important as well and was the case for the new endplate design.

5.1.1 Dynamic Dragster Model

The dragster model matched actual top-fuel dragster data very well. It functioned in a manner that allowed me to show how each of the aerodynamic parameters, lift and drag, affect the performance of the dragster. It led to the study of improving wind design by improving the current wing and also led to the knowledge of how a different style of wing might improve the performance even better.

5.1.2 Endplate Effects on a Top-Fuel Dragster Rear Wing

The study of endplate effects on top-fuel dragster wings proved to be beneficial in understanding how and to what extent an endplate has on the flow over a wing. The results presented led to vast improvements in rear wing design and helped two different top-fuel dragsters prevail on top of two different world records.

The addition of the new endplate improved the effectiveness of the wing. It allowed for a more uniform load distribution over the entire span of the wing. This in turn produced a greater down force and since it reduced the amount of spillover, or disruptive flow to the suction side, it reduced the amount of induced drag. With the new endplate design there was an increase of almost 7.2%, over the wing with the style 3 endplate, in terms of the ratio of down force to drag.

It should be noted that this solution does not take into consideration compressibility effects and since there is not any experimental data to compare it to the percent error cannot be provided.

5.1.3 Boxwing Design

The boxwing design compared to the currently used dragster wings showed much improvement to the overall performance of the dragster. The model was able to show how the lift and drag effected the performance of the dragster and this provided the insight as to what characteristics were needed for the new dragster rear wing. With this wing we were able to get to a lower elapsed time and a higher top speed.

This was done to reduce the drag since it takes so much horsepower to drag the currently used dragster rear wings through the air. By reducing the induced drag of the wing we were able to shift the horsepower that was saved into accelerating the car. This amounted to quicker elapsed times and faster speeds which was one of the motives behind this research.

5.2 Recommendations

Improvement to this research can be made in a number of ways. Recommendations will be made starting with modeling of the dragster and going thru to each of the parts of this project all the way to the boxwing design.

5.2.1 Dynamic Dragster Model

Although the dragster model worked well in showing the trends of the aerodynamic affects on performance it did not have some features that might be very beneficial to dragster teams. Many of the parameters for this program were not actual parameters but estimated parameters because this information was hard to get. Future work might include collecting data from actual runs that will show how close the estimations were to the actual parameters. The parameters did give accurate enough results to enable me to match actual run data that was shown in the validation section.

Other recommendations might be to add other features to the program that might enable a dragster team to get the dragster ready for a particular track and weather conditions. Such features could include track conditions as far as where the track is slippery or any conditions that a dragster team might look for when setting up the dragster. A feature that might be nice is adding a clutch that you can set up to shift for given parameters.

5.2.2 Endplate Design Improvements

Although improvements to the wing characteristics were made by changing the endplate geometry there can still be some changes made to further optimize the design. The shape of the wing was not truly optimized but merely a change in design of the endplate was chosen that would see the extent of the improvement that such a change could make. Further design could be done to improve upon this endplate so as to truly optimize it for design.

Another consideration would be to consider the cost of the wing and try to make changes that could not only improve the design but also reduce the cost of the wing itself. Since the wings are made of carbon fiber the cost can be expensive to produce. Improvements in design could reduce the amount of material used and therefore reduce the cost.

Further, structural analysis could be done using a finite element code, such as STARS, to look at the strength of the various parts of the wing. The inner workings of the wing as well as the attaching mechanism should be studied to see if modification could be done to reduce weigh.

5.2.3 Boxwing Design

The boxwing design showed to reduce the elapsed time of the dragster as well as increase the top speed when compared to a wing that is currently being used on several top-fuel dragsters. This wing was in no way optimized to its full potential. There are many parameters that can be looked at such as the decalage angle as well as the endplate design used and looking into the structural and support of the wing could also be studied.

The decalage angles of 0°, 8° and 12° were studied and analyzed. Refining these angles would more than likely show better performance characteristics could be achieved. Having this range allowed me to see how this parameter affected this wing performance but not a lot of time was spent on getting the best decalage angle.

5.2.4 Stability of the Dragster

It is good to note that before the implementation of this new dragster wing that careful analysis be done on the stability of the dragsters. Since these wings have less drag and they allow the dragsters to function at higher speeds they should be once again analyzed to make sure that they are still safe.

BIBLIOGRAPHY

Arena, A.S. Jr. (1998-2000). Associate Professor, Oklahoma State University. Personal Communications.

Cogotti, A., "Aerodynamic Characteristics of Car Wheels," *International Journal of Vehicle Design*, Technological Advances in Vehicle Design Series, SP3, Impact of Aerodynamics on Vehicle Design, pp. 173-196, 1983.

Gupta, K.K., "STARS-An Integrated, Multidisciplinary, Finite-Element, Structural, Fluids, Aeroelastic, and Aeroservoelastic Analysis Computer Program", NASA Technical Memorandum 4795, 1997.

Hallum, C., "The Magic of the Drag Tire", Society of Automotive Engineers Inc. Paper No. 942484, 1994.

Hawks, R.J. and C.L. Sayre, "Aerodynamics and Automobile Performance," *Advances in Road Vehicle Aerodynamics 1973*, pp. 1-13, BHRA Fluid Engineering (1973).

Katz, J., *Race Car Aerodynamics: Designing for Speed*, Robert Bentley Publishers, 1995.

Milliken, W.F. and D.L. Milliken, *Race Car Vehicle Dynamics*, Society of Automotive Engineers International, 1995.

Munson, B.R., Young, D.F., and T.H. Okiishi, *Fundamentals of Fluid Mechanics*, 2nd Edition, John Wiley and Sons Inc., 1994.

Raymer, D.P., *Aircraft Design: A Conceptual Approach*, 2nd Edition, American Institute of Aeronautics and Astronautics, 1992.

Selig, M., Airfoil data for Selig 1223, University of Illinois, Urbana, Illinois, July 14, 1995.

Smith, A.M.O., "High Lift Aerodynamics," *Journal of Aircraft*, Volume 12, Number 6, 1975, pp. 501-530.

Stapleford, W.R. and G.W. Carr, "Aerodynamic Characteristics of Exposed Rotating Wheels", MIRA Report No. 1970/2, 1969.

Stephens, C.H., "CFD-Based Aeroservoelastic Predictions on a Benchmark Configuration using the Transpiration Method", *Masters Thesis*, Oklahoma State University, July 1998.

Winn, R.C., Kohlman, D.L., and Kenner, M.T., "Optimal Wing Design for Top-Fuel Dragsters", American Institute of Aeronautics and Astronautics, Paper No. 99-0464, 1999.

2000 NHRA Rulebook, National Hot Rod Association, 1999.

APPENDICES

APPENDIX A-1

STARS-CFD Geometry Data File (*fin.sur*)

```
1  Geometry definition...fin
26  12
Curves
1  1
21
-123.0000  0.000  0.000
-121.7700  0.000  24.5680
-116.8500  0.000  54.6612
-107.0100  0.000  87.2439
-89.7900  0.000  123.4354
-68.8800  0.000  153.9419
-39.3600  0.000  184.8124
-7.3800  0.000  208.6080
29.5200  0.000  227.5475
71.3400  0.000  240.5142
123.0000  0.000  246.0000
174.6600  0.000  240.5142
216.4800  0.000  227.5475
253.3800  0.000  208.6080
285.3600  0.000  184.8124
314.8800  0.000  153.9419
335.7900  0.000  123.4354
353.0100  0.000  87.2439
362.8500  0.000  54.6612
367.7700  0.000  24.5680
369.0000  0.000  0.000
2  1
21
-123.00000  0.000  0.000
-121.77000  0.000  -24.56802
-116.85000  0.000  -54.66120
-107.01000  0.000  -87.24390
-89.79000  0.000  -123.43542
-68.88000  0.000  -153.94188
-39.36000  0.000  -184.81242
-7.38000  0.000  -208.60800
29.52000  0.000  -227.54754
71.34000  0.000  -240.51420
123.00000  0.000  -246.0000
174.66000  0.000  -240.5142
216.4800  0.000  -227.54754
253.3800  0.000  -208.6080
285.3600  0.000  -184.81242
314.8800  0.000  -153.94188
335.7900  0.000  -123.43542
353.0100  0.000  -87.24390
362.8500  0.000  -54.66120
367.7700  0.000  -24.56802
369.0000  0.000  0.000
3  1
36
0.000  0.000  0.000
0.0355  0.000  0.1008
0.0500  0.000  0.1280
0.1250  0.000  0.2295
0.1875  0.000  0.2700
0.3438  0.000  0.3338
0.5000  0.000  0.3677
0.7500  0.000  0.3750
1.0000  0.000  0.3969
1.5000  0.000  0.4207
2.0000  0.000  0.4431
2.5000  0.000  0.4654
3.0000  0.000  0.4892
3.5000  0.000  0.5135
4.0000  0.000  0.5392
4.5000  0.000  0.5639
5.0000  0.000  0.5880
5.5000  0.000  0.6091
6.0000  0.000  0.6275
6.5000  0.000  0.6417
7.0000  0.000  0.6471
7.5000  0.000  0.6386
8.0000  0.000  0.6120
8.5000  0.000  0.5693
9.0000  0.000  0.5103
9.5000  0.000  0.4324
10.000  0.000  0.3359
10.5000  0.000  0.2299
11.0000  0.000  0.1166
11.5000  0.000  0.000
12.0000  0.000  -0.0946
12.5000  0.000  -0.1530
13.0000  0.000  -0.1589
13.5000  0.000  -0.1024
14.0000  0.000  0.0251
14.1000  0.000  0.000
4  1
36
0.000  0.000  0.000
0.0355  0.000  -0.1650
0.0500  0.000  -0.2000
0.1250  0.000  -0.3438
0.1875  0.000  -0.4375
0.3438  0.000  -0.6560
0.5000  0.000  -0.8073
0.7500  0.000  -1.0500
1.0000  0.000  -1.2280
1.5000  0.000  -1.5251
2.0000  0.000  -1.7441
2.5000  0.000  -1.9078
3.0000  0.000  -2.0330
3.5000  0.000  -2.1265
4.0000  0.000  -2.1939
4.5000  0.000  -2.2383
5.0000  0.000  -2.2599
5.5000  0.000  -2.2648
6.0000  0.000  -2.2554
6.5000  0.000  -2.2329

7.0000  0.000  -2.1972
7.5000  0.000  -2.1456
8.0000  0.000  -2.0793
8.5000  0.000  -1.9994
9.0000  0.000  -1.9026
9.5000  0.000  -1.7891
10.000  0.000  -1.6611
10.5000  0.000  -1.5153
11.0000  0.000  -1.3543
11.5000  0.000  -1.1782
12.0000  0.000  -0.9868
12.5000  0.000  -0.7811
13.0000  0.000  -0.5588
13.5000  0.000  -0.3248
14.0000  0.000  -0.0699
14.1000  0.000  0.000
5  1
54
13.5405  0.000  0.7448
13.5428  0.000  0.7860
13.5549  0.000  0.8269
13.5766  0.000  0.8673
```

13.6076 0.000 0.9073
13.6475 0.000 0.9468
13.6960 0.000 0.9859
13.7525 0.000 1.0247
13.8167 0.000 1.0631
13.8880 0.000 1.1013
13.9660 0.000 1.1393
14.0503 0.000 1.1774
14.1403 0.000 1.2155
14.2355 0.000 1.2540
14.3354 0.000 1.2930
14.4398 0.000 1.3326
14.5480 0.000 1.3732
14.6598 0.000 1.4149
14.7746 0.000 1.4581
14.8923 0.000 1.5031
15.0123 0.000 1.5501
15.1343 0.000 1.5994
15.2581 0.000 1.6513
15.3861 0.000 1.7078
15.5197 0.000 1.7688
15.6547 0.000 1.8309
15.7906 0.000 1.8938
15.9269 0.000 1.9577
16.0631 0.000 2.0225
16.1987 0.000 2.0880
16.3332 0.000 2.1541
16.4662 0.000 2.2207
16.5971 0.000 2.2876
16.7255 0.000 2.3545
16.8509 0.000 2.4211
16.9729 0.000 2.4872
17.0911 0.000 2.5524
17.2050 0.000 2.6165
17.3142 0.000 2.6790
17.4184 0.000 2.7397
17.5171 0.000 2.7980
17.6101 0.000 2.8538
17.6970 0.000 2.9066
17.7774 0.000 2.9561
17.8512 0.000 3.0020
17.9179 0.000 3.0439
17.9774 0.000 3.0816
18.0295 0.000 3.1148
18.0739 0.000 3.1433
18.1104 0.000 3.1669
18.1390 0.000 3.1854
18.1595 0.000 3.1988
18.1719 0.000 3.2068
18.1760 0.000 3.2095
6 1
54
13.5405 0.000 0.7448
13.5483 0.000 0.7041
13.5664 0.000 0.6653
13.5948 0.000 0.6285
13.6336 0.000 0.5938
13.6826 0.000 0.5617
13.7418 0.000 0.5324
13.8110 0.000 0.5064
13.8898 0.000 0.4841
13.9779 0.000 0.4660
14.0748 0.000 0.4527
14.1800 0.000 0.4447
14.2930 0.000 0.4425
14.4130 0.000 0.4465
14.5394 0.000 0.4574
14.6714 0.000 0.4754
14.8081 0.000 0.5010
14.9486 0.000 0.5345
15.0921 0.000 0.5760
15.2376 0.000 0.6258
15.3843 0.000 0.6838
15.5312 0.000 0.7499
15.6774 0.000 0.8241
15.8192 0.000 0.9045
15.9552 0.000 0.9887
16.0900 0.000 1.0773
16.2233 0.000 1.1698
16.3544 0.000 1.2657
16.4830 0.000 1.3645
16.6087 0.000 1.4658
16.7310 0.000 1.5689
16.8496 0.000 1.6733
16.9643 0.000 1.7785
17.0747 0.000 1.8838
17.1805 0.000 1.9888
17.2816 0.000 2.0927
17.3777 0.000 2.1952
17.4687 0.000 2.2955
17.5544 0.000 2.3931
17.6348 0.000 2.4874
17.7097 0.000 2.5780
17.7790 0.000 2.6643
17.8428 0.000 2.7458
17.9009 0.000 2.8220
17.9535 0.000 2.8924
18.0004 0.000 2.9567
18.0417 0.000 3.0144
18.0775 0.000 3.0651
18.1076 0.000 3.1086
18.1323 0.000 3.1446
18.1514 0.000 3.1729
18.1651 0.000 3.1932
18.1733 0.000 3.2054
18.1760 0.000 3.2095
7 1
54
17.8359 0.000 3.4397
17.8074 0.000 3.4697
17.7857 0.000 3.5061
17.7707 0.000 3.5487
17.7621 0.000 3.5973
17.7599 0.000 3.6518
17.7637 0.000 3.7119
17.7734 0.000 3.7774
17.7886 0.000 3.8479
17.8091 0.000 3.9234
17.8346 0.000 4.0035
17.8647 0.000 4.0882
17.8992 0.000 4.1770
17.9376 0.000 4.2700
17.9797 0.000 4.3670
18.0250 0.000 4.4677
18.0732 0.000 4.5722
18.1239 0.000 4.6802
18.1766 0.000 4.7918
18.2314 0.000 4.9077
18.2905 0.000 5.0334
18.3530 0.000 5.1628
18.4185 0.000 5.2941
18.4864 0.000 5.4270
18.5565 0.000 5.5611
18.6283 0.000 5.6960
18.7015 0.000 5.8314
18.7757 0.000 5.9669
18.8505 0.000 6.1020
18.9255 0.000 6.2363
19.0004 0.000 6.3694
19.0748 0.000 6.5010
19.1485 0.000 6.6305
19.2209 0.000 6.7576
19.2920 0.000 6.8818
19.3613 0.000 7.0027
19.4286 0.000 7.1198
19.4936 0.000 7.2328
19.5561 0.000 7.3412
19.6159 0.000 7.4447
19.6726 0.000 7.5428
19.7262 0.000 7.6353
19.7763 0.000 7.7217
19.8228 0.000 7.8017
19.8655 0.000 7.8750
19.9042 0.000 7.9414
19.9388 0.000 8.0005
19.9691 0.000 8.0523
19.9950 0.000 8.0964
20.0163 0.000 8.1328
20.0330 0.000 8.1612
20.0450 0.000 8.1815
20.0522 0.000 8.1938
20.0546 0.000 8.1979
8 1
54
17.8359 0.000 3.4397
17.8704 0.000 3.4171
17.9104 0.000 3.4027
17.9558 0.000 3.3966
18.0063 0.000 3.3991
18.0619 0.000 3.4102
18.1221 0.000 3.4302
18.1867 0.000 3.4592
18.2551 0.000 3.4973
18.3268 0.000 3.5445
18.4013 0.000 3.6010
18.4780 0.000 3.6668
18.5561 0.000 3.7417

18.6349 0.000 3.8258
18.7138 0.000 3.9188
18.7921 0.000 4.0205
18.8690 0.000 4.1306
18.9439 0.000 4.2487
19.0161 0.000 4.3744
19.0846 0.000 4.5065
19.1466 0.000 4.6385
19.2062 0.000 4.7740
19.2642 0.000 4.9135
19.3204 0.000 5.0564
19.3747 0.000 5.2022
19.4270 0.000 5.3503
19.4772 0.000 5.5001
19.5253 0.000 5.6509
19.5712 0.000 5.8023
19.6149 0.000 5.9535
19.6564 0.000 6.1040
19.6956 0.000 6.2531
19.7325 0.000 6.4004
19.7671 0.000 6.5452
19.7995 0.000 6.6870
19.8296 0.000 6.8252
19.8576 0.000 6.9592
19.8833 0.000 7.0887
19.9069 0.000 7.2130
19.9284 0.000 7.3317
19.9479 0.000 7.4443
19.9654 0.000 7.5505
19.9811 0.000 7.6497
19.9950 0.000 7.7417
20.0072 0.000 7.8261
20.0178 0.000 7.9024
20.0269 0.000 7.9705
20.0345 0.000 8.0301
20.0408 0.000 8.0809
20.0459 0.000 8.1228
20.0497 0.000 8.1555
20.0524 0.000 8.1790
20.0541 0.000 8.1931
20.0546 0.000 8.1979
9 1
36
0.000 29.7500 0.000
0.0355 29.7500 0.1008
0.0500 29.7500 0.1280
0.1250 29.7500 0.2295
0.1875 29.7500 0.2700
0.3438 29.7500 0.3338
0.5000 29.7500 0.3677
0.7500 29.7500 0.3750
1.0000 29.7500 0.3969
1.5000 29.7500 0.4207
2.0000 29.7500 0.4431
2.5000 29.7500 0.4654
3.0000 29.7500 0.4892
3.5000 29.7500 0.5135
4.0000 29.7500 0.5392
4.5000 29.7500 0.5639
5.0000 29.7500 0.5880
5.5000 29.7500 0.6091
6.0000 29.7500 0.6275
6.5000 29.7500 0.6417
7.0000 29.7500 0.6471
7.5000 29.7500 0.6386
8.0000 29.7500 0.6120
8.5000 29.7500 0.5693
9.0000 29.7500 0.5103
9.5000 29.7500 0.4324
10.000 29.7500 0.3359
10.5000 29.7500 0.2299
11.0000 29.7500 0.1166
11.5000 29.7500 0.000
12.0000 29.7500 -0.0946
12.5000 29.7500 -0.1530
13.0000 29.7500 -0.1589
13.5000 29.7500 -0.1024
14.0000 29.7500 0.0251
14.1000 29.7500 0.000
10 1
36
0.000 29.7500 0.000
0.0355 29.7500 -0.1650
0.0500 29.7500 -0.2000
0.1250 29.7500 -0.3438
0.1875 29.7500 -0.4375
0.3438 29.7500 -0.6560
0.5000 29.7500 -0.8073
0.7500 29.7500 -1.0500
1.0000 29.7500 -1.2280
1.5000 29.7500 -1.5251
2.0000 29.7500 -1.7441
2.5000 29.7500 -1.9078
3.0000 29.7500 -2.0330
3.5000 29.7500 -2.1265
4.0000 29.7500 -2.1939
4.5000 29.7500 -2.2383
5.0000 29.7500 -2.2599
5.5000 29.7500 -2.2648
6.0000 29.7500 -2.2554
6.5000 29.7500 -2.2329
7.0000 29.7500 -2.1972
7.5000 29.7500 -2.1456
8.0000 29.7500 -2.0793
8.5000 29.7500 -1.9994
9.0000 29.7500 -1.9026
9.5000 29.7500 -1.7891
10.000 29.7500 -1.6611
10.5000 29.7500 -1.5153
11.0000 29.7500 -1.3543
11.5000 29.7500 -1.1782
12.0000 29.7500 -0.9868
12.5000 29.7500 -0.7811
13.0000 29.7500 -0.5588
13.5000 29.7500 -0.3248
14.0000 29.7500 -0.0699
14.1000 29.7500 0.000
11 1
54
13.5405 29.7500 0.7448
13.5428 29.7500 0.7860
13.5549 29.7500 0.8269
13.5766 29.7500 0.8673
13.6076 29.7500 0.9073
13.6475 29.7500 0.9468
13.6960 29.7500 0.9859
13.7525 29.7500 1.0247
13.8167 29.7500 1.0631
13.8880 29.7500 1.1013
13.9660 29.7500 1.1393
14.0503 29.7500 1.1774
14.1403 29.7500 1.2155
14.2355 29.7500 1.2540
14.3354 29.7500 1.2930
14.4398 29.7500 1.3326
14.5480 29.7500 1.3732
14.6598 29.7500 1.4149
14.7746 29.7500 1.4581
14.8923 29.7500 1.5031
15.0123 29.7500 1.5501
15.1343 29.7500 1.5994
15.2581 29.7500 1.6513
15.3861 29.7500 1.7078
15.5197 29.7500 1.7688
15.6547 29.7500 1.8309
15.7906 29.7500 1.8938
15.9269 29.7500 1.9577
16.0631 29.7500 2.0225
16.1987 29.7500 2.0880
16.3332 29.7500 2.1541
16.4662 29.7500 2.2207
16.5971 29.7500 2.2876
16.7255 29.7500 2.3545
16.8509 29.7500 2.4211
16.9729 29.7500 2.4872
17.0911 29.7500 2.5524
17.2050 29.7500 2.6165
17.3142 29.7500 2.6790
17.4184 29.7500 2.7397
17.5171 29.7500 2.7980
17.6101 29.7500 2.8538
17.6970 29.7500 2.9066
17.7774 29.7500 2.9561
17.8512 29.7500 3.0020
17.9179 29.7500 3.0439
17.9774 29.7500 3.0816
18.0295 29.7500 3.1148
18.0739 29.7500 3.1433
18.1104 29.7500 3.1669
18.1390 29.7500 3.1854
18.1595 29.7500 3.1988
18.1719 29.7500 3.2068
18.1760 29.7500 3.2095
12 1
54
13.5405 29.7500 0.7448
13.5483 29.7500 0.7041

13.5664 29.7500 0.6653
13.5948 29.7500 0.6285
13.6336 29.7500 0.5938
13.6826 29.7500 0.5617
13.7418 29.7500 0.5324
13.8110 29.7500 0.5064
13.8898 29.7500 0.4841
13.9779 29.7500 0.4660
14.0748 29.7500 0.4527
14.1800 29.7500 0.4447
14.2930 29.7500 0.4425
14.4130 29.7500 0.4465
14.5394 29.7500 0.4574
14.6714 29.7500 0.4754
14.8081 29.7500 0.5010
14.9486 29.7500 0.5345
15.0921 29.7500 0.5760
15.2376 29.7500 0.6258
15.3843 29.7500 0.6838
15.5312 29.7500 0.7499
15.6774 29.7500 0.8241
15.8192 29.7500 0.9045
15.9552 29.7500 0.9887
16.0900 29.7500 1.0773
16.2233 29.7500 1.1698
16.3544 29.7500 1.2657
16.4830 29.7500 1.3645
16.6087 29.7500 1.4658
16.7310 29.7500 1.5689
16.8496 29.7500 1.6733
16.9643 29.7500 1.7785
17.0747 29.7500 1.8838
17.1805 29.7500 1.9888
17.2816 29.7500 2.0927
17.3777 29.7500 2.1952
17.4687 29.7500 2.2955
17.5544 29.7500 2.3931
17.6348 29.7500 2.4874
17.7097 29.7500 2.5780
17.7790 29.7500 2.6643
17.8428 29.7500 2.7458
17.9009 29.7500 2.8220
17.9535 29.7500 2.8924
18.0004 29.7500 2.9567
18.0417 29.7500 3.0144
18.0775 29.7500 3.0651
18.1076 29.7500 3.1086
18.1323 29.7500 3.1446
18.1514 29.7500 3.1729
18.1651 29.7500 3.1932
18.1733 29.7500 3.2054
18.1760 29.7500 3.2095
13 1
54
17.8359 29.7500 3.4397
17.8074 29.7500 3.4697
17.7857 29.7500 3.5061
17.7707 29.7500 3.5487
17.7621 29.7500 3.5973
17.7599 29.7500 3.6518
17.7637 29.7500 3.7119
17.7734 29.7500 3.7774
17.7886 29.7500 3.8479
17.8091 29.7500 3.9234
17.8346 29.7500 4.0035
17.8647 29.7500 4.0882
17.8992 29.7500 4.1770
17.9376 29.7500 4.2700
17.9797 29.7500 4.3670
18.0250 29.7500 4.4677
18.0732 29.7500 4.5722
18.1239 29.7500 4.6802
18.1766 29.7500 4.7918
18.2314 29.7500 4.9077
18.2905 29.7500 5.0334
18.3530 29.7500 5.1628
18.4185 29.7500 5.2941
18.4864 29.7500 5.4270
18.5565 29.7500 5.5611
18.6283 29.7500 5.6960
18.7015 29.7500 5.8314
18.7757 29.7500 5.9669
18.8505 29.7500 6.1020
18.9255 29.7500 6.2363
19.0004 29.7500 6.3694
19.0748 29.7500 6.5010
19.1485 29.7500 6.6305
19.2209 29.7500 6.7576
19.2920 29.7500 6.8818
19.3613 29.7500 7.0027
19.4286 29.7500 7.1198
19.4936 29.7500 7.2328
19.5561 29.7500 7.3412
19.6159 29.7500 7.4447
19.6726 29.7500 7.5428
19.7262 29.7500 7.6353
19.7763 29.7500 7.7217
19.8228 29.7500 7.8017
19.8655 29.7500 7.8750
19.9042 29.7500 7.9414
19.9388 29.7500 8.0005
19.9691 29.7500 8.0523
19.9950 29.7500 8.0964
20.0163 29.7500 8.1328
20.0330 29.7500 8.1612
20.0450 29.7500 8.1815
20.0522 29.7500 8.1938
20.0546 29.7500 8.1979
14 1
54
17.8359 29.7500 3.4397
17.8704 29.7500 3.4171
17.9104 29.7500 3.4027
17.9558 29.7500 3.3966
18.0063 29.7500 3.3991
18.0619 29.7500 3.4102
18.1221 29.7500 3.4302
18.1867 29.7500 3.4592
18.2551 29.7500 3.4973
18.3268 29.7500 3.5445
18.4013 29.7500 3.6010
18.4780 29.7500 3.6668
18.5561 29.7500 3.7417
18.6349 29.7500 3.8258
18.7138 29.7500 3.9188
18.7921 29.7500 4.0205
18.8690 29.7500 4.1306
18.9439 29.7500 4.2487
19.0161 29.7500 4.3744
19.0846 29.7500 4.5065
19.1466 29.7500 4.6385
19.2062 29.7500 4.7740
19.2642 29.7500 4.9135
19.3204 29.7500 5.0564
19.3747 29.7500 5.2022
19.4270 29.7500 5.3503
19.4772 29.7500 5.5001
19.5253 29.7500 5.6509
19.5712 29.7500 5.8023
19.6149 29.7500 5.9535
19.6564 29.7500 6.1040
19.6956 29.7500 6.2531
19.7325 29.7500 6.4004
19.7671 29.7500 6.5452
19.7995 29.7500 6.6870
19.8296 29.7500 6.8252
19.8576 29.7500 6.9592
19.8833 29.7500 7.0887
19.9069 29.7500 7.2130
19.9284 29.7500 7.3317
19.9479 29.7500 7.4443
19.9654 29.7500 7.5505
19.9811 29.7500 7.6497
19.9950 29.7500 7.7417
20.0072 29.7500 7.8261
20.0178 29.7500 7.9024
20.0269 29.7500 7.9705
20.0345 29.7500 8.0301
20.0408 29.7500 8.0809
20.0459 29.7500 8.1228
20.0497 29.7500 8.1555
20.0524 29.7500 8.1790
20.0541 29.7500 8.1931
20.0546 29.7500 8.1979
15 1
2
0.000 0.000 0.000
0.000 29.7500 0.000
16 1
2
14.1000 0.000 0.000
14.1000 29.7500 0.000
17 1
2
13.5405 0.000 0.7448
13.5405 29.7500 0.7448
18 1

2
18.1760 0.000 3.2095
18.1760 29.7500 3.2095
19 1
2
17.8359 0.000 3.4397
17.8359 29.7500 3.4397
20 1
2
20.0546 0.000 8.1979
20.0546 29.7500 8.1979
21 1
41
21.3500 29.7500 -13.7000
15.0000 29.7500 -13.7000
10.000 29.7500 -13.7000
9.0000 29.7500 -13.7000
7.9500 29.7500 -13.7000
6.9500 29.7500 -13.2500
6.4500 29.7500 -12.9000
5.9000 29.7500 -12.3500
4.8000 29.7500 -11.0800
1.2000 29.7500 -6.6100
0.2000 29.7500 -5.1800
-0.3500 29.7500 -4.3000
-0.6800 29.7500 -3.7500
-0.9200 29.7500 -3.3500
-1.1800 29.7500 -2.7300
-1.3500 29.7500 -2.3500
-1.5000 29.7500 -1.9500
-1.6500 29.7500 -1.5500
-1.8600 29.7500 -1.0500
-2.0000 29.7500 -0.6200
-2.0600 29.7500 0.000
-2.0000 29.7500 0.6200
-1.8600 29.7500 1.0500
-1.6500 29.7500 1.5500
-1.5000 29.7500 1.9500
-1.3500 29.7500 2.3500
-1.1800 29.7500 2.7300
-0.9200 29.7500 3.3500
-0.6800 29.7500 3.7500
-0.3500 29.7500 4.3000
0.2000 29.7500 5.1800
1.2000 29.7500 6.6100
4.8000 29.7500 11.0800
5.9000 29.7500 12.3500
6.4500 29.7500 12.9000
6.9500 29.7500 13.2500
7.9500 29.7500 13.7000
9.0000 29.7500 13.7000
10.000 29.7500 13.7000
15.0000 29.7500 13.7000
21.3500 29.7500 13.7000
22 1
41
21.3500 30.000 -13.7000
15.0000 30.000 -13.7000
10.000 30.000 -13.7000
9.0000 30.000 -13.7000
7.9500 30.000 -13.7000
6.9500 30.000 -13.2500
6.4500 30.000 -12.9000
5.9000 30.000 -12.3500
4.8000 30.000 -11.0800
1.2000 30.000 -6.6100
0.2000 30.000 -5.1800
-0.3500 30.000 -4.3000
-0.6800 30.000 -3.7500
-0.9200 30.000 -3.3500
-1.1800 30.000 -2.7300
-1.3500 30.000 -2.3500
-1.5000 30.000 -1.9500
-1.6500 30.000 -1.5500
-1.8600 30.000 -1.0500
-2.0000 30.000 -0.6200
-2.0600 30.000 0.000
-2.0000 30.000 0.6200
-1.8600 30.000 1.0500
-1.6500 30.000 1.5500
-1.5000 30.000 1.9500
-1.3500 30.000 2.3500
-1.1800 30.000 2.7300
-0.9200 30.000 3.3500
-0.6800 30.000 3.7500
-0.3500 30.000 4.3000
0.2000 30.000 5.1800
1.2000 30.000 6.6100
4.8000 30.000 11.0800
5.9000 30.000 12.3500
6.4500 30.000 12.9000
6.9500 30.000 13.2500
7.9500 30.000 13.7000
9.0000 30.000 13.7000
10.000 30.000 13.7000
15.0000 30.000 13.7000
21.3500 30.000 13.7000
23 1
2
21.3500 29.7500 13.7
21.3500 29.7500 -13.7
24 1
2
21.3500 30.000 13.7
21.3500 30.000 -13.7
25 1
2
21.3500 29.7500 13.7
21.3500 30.000 13.7
26 1
2
21.3500 29.7500 -13.7
21.3500 30.000 -13.7
Surfaces
1 1
2 2
-140.000 0.000 -260.000
380.000 0.000 -260.000
-140.000 0.000 260.000
380.000 0.000 260.000
2 1
21 21
-123.0000 0.000 0.000
-121.7700 0.000 24.5680
-116.8500 0.000 54.6612
-107.0100 0.000 87.2439
-89.7900 0.000 123.4354
-68.8800 0.000 153.9419
-39.3600 0.000 184.8124
-7.3800 0.000 208.6080
29.5200 0.000 227.5475
71.3400 0.000 240.5142
123.0000 0.000 246.0000
174.6600 0.000 240.5142
216.4800 0.000 227.5475
253.3800 0.000 208.6080
285.3600 0.000 184.8124
314.8800 0.000 153.9419
335.7900 0.000 123.4354
353.0100 0.000 87.2439
362.8500 0.000 54.6612
367.7700 0.000 24.5680
369.0000 0.000 0.000
-123.0000 0.000 0.000
-121.7700 3.8435 24.2679
-116.8500 8.5511 53.9896
-107.010 13.6479 86.1689
-89.790 19.3096 121.9151
-68.880 24.0818 152.0477
-39.360 28.9108 182.5369
-7.3800 32.6334 206.0398
29.5200 35.5961 224.7456
71.3400 37.6247 237.5524
123.000 38.4828 242.9717
174.660 37.6247 237.5524
216.480 35.5961 224.7456
253.380 32.6334 206.0398
285.360 28.9108 182.5369
314.880 24.0818 152.0477
335.790 19.3096 121.9151
353.0100 13.6479 86.1689
362.8500 8.5511 53.9896
367.7700 3.8435 24.2679
369.0000 0.000 0.000
-123.0000 0.000 0.000
-121.7700 7.5923 23.3675
-116.850 16.8916 51.9872
-107.010 26.9597 82.9733
-89.7900 38.1438 117.3937
-68.880 47.5706 146.4069
-39.360 57.1098 175.7670
-7.3800 64.4632 198.3965
29.5200 70.3157 216.4087
71.3400 74.3230 228.7431
123.000 76.0181 233.9608
174.660 74.3230 228.7431
216.480 70.3157 216.4087

253.380	64.4632	198.3965
285.360	57.1098	175.7670
314.880	47.5706	146.4069
335.790	38.1438	117.3937
353.0100	26.9597	82.9733
362.8500	16.8916	51.9872
367.7700	7.5923	23.3675
369.0000	0.000	0.000
-123.0000	0.000	0.000
-121.770	11.1542	21.8915
-116.850	24.8162	48.7055
-107.010	39.6076	77.7335
-89.790	56.0387	109.9817
-68.880	69.8880	137.1622
-39.360	83.9025	164.6675
-7.3800	94.7057	185.8702
29.520	103.3039	202.7458
71.340	109.1912	214.3004
123.00	111.6816	219.1885
174.660	109.1912	214.3004
216.480	103.3039	202.7458
253.380	94.7057	185.8702
285.360	83.9025	164.6675
314.880	69.8880	137.1622
335.790	56.0387	109.9817
353.0100	39.6076	77.7335
362.8500	24.8162	48.7055
367.7700	11.1542	21.8915
369.0000	0.000	0.000
-123.0000	0.000	0.000
-121.770	14.4414	19.8768
-116.850	32.1297	44.2234
-107.010	51.2803	70.5823
-89.7900	72.5537	99.8612
-68.880	90.4846	124.5424
-39.360	108.6293	149.5163
-7.380	122.6163	168.7658
29.520	133.7485	184.0892
71.340	141.3708	194.5811
123.000	144.5951	199.0189
174.660	141.3708	194.5811
216.480	133.7485	184.0892
253.380	122.6163	168.7658
285.360	108.6293	149.5163
314.880	90.4846	124.5424
335.7900	72.5537	99.8612
353.0100	51.2803	70.5823
362.8500	32.1297	44.2234
367.7700	14.4414	19.8768
369.0000	0.000	0.000
-123.0000	0.000	0.000
-121.770	17.3731	17.3725
-116.850	38.6521	38.6515
-107.010	61.6903	61.6894
-89.7900	87.2823	87.2833
-68.880	108.8532	108.8525
-39.360	130.6813	130.6826
-7.3800	147.5076	147.5090
29.5200	160.8997	160.8988
71.3400	170.0694	170.0696
123.000	173.9482	173.9491
174.660	170.0694	170.0696
216.480	160.8997	160.8988
253.380	147.5076	147.5090
285.360	130.6813	130.6826
314.880	108.8532	108.8525
335.7900	87.2823	87.2833
353.0100	61.6903	61.6894
362.8500	38.6521	38.6515
367.7700	17.3731	17.3725
369.0000	0.000	0.000
-123.0000	0.000	0.000
-121.770	19.8769	14.4427
-116.850	44.2228	32.1301
-107.010	70.5813	51.2812
-89.7900	99.8617	72.5528
-68.880	124.5414	90.4837
-39.360	149.5154	108.6287
-7.3800	168.7669	122.6162
29.520	184.0890	133.7477
71.340	194.5802	141.3713
123.000	199.0181	144.5963
174.660	194.5802	141.3713
216.480	184.0890	133.7477
253.380	168.7669	122.6162
285.360	149.5154	108.6287
314.880	124.5414	90.4837
335.7900	99.8617	72.5528
353.0100	70.5813	51.2812
362.8500	44.2228	32.1301
367.7700	19.8769	14.4427
369.0000	0.000	0.000
-123.0000	0.000	0.000
-121.770	21.8913	11.1536
-116.850	48.7045	24.8165
-107.010	77.7343	39.6085
-89.7900	109.9821	56.0388
-68.8800	137.1630	69.8886
-39.3600	164.6680	83.9032
-7.3800	185.8705	94.7051
29.5200	202.7455	103.3052
71.3400	214.2999	109.1920
123.000	219.1875	111.6815
174.660	214.2999	109.1920
216.480	202.7455	103.3052
253.380	185.8705	94.7051
285.360	164.6680	83.9032
314.880	137.1630	69.8886
335.790	109.9821	56.0388
353.0100	77.7343	39.6085
362.8500	48.7045	24.8165
367.7700	21.8913	11.1536
369.0000	0.000	0.000
-123.0000	0.000	0.000
-121.7700	23.3667	7.5916
-116.850	51.9870	16.8928
-107.010	82.9733	26.9591
-89.7900	117.3945	38.1448
-68.880	146.4073	47.5715
-39.360	175.7660	57.1089
-7.3800	198.3974	64.4643
29.5200	216.4097	70.3166
71.3400	228.7428	74.3240
123.000	233.9598	76.0189
174.660	228.7428	74.3240
216.480	216.4097	70.3166
253.380	198.3974	64.4643
285.360	175.7660	57.1089
314.880	146.4073	47.5715
335.790	117.3945	38.1448
353.0100	82.9733	26.9591
362.8500	51.9870	16.8928
367.7700	23.3667	7.5916
369.0000	0.000	0.000
-123.0000	0.000	0.000
-121.7700	24.2667	3.8425
-116.8500	53.9894	8.5510
-107.010	86.1692	13.6481
-89.7900	121.9162	19.3110
-68.880	152.0465	24.0809
-39.360	182.5360	28.9099
-7.3800	206.0391	32.6344
29.5200	224.7452	35.5962
71.3400	237.5534	37.6257
123.000	242.9713	38.4842
174.660	237.5534	37.6257
216.480	224.7452	35.5962
253.380	206.0391	32.6344
285.360	182.5360	28.9099
314.880	152.0465	24.0809
335.790	121.9162	19.3110
353.0100	86.1692	13.6481
362.8500	53.9894	8.5510
367.7700	24.2667	3.8425
369.0000	0.000	0.000
-123.0000	0.000	0.000
-121.7700	24.5692	0.000
-116.8500	54.6624	0.000
-107.0100	87.2433	0.000
-89.7900	123.4359	0.000
-68.8800	153.9418	0.000
-39.3600	184.8113	0.000
-7.3800	208.6074	0.000
29.5200	227.5467	0.000
71.3400	240.5145	0.000
123.0000	246.0000	0.000
174.6600	240.5145	0.000
216.4800	227.5467	0.000
253.3800	208.6074	0.000
285.3600	184.8113	0.000
314.8800	153.9418	0.000
335.7900	123.4359	0.000
353.0100	87.2433	0.000
362.8500	54.6624	0.000
367.7700	24.5692	0.000
369.0000	0.000	0.000
-123.0000	0.000	0.000

-121.7700	24.2667	-3.8425
-116.8500	53.9894	-8.5510
-107.010	86.1692	-13.6481
-89.790	121.9162	-19.3085
-68.880	152.0465	-24.0809
-39.360	182.5360	-28.9099
-7.3800	206.0392	-32.6319
29.520	224.7453	-35.5962
71.340	237.5535	-37.6232
123.00	242.9714	-38.4818
174.660	237.5535	-37.6232
216.480	224.7453	-35.5962
253.380	206.0392	-32.6319
285.360	182.5360	-28.9099
314.880	152.0465	-24.0809
335.790	121.9162	-19.3085
353.010	86.1692	-13.6481
362.8500	53.9894	-8.5510
367.7700	24.2667	-3.8425
369.0000	0.000	0.000
-123.0000	0.000	0.000
-121.7700	23.3667	-7.5916
-116.850	51.9871	-16.8904
-107.010	82.9734	-26.9591
-89.790	117.3946	-38.1448
-68.880	146.4074	-47.5715
-39.360	175.7661	-57.1089
-7.3800	198.3975	-64.4618
29.520	216.4099	-70.3166
71.340	228.7430	-74.3215
123.00	233.9600	-76.0189
174.66	228.7430	-74.3215
216.48	216.4099	-70.3166
253.38	198.3975	-64.4618
285.36	175.7661	-57.1089
314.88	146.4074	-47.5715
335.79	117.3946	-38.1448
353.01	82.9734	-26.9591
362.85	51.9871	-16.8904
367.77	23.3667	-7.5916
369.00	0.000	0.000
-123.0000	0.000	0.000
-121.77	21.8914	-11.1536
-116.85	48.7046	-24.8165
-107.01	77.7345	-39.6085
-89.790	109.9823	-56.0388
-68.880	137.1632	-69.8886
-39.360	164.6683	-83.9032
-7.3800	185.8707	-94.7051
29.520	202.7458	-103.3028
71.340	214.3002	-109.1920
123.0	219.1878	-111.6815
174.66	214.3002	-109.1920
216.48	202.7458	-103.3028
253.38	185.8707	-94.7051
285.36	164.6683	-83.9032
314.88	137.1632	-69.8886
335.79	109.9823	-56.0388
353.010	77.7345	-39.6085

362.850	48.7046	-24.8165
367.770	21.8914	-11.1536
369.0000	0.000	0.000
-123.0000	0.000	0.000
-121.770	19.8770	-14.4402
-116.850	44.2229	-32.1301
-107.010	70.5814	-51.2812
-89.7900	99.8619	-72.5528
-68.880	124.5417	-90.4837
-39.36	149.5157	-108.6287
-7.380	168.7672	-122.6162
29.520	184.0894	-133.7477
71.340	194.5806	-141.3713
123.00	199.0184	-144.5939
174.66	194.5806	-141.3713
216.48	184.0894	-133.7477
253.38	168.7672	-122.6162
285.36	149.5157	-108.6287
314.88	124.5417	-90.4837
335.79	99.8619	-72.5528
353.010	70.5814	-51.2812
362.850	44.2229	-32.1301
367.770	19.8770	-14.4402
369.0000	0.000	0.000
-123.0000	0.000	0.000
-121.770	17.3731	-17.3725
-116.850	38.6522	-38.6515
-107.010	61.6905	-61.6894
-89.7900	87.2825	-87.2833
-68.88	108.8535	-108.8525
-39.36	130.6816	-130.6801
-7.380	147.5080	-147.5065
29.520	160.9001	-160.8988
71.340	170.0698	-170.0696
123.00	173.9486	-173.9491
174.66	170.0698	-170.0696
216.48	160.9001	-160.8988
253.38	147.5080	-147.5065
285.36	130.6816	-130.6801
314.88	108.8535	-108.8525
335.79	87.2825	-87.2833
353.010	61.6905	-61.6894
362.850	38.6522	-38.6515
367.770	17.3731	-17.3725
369.0000	0.000	0.000
-123.0000	0.000	0.000
-121.770	14.4415	-19.8768
-116.850	32.1298	-44.2234
-107.010	51.2805	-70.5823
-89.7900	72.5540	-99.8612
-68.880	90.4850	-124.5424
-39.36	108.6297	-149.5163
-7.380	122.6167	-168.7658
29.520	133.7490	-184.0892
71.340	141.3713	-194.5811
123.00	144.5956	-199.0189
174.66	141.3713	-194.5811
216.48	133.7490	-184.0892
253.38	122.6167	-168.7658

285.36	108.6297	-149.5163
314.88	90.4850	-124.5424
335.790	72.5540	-99.8612
353.010	51.2805	-70.5823
362.850	32.1298	-44.2234
367.7700	14.4415	-19.8768
369.0000	0.000	0.000
-123.0000	0.000	0.000
-121.770	11.1542	-21.8915
-116.850	24.8163	-48.7055
-107.010	39.6078	-77.7335
-89.790	56.0390	-109.9817
-68.880	69.8884	-137.1622
-39.360	83.9030	-164.6675
-7.3800	94.7062	-185.8702
29.52	103.3045	-202.7458
71.34	109.1918	-214.3004
123.0	111.6822	-219.1885
174.66	109.1918	-214.3004
216.48	103.3045	-202.7458
253.38	94.7062	-185.8702
285.36	83.9030	-164.6675
314.88	69.8884	-137.1622
335.79	56.0390	-109.9817
353.01	39.6078	-77.7335
362.850	24.8163	-48.7055
367.770	11.1542	-21.8915
369.0000	0.000	0.000
-123.0000	0.000	0.000
-121.7700	7.5924	-23.3675
-116.850	16.8917	-51.9872
-107.010	26.9599	-82.9733
-89.790	38.1441	-117.3937
-68.880	47.5710	-146.4069
-39.360	57.1103	-175.7670
-7.3800	64.4637	-198.3965
29.520	70.3163	-216.4087
71.340	74.3236	-228.7431
123.00	76.0187	-233.9608
174.66	74.3236	-228.7431
216.48	70.3163	-216.4087
253.38	64.4637	-198.3965
285.36	57.1103	-175.7670
314.88	47.5710	-146.4069
335.79	38.1441	-117.3937
353.010	26.9599	-82.9733
362.850	16.8917	-51.9872
367.7700	7.5924	-23.3675
369.0000	0.000	0.000
-123.0000	0.000	0.000
-121.7700	3.8435	-24.2679
-116.8500	8.5512	-53.9896
-107.010	13.6481	-86.1689
-89.790	19.3099	-121.9151
-68.880	24.0822	-152.0452
-39.360	28.9113	-182.5369
-7.3800	32.6339	-206.0398
29.520	35.5967	-224.7456
71.340	37.6254	-237.5524

123.00 38.4835 -242.9717
174.66 37.6254 -237.5524
216.48 35.5967 -224.7456
253.38 32.6339 -206.0398
285.36 28.9113 -182.5369
314.88 24.0822 -152.0452
335.79 19.3099 -121.9151
353.010 13.6481 -86.1689
362.8500 8.5512 -53.9896
367.7700 3.8435 -24.2679
369.0000 0.000 0.000
-123.0000 0.000 0.000
-121.7700 0.000 -24.5680
-116.8500 0.000 -54.6612
-107.0100 0.000 -87.2439
-89.7900 0.000 -123.4354
-68.8800 0.000 -153.9419
-39.3600 0.000 -184.8124
-7.3800 0.000 -208.6080
29.5200 0.000 -227.5475
71.3400 0.000 -240.5142
123.0000 0.000 -246.0000
174.6600 0.000 -240.5142
216.4800 0.000 -227.5475
253.3800 0.000 -208.6080
285.3600 0.000 -184.8124
314.8800 0.000 -153.9419
335.7900 0.000 -123.4354
353.0100 0.000 -87.2439
362.8500 0.000 -54.6612
367.7700 0.000 -24.5680
369.0000 0.000 0.000
3 1
36 2
0.000 0.000 0.000
0.0355 0.000 0.1008
0.0500 0.000 0.1280
0.1250 0.000 0.2295
0.1875 0.000 0.2700
0.3438 0.000 0.3338
0.5000 0.000 0.3677
0.7500 0.000 0.3750
1.0000 0.000 0.3969
1.5000 0.000 0.4207
2.0000 0.000 0.4431
2.5000 0.000 0.4654
3.0000 0.000 0.4892
3.5000 0.000 0.5135
4.0000 0.000 0.5392
4.5000 0.000 0.5639
5.0000 0.000 0.5880
5.5000 0.000 0.6091
6.0000 0.000 0.6275
6.5000 0.000 0.6417
7.0000 0.000 0.6471
7.5000 0.000 0.6386
8.0000 0.000 0.6120
8.5000 0.000 0.5693
9.0000 0.000 0.5103
9.5000 0.000 0.4324
10.000 0.000 0.3359
10.5000 0.000 0.2299
11.0000 0.000 0.1166
11.5000 0.000 0.000
12.0000 0.000 -0.0946
12.5000 0.000 -0.1530
13.0000 0.000 -0.1589
13.5000 0.000 -0.1024
14.0000 0.000 0.0251
14.1000 0.000 0.000
0.000 29.7500 0.000
0.0355 29.7500 0.1008
0.0500 29.7500 0.1280
0.1250 29.7500 0.2295
0.1875 29.7500 0.2700
0.3438 29.7500 0.3338
0.5000 29.7500 0.3677
0.7500 29.7500 0.3750
1.0000 29.7500 0.3969
1.5000 29.7500 0.4207
2.0000 29.7500 0.4431
2.5000 29.7500 0.4654
3.0000 29.7500 0.4892
3.5000 29.7500 0.5135
4.0000 29.7500 0.5392
4.5000 29.7500 0.5639
5.0000 29.7500 0.5880
5.5000 29.7500 0.6091
6.0000 29.7500 0.6275
6.5000 29.7500 0.6417
7.0000 29.7500 0.6471
7.5000 29.7500 0.6386
8.0000 29.7500 0.6120
8.5000 29.7500 0.5693
9.0000 29.7500 0.5103
9.5000 29.7500 0.4324
10.000 29.7500 0.3359
10.5000 29.7500 0.2299
11.0000 29.7500 0.1166
11.5000 29.7500 0.000
12.0000 29.7500 -0.0946
12.5000 29.7500 -0.1530
13.0000 29.7500 -0.1589
13.5000 29.7500 -0.1024
14.0000 29.7500 0.0251
14.1000 29.7500 0.000
4 1
36 2
0.000 0.000 0.000
0.0355 0.000 -0.1650
0.0500 0.000 -0.2000
0.1250 0.000 -0.3438
0.1875 0.000 -0.4375
0.3438 0.000 -0.6560
0.5000 0.000 -0.8073
0.7500 0.000 -1.0500
1.0000 0.000 -1.2280
1.5000 0.000 -1.5251
2.0000 0.000 -1.7441
2.5000 0.000 -1.9078
3.0000 0.000 -2.0330
3.5000 0.000 -2.1265
4.0000 0.000 -2.1939
4.5000 0.000 -2.2383
5.0000 0.000 -2.2599
5.5000 0.000 -2.2648
6.0000 0.000 -2.2554
6.5000 0.000 -2.2329
7.0000 0.000 -2.1972
7.5000 0.000 -2.1456
8.0000 0.000 -2.0793
8.5000 0.000 -1.9994
9.0000 0.000 -1.9026
9.5000 0.000 -1.7891
10.000 0.000 -1.6611
10.5000 0.000 -1.5153
11.0000 0.000 -1.3543
11.5000 0.000 -1.1782
12.0000 0.000 -0.9868
12.5000 0.000 -0.7811
13.0000 0.000 -0.5588
13.5000 0.000 -0.3248
14.0000 0.000 -0.0699
14.1000 0.000 0.000
0.000 29.7500 0.000
0.0355 29.7500 -0.1650
0.0500 29.7500 -0.2000
0.1250 29.7500 -0.3438
0.1875 29.7500 -0.4375
0.3438 29.7500 -0.6560
0.5000 29.7500 -0.8073
0.7500 29.7500 -1.0500
1.0000 29.7500 -1.2280
1.5000 29.7500 -1.5251
2.0000 29.7500 -1.7441
2.5000 29.7500 -1.9078
3.0000 29.7500 -2.0330
3.5000 29.7500 -2.1265
4.0000 29.7500 -2.1939
4.5000 29.7500 -2.2383
5.0000 29.7500 -2.2599
5.5000 29.7500 -2.2648
6.0000 29.7500 -2.2554
6.5000 29.7500 -2.2329
7.0000 29.7500 -2.1972
7.5000 29.7500 -2.1456
8.0000 29.7500 -2.0793
8.5000 29.7500 -1.9994
9.0000 29.7500 -1.9026
9.5000 29.7500 -1.7891
10.000 29.7500 -1.6611
10.5000 29.7500 -1.5153
11.0000 29.7500 -1.3543
11.5000 29.7500 -1.1782
12.0000 29.7500 -0.9868
12.5000 29.7500 -0.7811
13.0000 29.7500 -0.5588

13.5000 29.7500 -0.3248
14.0000 29.7500 -0.0699
14.1000 29.7500 0.000
5 1
54 2
13.5405 0.000 0.7448
13.5428 0.000 0.7860
13.5549 0.000 0.8269
13.5766 0.000 0.8673
13.6076 0.000 0.9073
13.6475 0.000 0.9468
13.6960 0.000 0.9859
13.7525 0.000 1.0247
13.8167 0.000 1.0631
13.8880 0.000 1.1013
13.9660 0.000 1.1393
14.0503 0.000 1.1774
14.1403 0.000 1.2155
14.2355 0.000 1.2540
14.3354 0.000 1.2930
14.4398 0.000 1.3326
14.5480 0.000 1.3732
14.6598 0.000 1.4149
14.7746 0.000 1.4581
14.8923 0.000 1.5031
15.0123 0.000 1.5501
15.1343 0.000 1.5994
15.2581 0.000 1.6513
15.3861 0.000 1.7078
15.5197 0.000 1.7688
15.6547 0.000 1.8309
15.7906 0.000 1.8938
15.9269 0.000 1.9577
16.0631 0.000 2.0225
16.1987 0.000 2.0880
16.3332 0.000 2.1541
16.4662 0.000 2.2207
16.5971 0.000 2.2876
16.7255 0.000 2.3545
16.8509 0.000 2.4211
16.9729 0.000 2.4872
17.0911 0.000 2.5524
17.2050 0.000 2.6165
17.3142 0.000 2.6790
17.4184 0.000 2.7397
17.5171 0.000 2.7980
17.6101 0.000 2.8538
17.6970 0.000 2.9066
17.7774 0.000 2.9561
17.8512 0.000 3.0020
17.9179 0.000 3.0439
17.9774 0.000 3.0816
18.0295 0.000 3.1148
18.0739 0.000 3.1433
18.1104 0.000 3.1669
18.1390 0.000 3.1854
18.1595 0.000 3.1988
18.1719 0.000 3.2068
18.1760 0.000 3.2095
13.5405 29.7500 0.7448
13.5428 29.7500 0.7860
13.5549 29.7500 0.8269
13.5766 29.7500 0.8673
13.6076 29.7500 0.9073
13.6475 29.7500 0.9468
13.6960 29.7500 0.9859
13.7525 29.7500 1.0247
13.8167 29.7500 1.0631
13.8880 29.7500 1.1013
13.9660 29.7500 1.1393
14.0503 29.7500 1.1774
14.1403 29.7500 1.2155
14.2355 29.7500 1.2540
14.3354 29.7500 1.2930
14.4398 29.7500 1.3326
14.5480 29.7500 1.3732
14.6598 29.7500 1.4149
14.7746 29.7500 1.4581
14.8923 29.7500 1.5031
15.0123 29.7500 1.5501
15.1343 29.7500 1.5994
15.2581 29.7500 1.6513
15.3861 29.7500 1.7078
15.5197 29.7500 1.7688
15.6547 29.7500 1.8309
15.7906 29.7500 1.8938
15.9269 29.7500 1.9577
16.0631 29.7500 2.0225
16.1987 29.7500 2.0880
16.3332 29.7500 2.1541
16.4662 29.7500 2.2207
16.5971 29.7500 2.2876
16.7255 29.7500 2.3545
16.8509 29.7500 2.4211
16.9729 29.7500 2.4872
17.0911 29.7500 2.5524
17.2050 29.7500 2.6165
17.3142 29.7500 2.6790
17.4184 29.7500 2.7397
17.5171 29.7500 2.7980
17.6101 29.7500 2.8538
17.6970 29.7500 2.9066
17.7774 29.7500 2.9561
17.8512 29.7500 3.0020
17.9179 29.7500 3.0439
17.9774 29.7500 3.0816
18.0295 29.7500 3.1148
18.0739 29.7500 3.1433
18.1104 29.7500 3.1669
18.1390 29.7500 3.1854
18.1595 29.7500 3.1988
18.1719 29.7500 3.2068
18.1760 29.7500 3.2095
6 1
54 2
13.5405 0.000 0.7448
13.5483 0.000 0.7041
13.5664 0.000 0.6653
13.5948 0.000 0.6285
13.6336 0.000 0.5938
13.6826 0.000 0.5617
13.7418 0.000 0.5324
13.8110 0.000 0.5064
13.8898 0.000 0.4841
13.9779 0.000 0.4660
14.0748 0.000 0.4527
14.1800 0.000 0.4447
14.2930 0.000 0.4425
14.4130 0.000 0.4465
14.5394 0.000 0.4574
14.6714 0.000 0.4754
14.8081 0.000 0.5010
14.9486 0.000 0.5345
15.0921 0.000 0.5760
15.2376 0.000 0.6258
15.3843 0.000 0.6838
15.5312 0.000 0.7499
15.6774 0.000 0.8241
15.8192 0.000 0.9045
15.9552 0.000 0.9887
16.0900 0.000 1.0773
16.2233 0.000 1.1698
16.3544 0.000 1.2657
16.4830 0.000 1.3645
16.6087 0.000 1.4658
16.7310 0.000 1.5689
16.8496 0.000 1.6733
16.9643 0.000 1.7785
17.0747 0.000 1.8838
17.1805 0.000 1.9888
17.2816 0.000 2.0927
17.3777 0.000 2.1952
17.4687 0.000 2.2955
17.5544 0.000 2.3931
17.6348 0.000 2.4874
17.7097 0.000 2.5780
17.7790 0.000 2.6643
17.8428 0.000 2.7458
17.9009 0.000 2.8220
17.9535 0.000 2.8924
18.0004 0.000 2.9567
18.0417 0.000 3.0144
18.0775 0.000 3.0651
18.1076 0.000 3.1086
18.1323 0.000 3.1446
18.1514 0.000 3.1729
18.1651 0.000 3.1932
18.1733 0.000 3.2054
18.1760 0.000 3.2095
13.5405 29.7500 0.7448
13.5483 29.7500 0.7041
13.5664 29.7500 0.6653
13.5948 29.7500 0.6285
13.6336 29.7500 0.5938
13.6826 29.7500 0.5617
13.7418 29.7500 0.5324
13.8110 29.7500 0.5064

13.8898	29.7500	0.4841
13.9779	29.7500	0.4660
14.0748	29.7500	0.4527
14.1800	29.7500	0.4447
14.2930	29.7500	0.4425
14.4130	29.7500	0.4465
14.5394	29.7500	0.4574
14.6714	29.7500	0.4754
14.8081	29.7500	0.5010
14.9486	29.7500	0.5345
15.0921	29.7500	0.5760
15.2376	29.7500	0.6258
15.3843	29.7500	0.6838
15.5312	29.7500	0.7499
15.6774	29.7500	0.8241
15.8192	29.7500	0.9045
15.9552	29.7500	0.9887
16.0900	29.7500	1.0773
16.2233	29.7500	1.1698
16.3544	29.7500	1.2657
16.4830	29.7500	1.3645
16.6087	29.7500	1.4658
16.7310	29.7500	1.5689
16.8496	29.7500	1.6733
16.9643	29.7500	1.7785
17.0747	29.7500	1.8838
17.1805	29.7500	1.9888
17.2816	29.7500	2.0927
17.3777	29.7500	2.1952
17.4687	29.7500	2.2955
17.5544	29.7500	2.3931
17.6348	29.7500	2.4874
17.7097	29.7500	2.5780
17.7790	29.7500	2.6643
17.8428	29.7500	2.7458
17.9009	29.7500	2.8220
17.9535	29.7500	2.8924
18.0004	29.7500	2.9567
18.0417	29.7500	3.0144
18.0775	29.7500	3.0651
18.1076	29.7500	3.1086
18.1323	29.7500	3.1446
18.1514	29.7500	3.1729
18.1651	29.7500	3.1932
18.1733	29.7500	3.2054
18.1760	29.7500	3.2095
7	1	
54	2	
17.8359	0.000	3.4397
17.8074	0.000	3.4697
17.7857	0.000	3.5061
17.7707	0.000	3.5487
17.7621	0.000	3.5973
17.7599	0.000	3.6518
17.7637	0.000	3.7119
17.7734	0.000	3.7774
17.7886	0.000	3.8479
17.8091	0.000	3.9234
17.8346	0.000	4.0035
17.8647	0.000	4.0882
17.8992	0.000	4.1770
17.9376	0.000	4.2700
17.9797	0.000	4.3670
18.0250	0.000	4.4677
18.0732	0.000	4.5722
18.1239	0.000	4.6802
18.1766	0.000	4.7918
18.2314	0.000	4.9077
18.2905	0.000	5.0334
18.3530	0.000	5.1628
18.4185	0.000	5.2941
18.4864	0.000	5.4270
18.5565	0.000	5.5611
18.6283	0.000	5.6960
18.7015	0.000	5.8314
18.7757	0.000	5.9669
18.8505	0.000	6.1020
18.9255	0.000	6.2363
19.0004	0.000	6.3694
19.0748	0.000	6.5010
19.1485	0.000	6.6305
19.2209	0.000	6.7576
19.2920	0.000	6.8818
19.3613	0.000	7.0027
19.4286	0.000	7.1198
19.4936	0.000	7.2328
19.5561	0.000	7.3412
19.6159	0.000	7.4447
19.6726	0.000	7.5428
19.7262	0.000	7.6353
19.7763	0.000	7.7217
19.8228	0.000	7.8017
19.8655	0.000	7.8750
19.9042	0.000	7.9414
19.9388	0.000	8.0005
19.9691	0.000	8.0523
19.9950	0.000	8.0964
20.0163	0.000	8.1328
20.0330	0.000	8.1612
20.0450	0.000	8.1815
20.0522	0.000	8.1938
20.0546	0.000	8.1979
17.8359	29.7500	3.4397
17.8074	29.7500	3.4697
17.7857	29.7500	3.5061
17.7707	29.7500	3.5487
17.7621	29.7500	3.5973
17.7599	29.7500	3.6518
17.7637	29.7500	3.7119
17.7734	29.7500	3.7774
17.7886	29.7500	3.8479
17.8091	29.7500	3.9234
17.8346	29.7500	4.0035
17.8647	29.7500	4.0882
17.8992	29.7500	4.1770
17.9376	29.7500	4.2700
17.9797	29.7500	4.3670
18.0250	29.7500	4.4677
18.0732	29.7500	4.5722
18.1239	29.7500	4.6802
18.1766	29.7500	4.7918
18.2314	29.7500	4.9077
18.2905	29.7500	5.0334
18.3530	29.7500	5.1628
18.4185	29.7500	5.2941
18.4864	29.7500	5.4270
18.5565	29.7500	5.5611
18.6283	29.7500	5.6960
18.7015	29.7500	5.8314
18.7757	29.7500	5.9669
18.8505	29.7500	6.1020
18.9255	29.7500	6.2363
19.0004	29.7500	6.3694
19.0748	29.7500	6.5010
19.1485	29.7500	6.6305
19.2209	29.7500	6.7576
19.2920	29.7500	6.8818
19.3613	29.7500	7.0027
19.4286	29.7500	7.1198
19.4936	29.7500	7.2328
19.5561	29.7500	7.3412
19.6159	29.7500	7.4447
19.6726	29.7500	7.5428
19.7262	29.7500	7.6353
19.7763	29.7500	7.7217
19.8228	29.7500	7.8017
19.8655	29.7500	7.8750
19.9042	29.7500	7.9414
19.9388	29.7500	8.0005
19.9691	29.7500	8.0523
19.9950	29.7500	8.0964
20.0163	29.7500	8.1328
20.0330	29.7500	8.1612
20.0450	29.7500	8.1815
20.0522	29.7500	8.1938
20.0546	29.7500	8.1979
8	1	
54	2	
17.8359	0.000	3.4397
17.8704	0.000	3.4171
17.9104	0.000	3.4027
17.9558	0.000	3.3966
18.0063	0.000	3.3991
18.0619	0.000	3.4102
18.1221	0.000	3.4302
18.1867	0.000	3.4592
18.2551	0.000	3.4973
18.3268	0.000	3.5445
18.4013	0.000	3.6010
18.4780	0.000	3.6668
18.5561	0.000	3.7417
18.6349	0.000	3.8258
18.7138	0.000	3.9188
18.7921	0.000	4.0205
18.8690	0.000	4.1306
18.9439	0.000	4.2487
19.0161	0.000	4.3744

19.0846 0.000 4.5065
19.1466 0.000 4.6385
19.2062 0.000 4.7740
19.2642 0.000 4.9135
19.3204 0.000 5.0564
19.3747 0.000 5.2022
19.4270 0.000 5.3503
19.4772 0.000 5.5001
19.5253 0.000 5.6509
19.5712 0.000 5.8023
19.6149 0.000 5.9535
19.6564 0.000 6.1040
19.6956 0.000 6.2531
19.7325 0.000 6.4004
19.7671 0.000 6.5452
19.7995 0.000 6.6870
19.8296 0.000 6.8252
19.8576 0.000 6.9592
19.8833 0.000 7.0887
19.9069 0.000 7.2130
19.9284 0.000 7.3317
19.9479 0.000 7.4443
19.9654 0.000 7.5505
19.9811 0.000 7.6497
19.9950 0.000 7.7417
20.0072 0.000 7.8261
20.0178 0.000 7.9024
20.0269 0.000 7.9705
20.0345 0.000 8.0301
20.0408 0.000 8.0809
20.0459 0.000 8.1228
20.0497 0.000 8.1555
20.0524 0.000 8.1790
20.0541 0.000 8.1931
20.0546 0.000 8.1979
17.8359 29.7500 3.4397
17.8704 29.7500 3.4171
17.9104 29.7500 3.4027
17.9558 29.7500 3.3966
18.0063 29.7500 3.3991
18.0619 29.7500 3.4102
18.1221 29.7500 3.4302
18.1867 29.7500 3.4592
18.2551 29.7500 3.4973
18.3268 29.7500 3.5445
18.4013 29.7500 3.6010
18.4780 29.7500 3.6668
18.5561 29.7500 3.7417
18.6349 29.7500 3.8258
18.7138 29.7500 3.9188
18.7921 29.7500 4.0205
18.8690 29.7500 4.1306
18.9439 29.7500 4.2487
19.0161 29.7500 4.3744
19.0846 29.7500 4.5065
19.1466 29.7500 4.6385
19.2062 29.7500 4.7740
19.2642 29.7500 4.9135
19.3204 29.7500 5.0564
19.3747 29.7500 5.2022
19.4270 29.7500 5.3503
19.4772 29.7500 5.5001
19.5253 29.7500 5.6509
19.5712 29.7500 5.8023
19.6149 29.7500 5.9535
19.6564 29.7500 6.1040
19.6956 29.7500 6.2531
19.7325 29.7500 6.4004
19.7671 29.7500 6.5452
19.7995 29.7500 6.6870
19.8296 29.7500 6.8252
19.8576 29.7500 6.9592
19.8833 29.7500 7.0887
19.9069 29.7500 7.2130
19.9284 29.7500 7.3317
19.9479 29.7500 7.4443
19.9654 29.7500 7.5505
19.9811 29.7500 7.6497
19.9950 29.7500 7.7417
20.0072 29.7500 7.8261
20.0178 29.7500 7.9024
20.0269 29.7500 7.9705
20.0345 29.7500 8.0301
20.0408 29.7500 8.0809
20.0459 29.7500 8.1228
20.0497 29.7500 8.1555
20.0524 29.7500 8.1790
20.0541 29.7500 8.1931
20.0546 29.7500 8.1979
9 1
2 2
-30.000 29.7500 -30.000
30.000 29.7500 -30.000
-30.000 29.7500 30.000
30.000 29.7500 30.000
10 1
2 2
-30.000 30.000 -30.000
30.000 30.000 -30.000
-30.000 30.000 30.000
30.000 30.000 30.000
11 1
2 2
21.3500 29.7500 -13.7000
21.3500 30.000 -13.7000
21.3500 29.7500 13.7000
21.3500 30.000 13.7000
12 1
41 2
21.3500 29.7500 -13.7000
15.0000 29.7500 -13.7000
10.000 29.7500 -13.7000
9.0000 29.7500 -13.7000
7.9500 29.7500 -13.7000
6.9500 29.7500 -13.2500
6.4500 29.7500 -12.9000
5.9000 29.7500 -12.3500
4.8000 29.7500 -11.0800
1.2000 29.7500 -6.6100
0.2000 29.7500 -5.1800
-0.3500 29.7500 -4.3000
-0.6800 29.7500 -3.7500
-0.9200 29.7500 -3.3500
-1.1800 29.7500 -2.7300
-1.3500 29.7500 -2.3500
-1.5000 29.7500 -1.9500
-1.6500 29.7500 -1.5500
-1.8600 29.7500 -1.0500
-2.0000 29.7500 -0.6200
-2.0600 29.7500 0.000
-2.0000 29.7500 0.6200
-1.8600 29.7500 1.0500
-1.6500 29.7500 1.5500
-1.5000 29.7500 1.9500
-1.3500 29.7500 2.3500
-1.1800 29.7500 2.7300
-0.9200 29.7500 3.3500
-0.6800 29.7500 3.7500
-0.3500 29.7500 4.3000
0.2000 29.7500 5.1800
1.2000 29.7500 6.6100
4.8000 29.7500 11.0800
5.9000 29.7500 12.3500
6.4500 29.7500 12.9000
6.9500 29.7500 13.2500
7.9500 29.7500 13.7000
9.0000 29.7500 13.7000
10.000 29.7500 13.7000
15.0000 29.7500 13.7000
21.3500 29.7500 13.7000
21.3500 30.000 -13.7000
15.0000 30.000 -13.7000
10.000 30.000 -13.7000
9.0000 30.000 -13.7000
7.9500 30.000 -13.7000
6.9500 30.000 -13.2500
6.4500 30.000 -12.9000
5.9000 30.000 -12.3500
4.8000 30.000 -11.0800
1.2000 30.000 -6.6100
0.2000 30.000 -5.1800
-0.3500 30.000 -4.3000
-0.6800 30.000 -3.7500
-0.9200 30.000 -3.3500
-1.1800 30.000 -2.7300
-1.3500 30.000 -2.3500
-1.5000 30.000 -1.9500
-1.6500 30.000 -1.5500
-1.8600 30.000 -1.0500
-2.0000 30.000 -0.6200
-2.0600 30.000 0.000
-2.0000 30.000 0.6200
-1.8600 30.000 1.0500
-1.6500 30.000 1.5500
-1.5000 30.000 1.9500
-1.3500 30.000 2.3500
-1.1800 30.000 2.7300

-0.9200 30.000 3.3500
-0.6800 30.000 3.7500
-0.3500 30.000 4.3000
0.2000 30.000 5.1800
1.2000 30.000 6.6100
4.8000 30.000 11.0800
5.9000 30.000 12.3500
6.4500 30.000 12.9000
6.9500 30.000 13.2500
7.9500 30.000 13.7000
9.0000 30.000 13.7000
10.000 30.000 13.7000
15.0000 30.000 13.7000
21.3500 30.000 13.7000
Mesh generation
26 12
Curves segments
1 1 1
2 2 1
3 3 1
4 4 1
5 5 1
6 6 1
7 7 1
8 8 1
9 9 1
10 10 1
11 11 1
12 12 1
13 13 1
14 14 1
15 15 1
16 16 1
17 17 1
18 18 1
19 19 1
20 20 1
21 21 1
22 22 1
23 23 1
24 24 1
25 25 1
26 26 1
Surface Regions
1 1 1
8
1 -2 -3 4 -5 6 -7 8
2 2 1
2
1 2
3 3 1
4
15 3 16 9
4 4 1
4
15 10 16 4
5 5 1
4
17 5 18 11
6 6 1
4
17 12 18 6
7 7 1
4
19 7 20 13
8 8 1
4
19 14 20 8
9 9 1
8
21 23 9 -10 11 -12 13 -14
10 10 1
2
22 24
11 11 1
4
23 26 24 25
12 12 1
4
21 25 -22 -26

APPENDIX A-2

STARS-CFD Background Mesh Data File (*fin.bac*)

```
Background Mesh....fin
4  1  0  0  7
1  -1800  -100  -2400
  1  0  0  20
  0  1  0  20
  0  0  1  20
2  1800  -100  -2400
  1  0  0  20
  0  1  0  20
  0  0  1  20
3  0  -100  2400
  1  0  0  20
  0  1  0  20
  0  0  1  20
4  0  2400  0
  1  0  0  20
  0  1  0  20
  0  0  1  20
1  1  2  3  4
* Point Sources
* Line Sources
* Triangle Sources
1. Source for fin 1
0.000  0.000  0.000  0.4  0.8  3
0.000  30.000  0.000  0.4  0.8  3
14.10000  0.000  0.000  0.4  0.8  3
2. Source for fin 1
14.10000  0.000  0.000  0.4  0.8  3
0.000  30.000  0.000  0.4  0.8  3
14.10000  30.000  0.000  0.4  0.8  3
3. Source for fin 2
13.54051  0.000  0.74475  0.4  0.8  3
13.54051  30.000  0.74475  0.4  0.8  3
18.17598  0.000  3.20948  0.4  0.8  3
```

4. Source for fin 2

18.17598	0.000	3.20948	0.4	0.8	3
13.54051	30.000	0.74475	0.4	0.8	3
18.17598	30.000	3.20948	0.4	0.8	3

5. Source for fin 3

17.83585	0.000	3.43973	0.4	0.8	3
17.83585	30.000	3.43973	0.4	0.8	3
20.05219	0.000	8.19376	0.4	0.8	3

6. Source for fin 3

20.05219	0.000	8.19376	0.4	0.8	3
17.83585	30.000	3.43973	0.4	0.8	3
20.05219	30.000	8.19376	0.4	0.8	3

7. Source for endplate

21.00000	30.000	13.0000	0.6	0.8	5
21.00000	30.000	-13.000	0.6	0.8	5
-2.00000	30.000	0.000	0.6	0.8	5

APPENDIX A-3

STARS-CFD Boundary Conditions Data File (*fin.bco*)

```
Fin Boundary Condition File
12    26
Surface Regions
1     2
2     3
3     1
4     1
5     1
6     1
7     1
8     1
9     1
10    1
11    1
12    1
Curve Segments
1     0
2     0
3     4
4     4
5     4
6     4
7     4
8     4
9     4
10    4
11    4
12    4
13    4
14    4
15    0
16    1
17    0
18    1
19    0
20    1
21    1
22    1
23    1
24    1
25    1
26    1
```

APPENDIX A-4

STARS-CFD Parameter Control File (*fin.cons*)

```
&control
 nout    = 50,
 nstep   = 1,
 ncycl   = 5000,
 nstpe   = 20,
 cfl     = 0.3,
 nsmth   = 0,
 smofc   = 0.2,
 relax   = 1.0,
 mach    = 0.434,
 alpha   = 0.0,
 beta    = 0.0,
 restart = 0,
 amplitude= 1.0,
/
```

APPENDIX B-1

STARS-CFD Geometry Data File (*boxwing.sur*)

```
1  Geometry definition...felisa
boxwing
26  12
Curves
1  1
21
-123.0000  0.000  0.000
-121.7700  0.000  24.5680
-116.8500  0.000  54.6612
-107.0100  0.000  87.2439
-89.7900  0.000  123.4354
-68.8800  0.000  153.9419
-39.3600  0.000  184.8124
-7.3800  0.000  208.6080
29.5200  0.000  227.5475
71.3400  0.000  240.5142
123.0000  0.000  246.0000
174.6600  0.000  240.5142
216.4800  0.000  227.5475
253.3800  0.000  208.6080
285.3600  0.000  184.8124
314.8800  0.000  153.9419
335.7900  0.000  123.4354
353.0100  0.000  87.2439
362.8500  0.000  54.6612
367.7700  0.000  24.5680
369.0000  0.000  0.000
2  1
21
-123.0000  0.000  0.000
-121.7700  0.000  -24.5680
-116.8500  0.000  -54.6612
-107.0100  0.000  -87.2439
-89.7900  0.000  -123.4354
-68.8800  0.000  -153.9419
-39.3600  0.000  -184.8124
-7.3800  0.000  -208.6080
29.5200  0.000  -227.5475
71.3400  0.000  -240.5142
123.0000  0.000  -246.0000
174.6600  0.000  -240.5142
216.4800  0.000  -227.5475
253.3800  0.000  -208.6080
285.3600  0.000  -184.8124
314.8800  0.000  -153.9419
335.7900  0.000  -123.4354
353.0100  0.000  -87.2439
362.8500  0.000  -54.6612
367.7700  0.000  -24.5680
369.0000  0.000  0.000
3  1
36
100.000625 0.000  -0.02225
100.0055  0.000  0.070125
100.033  0.000  0.140000
100.098625 0.0000  0.178375
100.21475  0.000  0.193750
100.37575  0.000  0.198000
100.578375 0.0000  0.191500
100.820125 0.0000  0.175500
101.098375 0.0000  0.150250
101.41025  0.000  0.115625
101.7525  0.000  0.070375
102.12575  0.000  0.009375
102.53475  0.0000  -0.066875
102.98  0.000  -0.151625
103.459125 0.0000 -0.241000
103.96875  0.0000  -0.331500
104.5055  0.000  -0.419750
105.064875  0.000  -0.502625
105.642375  0.000  -0.577250
106.2325  0.000  -0.641125
106.829875  0.000  -0.691750
107.4285  0.000  -0.727500
108.022  0.000  -0.747000
108.604  0.000  -0.749250
109.168  0.000  -0.734000
109.7075  0.000  -0.701500
110.216125  0.000  -0.652375
110.6875  0.000  -0.588250
111.116  0.000  -0.511000
111.49575  0.000  -0.423375
111.821625  0.000  -0.328000
112.086625  0.000  -0.227750
112.281875  0.000  -0.132500
112.4085  0.000  -0.058500
112.478125  0.000  -0.014375
112.5  0.000  0.000
4  1
46
100.000625  0.000  -0.022250
100.019375  0.000  -0.129125
100.061875  0.000  -0.246125
100.1285  0.000  -0.369250
100.219375  0.000  -0.495125
100.33675  0.000  -0.620750
100.481875  0.000  -0.746000
100.652875  0.000  -0.870625
100.848625  0.000  -0.992500
101.068125  0.000  -1.109875
101.31025  0.000  -1.221250
101.573875  0.000  -1.324750
101.857875  0.000  -1.419375
102.16075  0.000  -1.503250
102.48075  0.000  -1.574250
102.817625  0.000  -1.629625
103.17125  0.000  -1.668250
103.543375  0.000  -1.688125
103.936  0.000  -1.690750
104.347125  0.000  -1.680875
104.774125  0.000  -1.658875
105.215125  0.000  -1.626375
105.6675  0.000  -1.585375
106.128125  0.000  -1.537875
106.593  0.000  -1.485125
107.058125  0.000  -1.428125
107.51975  0.000  -1.366875
107.97475  0.000  -1.301500
108.42  0.000  -1.232375
108.852875  0.000  -1.159625
109.27075  0.000  -1.083875
109.671125  0.000  -1.005500
110.0515  0.000  -0.925250
110.409625  0.000  -0.843625
110.743375  0.000  -0.761125
111.05075  0.000  -0.678375
111.330125  0.000  -0.596000
111.579875  0.000  -0.514500
111.798625  0.000  -0.434500
111.9855  0.000  -0.356625
112.138875  0.000  -0.281250
112.259375  0.000  -0.205750
```

112.353125 0.000 -0.129625
112.427125 0.000 -0.061750
112.47975 0.000 -0.015750
112.5 0.000 0.000
5 1
36
112.500625 0.000 12.477750
112.5055 0.000 12.570125
112.533 0.000 12.640000
112.598625 0.000 12.678375
112.71475 0.000 12.693750
112.87575 0.000 12.698000
113.078375 0.000 12.691500
113.320125 0.000 12.675500
113.598375 0.000 12.650250
113.91025 0.000 12.615625
114.2525 0.000 12.570375
114.62575 0.000 12.509375
115.03475 0.000 12.433125
115.48 0.000 12.348375
115.959125 0.000 12.259000
116.46875 0.000 12.168500
117.0055 0.000 12.080250
117.564875 0.000 11.997375
118.142375 0.000 11.922750
118.7325 0.000 11.858875
119.329875 0.000 11.808250
119.9285 0.000 11.772500
120.522 0.000 11.753000
121.104 0.000 11.750750
121.668 0.000 11.766000
122.2075 0.000 11.798500
122.716125 0.000 11.847625
123.1875 0.000 11.911750
123.616 0.000 11.989000
123.99575 0.000 12.076625
124.321625 0.000 12.172000
124.586625 0.000 12.272250
124.781875 0.000 12.367500
124.9085 0.000 12.441500
124.978125 0.000 12.485625
125 0.000 12.500000
6 1
46
112.500625 0.000 12.477750
112.519375 0.000 12.370875
112.561875 0.000 12.253875
112.6285 0.000 12.130750
112.719375 0.000 12.004875
112.83675 0.000 11.879250
112.981875 0.000 11.754000
113.152875 0.000 11.629375
113.348625 0.000 11.507500
113.568125 0.000 11.390125
113.81025 0.000 11.278750
114.073875 0.000 11.175250
114.357875 0.000 11.080625
114.66075 0.000 10.996750
114.98075 0.000 10.925750
115.317625 0.000 10.870375
115.67125 0.000 10.831750
116.043375 0.000 10.811875
116.436 0.000 10.809250
116.847125 0.000 10.819125
117.274125 0.000 10.841125
117.715125 0.000 10.873625
118.1675 0.000 10.914625
118.628125 0.000 10.962125
119.093 0.000 11.014875
119.558125 0.000 11.071875
120.01975 0.000 11.133125
120.47475 0.000 11.198500
120.92 0.000 11.267625
121.352875 0.000 11.340375
121.77075 0.000 11.416125
122.171125 0.000 11.494500
122.5515 0.000 11.574750
122.909625 0.000 11.656375
123.243375 0.000 11.738875
123.55075 0.000 11.821625
123.830125 0.000 11.904000
124.079875 0.000 11.985500
124.298625 0.000 12.065500
124.4855 0.000 12.143375
124.638875 0.000 12.218750
124.759375 0.000 12.294250
124.853125 0.000 12.370375
124.927125 0.000 12.438250
124.97975 0.000 12.484250
125 0.000 12.500000
7 1
36
100.000625 29.7500 -0.02225
100.0055 29.7500 0.070125
100.033 29.75000 0.140000
100.098625 29.750 0.178375
100.21475 29.750 0.193750
100.37575 29.750 0.198000
100.578375 29.750 0.191500
100.820125 29.750 0.175500
101.098375 29.750 0.150250
101.41025 29.750 0.115625
101.7525 29.750 0.070375
102.12575 29.750 0.009375
102.53475 29.750 -0.066875
102.98 29.750 -0.151625
103.459125 29.750 -0.24100
103.96875 29.750 -0.331500
104.5055 29.750 -0.419750
105.064875 29.750 -0.502625
105.642375 29.750 -0.577250
106.2325 29.750 -0.641125
106.829875 29.750 -0.691750
107.4285 29.750 -0.727500
108.022 29.750 -0.747000
108.604 29.750 -0.749250
109.168 29.750 -0.734000
109.7075 29.750 -0.701500
110.216125 29.750 -0.652375
110.6875 29.750 -0.588250
111.116 29.750 -0.511000
111.49575 29.750 -0.423375
111.821625 29.750 -0.32800
112.086625 29.750 -0.22775
112.281875 29.750 -0.13250
112.4085 29.750 -0.058500
112.478125 29.750 -0.014375
112.5 29.750 0.000
8 1
46
100.000625 29.750 -0.02225
100.019375 29.750 -0.129125
100.061875 29.75 -0.246125
100.12850 29.750 -0.369250
100.219375 29.750 -0.495125
100.336750 29.750 -0.62075
100.481875 29.750 -0.74600
100.652875 29.750 -0.870625
100.848625 29.750 -0.99250
101.068125 29.750 -1.109875
101.310250 29.750 -1.22125
101.573875 29.750 -1.32475
101.857875 29.750 -1.419375
102.160750 29.750 -1.50325
102.480750 29.750 -1.57425
102.817625 29.750 -1.629625
103.171250 29.750 -1.66825
103.543375 29.750 -1.688125
103.93600 29.750 -1.69075
104.347125 29.750 -1.680875
104.774125 29.750 -1.658875
105.215125 29.750 -1.626375
105.66750 29.750 -1.585375
106.128125 29.750 -1.537875
106.593000 29.750 -1.485125
107.058125 29.750 -1.428125
107.519750 29.750 -1.366875
107.974750 29.750 -1.30150
108.420000 29.750 -1.232375
108.852875 29.750 -1.159625
109.270750 29.750 -1.083875
109.671125 29.750 -1.00550
110.051500 29.750 -0.92525
110.409625 29.750 -0.843625
110.743375 29.750 -0.761125
111.050750 29.750 -0.678375
111.330125 29.750 -0.596000
111.579875 29.750 -0.514500
111.798625 29.750 -0.434500
111.985500 29.750 -0.356625
112.138875 29.750 -0.281250
112.259375 29.750 -0.205750
112.353125 29.750 -0.129625
112.427125 29.750 -0.061750
112.479750 29.750 -0.015750
112.500000 29.750 0.000
9 1

36
112.500625 29.750 12.47775
112.50550 29.750 12.570125
112.53300 29.750 12.640000
112.598625 29.750 12.67837
112.71475 29.750 12.693750
112.87575 29.750 12.698000
113.078375 29.750 12.69150
113.320125 29.750 12.67550
113.598375 29.750 12.65025
113.91025 29.750 12.615625
114.25250 29.750 12.570375
114.62575 29.750 12.509375
115.03475 29.750 12.433125
115.48000 29.750 12.348375
115.959125 29.750 12.25900
116.468750 29.750 12.16850
117.005500 29.750 12.08025
117.564875 29.750 11.99737
118.142375 29.750 11.92275
118.73250 29.750 11.858875
119.329875 29.750 11.80825
119.92850 29.750 11.772500
120.52200 29.750 11.753000
121.10400 29.750 11.750750
121.66800 29.750 11.766000
122.20750 29.750 11.798500
122.716125 29.75 11.847625
123.18750 29.750 11.911750
123.61600 29.750 11.989000
123.99575 29.750 12.076625
124.321625 29.750 12.17200
124.586625 29.750 12.27225
124.781875 29.750 12.36750
124.908500 29.750 12.44150
124.978125 29.75 12.485625
125.00000 29.750 12.500000
10 1
46
112.500625 29.750 12.47775
112.519375 29.75 12.370875
112.561875 29.75 12.253875
112.62850 29.750 12.130750
112.719375 29.75 12.004875
112.83675 29.750 11.879250
112.981875 29.750 11.75400
113.152875 29.75 11.629375
113.348625 29.750 11.50750
113.568125 29.75 11.390125
113.810250 29.750 11.27875
114.073875 29.750 11.17525
114.357875 29.75 11.080625
114.660750 29.750 10.99675
114.980750 29.750 10.92575
115.317625 29.75 10.870375
115.671250 29.750 10.83175
116.043375 29.75 10.811875
116.43600 29.750 10.809250
116.847125 29.75 10.819125
117.274125 29.75 10.841125
117.715125 29.75 10.873625
118.16750 29.75 10.914625
118.628125 29.75 10.962125
119.093000 29.75 11.014875
119.558125 29.75 11.071875
120.019750 29.75 11.133125
120.474750 29.75 11.198500
120.920000 29.75 11.267625
121.352875 29.75 11.340375
121.770750 29.75 11.416125
122.171125 29.75 11.494500
122.551500 29.75 11.574750
122.909625 29.75 11.656375
123.243375 29.75 11.738875
123.550750 29.75 11.821625
123.830125 29.75 11.904000
124.079875 29.75 11.985500
124.298625 29.75 12.065500
124.485500 29.75 12.143375
124.638875 29.75 12.218750
124.759375 29.75 12.294250
124.853125 29.75 12.370375
124.927125 29.75 12.438250
124.979750 29.75 12.484250
125.000000 29.75 12.500000
11 1
2
100.000625 0.000 -0.022250
100.000625 29.750 -0.022250
12 1
2
112.500000 0.000 0.000
112.500000 29.750 0.000
13 1
2
112.500625 0.000 12.477750
112.500625 29.750
12.477750
14 1
2
125.000000 0.000 12.500000
125.000000 29.75 12.500000
15 1
2
98.6 29.750 14.400000
98.6 29.750 -3.200000
16 1
2
98.600000 30.000 14.400000
98.600000 30.000 -3.200000
17 1
2
98.6 29.750 14.400000
98.6 30.000 14.400000
18 1
2
98.6 29.750 -3.200000
98.6 30.000 -3.200000
19 1
2
125.8 29.750 -3.200000
98.6 29.750 -3.200000
20 1
2
125.80000 30.000 -3.200000
98.600000 30.000 -3.200000
21 1
2
125.8 29.750 -3.200000
125.8 30.000 -3.200000
22 1
2
125.8 29.750 14.400000
125.8 29.750 -3.200000
23 1
2
125.8000 30.000 14.400000
125.8000 30.000 -3.200000
24 1
2
125.8 29.750 14.400000
125.8 30.000 14.400000
25 1
2
125.8 29.750 14.400000
98.6 29.750 14.400000
26 1
2
125.8000 30.000 14.400000
98.60000 30.000 14.400000
Surfaces
1 1
2 2
-140.000 0.000 -260.000
380.000 0.000 -260.000
-140.000 0.000 260.000
380.000 0.000 260.000
2 1
21 21
-123.0000 0.000 0.000
-121.7700 0.000 24.5680
-116.8500 0.000 71.3400
-107.0100 0.000 87.2439
-89.7900 0.000 123.4354
-68.8800 0.000 153.9419
-39.3600 0.000 184.8124
-7.3800 0.000 208.6080
29.5200 0.000 227.5475
71.3400 0.000 240.5142
123.0000 0.000 246.0000
174.6600 0.000 240.5142
216.4800 0.000 227.5475
253.3800 0.000 208.6080
285.3600 0.000 184.8124
314.8800 0.000 153.9419
335.7900 0.000 123.4354
353.0100 0.000 87.2439

362.8500	0.000	54.6612
367.7700	0.000	24.5680
369.0000	0.000	0.000
-123.0000	0.000	0.000
-121.7700	3.8435	24.2679
-116.8500	8.5511	53.9896
-107.0100	13.6479	86.1689
-89.7900	19.3096	121.9151
-68.8800	24.0818	152.0477
-39.3600	28.9108	182.5369
-7.3800	32.6334	206.0398
29.5200	35.5961	224.7456
71.3400	37.6247	237.5524
123.0000	38.4828	242.9717
174.6600	37.6247	237.5524
216.4800	35.5961	224.7456
253.3800	32.6334	206.0398
285.3600	28.9108	182.5369
314.8800	24.0818	152.0477
335.7900	19.3096	121.9151
353.0100	13.6479	86.1689
362.8500	8.5511	53.9896
367.7700	3.8435	24.2679
369.0000	0.000	0.000
-123.0000	0.000	0.000
-121.7700	7.5923	23.3675
-116.8500	16.8916	51.9872
-107.0100	26.9597	82.9733
-89.7900	38.1438	117.3937
-68.8800	51.6600	120.5400
-39.3600	57.1098	175.7670
-7.3800	64.4632	198.3965
29.5200	66.4200	204.1800
71.3400	70.3157	216.4087
123.0000	76.0181	233.9608
174.6600	74.3230	228.7431
216.4800	70.3157	216.4087
253.3800	64.4632	198.3965
285.3600	57.1098	175.7670
314.8800	47.5706	146.4069
335.7900	38.1438	117.3937
353.0100	26.9597	82.9733
362.8500	16.8916	51.9872
367.7700	7.5923	23.3675
369.0000	0.000	0.000
-123.0000	0.000	0.000
-121.7700	11.1542	21.8915
-116.8500	24.8162	48.7055
-107.0100	39.6076	77.7335
-89.7900	56.0387	109.9817
-68.8800	69.8880	137.1622
-39.3600	83.9025	164.6675
-7.3800	94.7057	185.8702
29.5200	103.3039	202.7458
71.3400	109.1912	214.3004
123.000	111.6816	219.1885
174.660	109.1912	214.3004
216.480	103.3039	202.7458
253.3800	94.7057	185.8702

285.3600	83.9025	164.6675
314.8800	69.8880	137.1622
335.7900	56.0387	109.9817
353.0100	39.6076	77.7335
362.8500	24.8162	48.7055
367.7700	11.1542	21.8915
369.0000	0.000	0.000
-123.0000	0.000	0.000
-121.7700	14.4414	19.8768
-116.8500	32.1297	44.2234
-107.0100	51.2803	70.5823
-89.7900	72.5537	99.8612
-68.8800	90.4846	124.5424
-39.3600	108.6293	149.5163
-7.3800	122.6163	168.7658
29.5200	133.7485	184.0892
71.3400	141.3708	194.5811
123.000	144.5951	199.0189
174.660	141.3708	194.5811
216.480	133.7485	184.0892
253.380	122.6163	168.7658
285.360	108.6293	149.5163
314.8800	90.4846	124.5424
335.7900	72.5537	99.8612
353.0100	51.2803	70.5823
362.8500	32.1297	44.2234
367.7700	14.4414	19.8768
369.0000	0.000	0.000
-123.0000	0.000	0.000
-121.7700	17.3731	17.3725
-116.8500	38.6521	38.6515
-107.0100	61.6903	61.6894
-89.7900	87.2823	87.2833
-68.8800	108.8532	108.8525
-39.3600	130.6813	130.6826
-7.3800	147.5076	147.5090
29.5200	160.8997	160.8988
71.3400	170.0694	170.0696
123.000	173.9482	173.9491
174.660	170.0694	170.0696
216.480	160.8997	160.8988
253.380	147.5076	147.5090
285.360	130.6813	130.6826
314.880	108.8532	108.8525
335.7900	87.2823	87.2833
353.0100	61.6903	61.6894
362.8500	38.6521	38.6515
367.7700	17.3731	17.3725
369.0000	0.000	0.000
-123.0000	0.000	0.000
-121.7700	19.8769	14.4427
-116.8500	44.2228	32.1301
-107.0100	70.5813	51.2812
-89.7900	99.8617	72.5528
-68.8800	124.5414	90.4837
-39.3600	149.5154	108.6287
-7.3800	168.7669	122.6162
29.5200	184.0890	133.7477
71.3400	194.5802	141.3713

123.000	199.0181	144.5963
174.660	194.5802	141.3713
216.480	184.0890	133.7477
253.380	168.7669	122.6162
285.360	149.5154	108.6287
314.8800	124.5414	90.4837
335.7900	99.8617	72.5528
353.0100	70.5813	51.2812
362.8500	44.2228	32.1301
367.7700	19.8769	14.4427
369.0000	0.000	0.000
-123.0000	0.000	0.000
-121.7700	21.8913	11.1536
-116.8500	48.7045	24.8165
-107.0100	77.7343	39.6085
-89.7900	109.9821	56.0388
-68.8800	137.1630	69.8886
-39.3600	164.6680	83.9032
-7.3800	185.8705	94.7051
29.5200	202.7455	103.3052
71.3400	214.2999	109.1920
123.000	219.1875	111.6815
174.660	214.2999	109.1920
216.480	202.7455	103.3052
253.3800	185.8705	94.7051
285.3600	164.6680	83.9032
314.8800	137.1630	69.8886
335.7900	109.9821	56.0388
353.0100	77.7343	39.6085
362.8500	48.7045	24.8165
367.7700	21.8913	11.1536
369.0000	0.000	0.000
-123.0000	0.000	0.000
-121.7700	23.3667	7.5916
-116.8500	51.9870	16.8928
-107.0100	82.9733	26.9591
-89.7900	117.3945	38.1448
-68.8800	146.4073	47.5715
-39.3600	175.7660	57.1089
-7.3800	198.3974	64.4643
29.5200	216.4097	70.3166
71.3400	228.7428	74.3240
123.0000	233.9598	76.0189
174.6600	228.7428	74.3240
216.4800	216.4097	70.3166
253.3800	198.3974	64.4643
285.3600	175.7660	57.1089
314.8800	146.4073	47.5715
335.7900	117.3945	38.1448
353.0100	82.9733	26.9591
362.8500	51.9870	16.8928
367.7700	23.3667	7.5916
369.0000	0.000	0.000
-123.0000	0.000	0.000
-121.7700	24.2667	3.8425
-116.8500	53.9894	8.5510
-107.0100	86.1692	13.6481
-89.7900	121.9162	19.3110
-68.8800	152.0465	24.0809

-39.3600	182.5360	28.9099
-7.3800	206.0391	32.6344
29.5200	224.7452	35.5962
71.3400	237.5534	37.6257
123.0000	242.9713	38.4842
174.6600	237.5534	37.6257
216.4800	224.7452	35.5962
253.3800	206.0391	32.6344
285.3600	182.5360	28.9099
314.8800	152.0465	24.0809
335.7900	121.9162	19.3110
353.0100	86.1692	13.6481
362.8500	53.9894	8.5510
367.7700	24.2667	3.8425
369.0000	0.000	0.000
-123.0000	0.000	0.000
-121.7700	24.5692	0.000
-116.8500	54.6624	0.000
-107.0100	87.2433	0.000
-89.7900	123.4359	0.000
-68.8800	153.9418	0.000
-39.3600	184.8113	0.000
-7.3800	208.6074	0.000
29.5200	227.5467	0.000
71.3400	240.5145	0.000
123.0000	246.0000	0.000
174.6600	240.5145	0.000
216.4800	227.5467	0.000
253.3800	208.6074	0.000
285.3600	184.8113	0.000
314.8800	153.9418	0.000
335.7900	123.4359	0.000
353.0100	87.2433	0.000
362.8500	54.6624	0.000
367.7700	24.5692	0.000
369.0000	0.000	0.000
-123.0000	0.000	0.000
-121.7700	24.2667	-3.8425
-116.8500	53.9894	-8.5510
-107.0100	86.1692	-13.6481
-89.7900	121.9162	-19.3085
-68.8800	152.0465	-24.0809
-39.3600	182.5360	-28.9099
-7.3800	206.0392	-32.6319
29.5200	224.7453	-35.5962
71.3400	237.5535	-37.6232
123.0000	242.9714	-38.4818
174.6600	237.5535	-37.6232
216.4800	224.7453	-35.5962
253.3800	206.0392	-32.6319
285.3600	182.5360	-28.9099
314.8800	152.0465	-24.0809
335.7900	121.9162	-19.3085
353.0100	86.1692	-13.6481
362.8500	53.9894	-8.5510
367.7700	24.2667	-3.8425
369.0000	0.000	0.000
-123.0000	0.000	0.000
-121.7700	23.3667	-7.5916
-116.8500	51.9871	-16.8904
-107.0100	82.9734	-26.9591
-89.7900	117.3946	-38.1448
-68.8800	146.4074	-47.5715
-39.3600	175.7661	-57.1089
-7.3800	198.3975	-64.4618
29.5200	216.4099	-70.3166
71.3400	228.7430	-74.3215
123.0000	233.9600	-76.0189
174.6600	228.7430	-74.3215
216.4800	216.4099	-70.3166
253.3800	198.3975	-64.4618
285.3600	175.7661	-57.1089
314.8800	146.4074	-47.5715
335.7900	117.3946	-38.1448
353.0100	82.9734	-26.9591
362.8500	51.9871	-16.8904
367.7700	23.3667	-7.5916
369.0000	0.000	0.000
-123.0000	0.000	0.000
-121.7700	21.8914	-11.1536
-116.8500	48.7046	-24.8165
-107.0100	77.7345	-39.6085
-89.7900	109.9823	-56.0388
-68.8800	137.1632	-69.8886
-39.3600	164.6683	-83.9032
-7.3800	185.8707	-94.7051
29.5200	202.7458	-103.3028
71.3400	214.3002	-109.1920
123.000	219.1878	-111.6815
174.660	214.3002	-109.1920
216.480	202.7458	-103.3028
253.3800	185.8707	-94.7051
285.3600	164.6683	-83.9032
314.8800	137.1632	-69.8886
335.7900	109.9823	-56.0388
353.0100	77.7345	-39.6085
362.8500	48.7046	-24.8165
367.7700	21.8914	-11.1536
369.0000	0.000	0.000
-123.0000	0.000	0.000
-121.7700	19.8770	-14.4402
-116.8500	44.2229	-32.1301
-107.0100	70.5814	-51.2812
-89.7900	99.8619	-72.5528
-68.8800	124.5417	-90.4837
-39.360	149.5157	-108.6287
-7.3800	168.7672	-122.6162
29.5200	184.0894	-133.7477
71.3400	194.5806	-141.3713
123.000	199.0184	-144.5939
174.660	194.5806	-141.3713
216.480	184.0894	-133.7477
253.380	168.7672	-122.6162
285.360	149.5157	-108.6287
314.8800	124.5417	-90.4837
335.7900	99.8619	-72.5528
353.0100	70.5814	-51.2812
362.8500	44.2229	-32.1301
367.7700	19.8770	-14.4402
369.0000	0.000	0.000
-123.0000	0.000	0.000
-121.7700	17.3731	-17.3725
-116.8500	38.6522	-38.6515
-107.0100	61.6905	-61.6894
-89.7900	87.2825	-87.2833
-68.880	108.8535	-108.8525
-39.360	130.6816	-130.6801
-7.3800	147.5080	-147.5065
29.5200	160.9001	-160.8988
71.3400	170.0698	-170.0696
123.000	173.9486	-173.9491
174.660	170.0698	-170.0696
216.480	160.9001	-160.8988
253.380	147.5080	-147.5065
285.360	130.6816	-130.6801
314.880	108.8535	-108.8525
335.7900	87.2825	-87.2833
353.0100	61.6905	-61.6894
362.8500	38.6522	-38.6515
367.7700	17.3731	-17.3725
369.0000	0.000	0.000
-123.0000	0.000	0.000
-121.7700	14.4415	-19.8768
-116.8500	32.1298	-44.2234
-107.0100	51.2805	-70.5823
-89.7900	72.5540	-99.8612
-68.8800	90.4850	-124.5424
-39.360	108.6297	-149.5163
-7.3800	122.6167	-168.7658
29.5200	133.7490	-184.0892
71.3400	141.3713	-194.5811
123.000	144.5956	-199.0189
174.660	141.3713	-194.5811
216.480	133.7490	-184.0892
253.380	122.6167	-168.7658
285.360	108.6297	-149.5163
314.8800	90.4850	-124.5424
335.7900	72.5540	-99.8612
353.0100	51.2805	-70.5823
362.8500	32.1298	-44.2234
367.7700	14.4415	-19.8768
369.0000	0.000	0.000
-123.0000	0.000	0.000
-121.7700	11.1542	-21.8915
-116.8500	24.8163	-48.7055
-107.0100	39.6078	-77.7335
-89.7900	56.0390	-109.9817
-68.8800	69.8884	-137.1622
-39.3600	83.9030	-164.6675
-7.3800	94.7062	-185.8702
29.5200	103.3045	-202.7458
71.3400	109.1918	-214.3004
123.000	111.6822	-219.1885
174.660	109.1918	-214.3004
216.480	103.3045	-202.7458
253.3800	94.7062	-185.8702
285.3600	83.9030	-164.6675

314.8800 69.8884 -137.1622
335.7900 56.0390 -109.9817
353.0100 39.6078 -77.7335
362.8500 24.8163 -48.7055
367.7700 11.1542 -21.8915
369.0000 0.000 0.000
-123.0000 0.000 0.000
-121.7700 7.5924 -23.3675
-116.8500 16.8917 -51.9872
-107.0100 26.9599 -82.9733
-89.7900 38.1441 -117.3937
-68.8800 47.5710 -146.4069
-39.3600 57.1103 -175.7670
-7.3800 64.4637 -198.3965
29.5200 70.3163 -216.4087
71.3400 74.3236 -228.7431
123.0000 76.0187 -233.9608
174.6600 74.3236 -228.7431
216.4800 70.3163 -216.4087
253.3800 64.4637 -198.3965
285.3600 57.1103 -175.7670
314.8800 47.5710 -146.4069
335.7900 38.1441 -117.3937
353.0100 26.9599 -82.9733
362.8500 16.8917 -51.9872
367.7700 7.5924 -23.3675
369.0000 0.000 0.000
-123.0000 0.000 0.000
-121.7700 3.8435 -24.2679
-116.8500 8.5512 -53.9896
-107.0100 13.6481 -86.1689
-89.7900 19.3099 -121.9151
-68.8800 24.0822 -152.0452
-39.3600 28.9113 -182.5369
-7.3800 32.6339 -206.0398
29.5200 35.5967 -224.7456
71.3400 37.6254 -237.5524
123.0000 38.4835 -242.9717
174.6600 37.6254 -237.5524
216.4800 35.5967 -224.7456
253.3800 32.6339 -206.0398
285.3600 28.9113 -182.5369
314.8800 24.0822 -152.0452
335.7900 19.3099 -121.9151
353.0100 13.6481 -86.1689
362.8500 8.5512 -53.9896
367.7700 3.8435 -24.2679
369.0000 0.000 0.000
-123.0000 0.000 0.000
-121.7700 0.000 -24.5680
-116.8500 0.000 -54.6612
-107.0100 0.000 -87.2439
-89.7900 0.000 -123.4354
-68.8800 0.000 -153.9419
-39.3600 0.000 -184.8124
-7.3800 0.000 -208.6080
29.5200 0.000 -227.5475
71.3400 0.000 -240.5142
123.0000 0.000 -246.0000
174.6600 0.000 -240.5142
216.4800 0.000 -227.5475
253.3800 0.000 -208.6080
285.3600 0.000 -184.8124
314.8800 0.000 -153.9419
335.7900 0.000 -123.4354
353.0100 0.000 -87.2439
362.8500 0.000 -54.6612
367.7700 0.000 -24.5680
369.0000 0.000 0.000
3 1
36 2
100.000625 0.000 -0.022250
100.0055 0.000 0.070125
100.033 0.000 0.140000
100.098625 0.000 0.178375
100.21475 0.000 0.193750
100.37575 0.000 0.198000
100.578375 0.000 0.191500
100.820125 0.000 0.175500
101.098375 0.000 0.150250
101.41025 0.000 0.115625
101.7525 0.000 0.070375
102.12575 0.000 0.009375
102.53475 0.000 -0.066875
102.98 0.000 -0.151625
103.459125 0.000 -0.241000
103.96875 0.000 -0.331500
104.5055 0.000 -0.419750
105.064875 0.000 -0.502625
105.642375 0.000 -0.577250
106.2325 0.000 -0.641125
106.829875 0.000 -0.691750
107.4285 0.000 -0.727500
108.022 0.000 -0.747000
108.604 0.000 -0.749250
109.168 0.000 -0.734000
109.7075 0.000 -0.701500
110.216125 0.000 -0.652375
110.6875 0.000 -0.588250
111.116 0.000 -0.511000
111.49575 0.000 -0.423375
111.821625 0.000 -0.328000
112.086625 0.000 -0.227750
112.281875 0.000 -0.132500
112.4085 0.000 -0.058500
112.478125 0.000 -0.014375
112.5 0.000 0.000
100.000625 29.750 -0.02225
100.0055 29.750 0.070125
100.033 29.750 0.140000
100.098625 29.75 0.178375
100.21475 29.750 0.193750
100.37575 29.750 0.198000
100.578375 29.75 0.191500
100.820125 29.750 0.17550
101.098375 29.75 0.150250
101.41025 29.750 0.115625
101.7525 29.750 0.070375
102.12575 29.750 0.009375
102.53475 29.750 -0.066875
102.98 29.750 -0.151625
103.459125 29.75 -0.241000
103.96875 29.750 -0.331500
104.5055 29.750 -0.419750
105.064875 29.75 -0.502625
105.642375 29.75 -0.577250
106.2325 29.750 -0.641125
106.829875 29.75 -0.691750
107.4285 29.750 -0.727500
108.022 29.750 -0.747000
108.604 29.750 -0.749250
109.168 29.750 -0.734000
109.7075 29.750 -0.701500
110.216125 29.75 -0.652375
110.6875 29.750 -0.588250
111.116 29.750 -0.511000
111.49575 29.750 -0.423375
111.821625 29.75 -0.328000
112.086625 29.75 -0.227750
112.281875 29.75 -0.132500
112.4085 29.750 -0.058500
112.478125 29.75 -0.014375
112.5 29.750 0.000
4 1
46 2
100.000625 0.000 -0.022250
100.019375 0.000 -0.129125
100.061875 0.000 -0.246125
100.1285 0.000 -0.369250
100.219375 0.000 -0.495125
100.33675 0.000 -0.620750
100.481875 0.000 -0.746000
100.652875 0.000 -0.870625
100.848625 0.000 -0.992500
101.068125 0.000 -1.109875
101.31025 0.000 -1.221250
101.573875 0.000 -1.324750
101.857875 0.000 -1.419375
102.16075 0.000 -1.503250
102.48075 0.000 -1.574250
102.817625 0.000 -1.629625
103.17125 0.000 -1.668250
103.543375 0.000 -1.688125
103.936 0.000 -1.690750
104.347125 0.000 -1.680875
104.774125 0.000 -1.658875
105.215125 0.000 -1.626375
105.6675 0.000 -1.585375
106.128125 0.000 -1.537875
106.593 0.000 -1.485125
107.058125 0.000 -1.428125
107.51975 0.000 -1.366875
107.97475 0.000 -1.301500
108.42 0.000 -1.232375
108.852875 0.000 -1.159625
109.27075 0.000 -1.083875
109.671125 0.000 -1.005500

110.0515 0.000 -0.925250
110.409625 0.000 -0.843625
110.743375 0.000 -0.761125
111.05075 0.000 -0.678375
111.330125 0.000 -0.596000
111.579875 0.000 -0.514500
111.798625 0.000 -0.434500
111.9855 0.000 -0.356625
112.138875 0.000 -0.281250
112.259375 0.000 -0.205750
112.353125 0.000 -0.129625
112.427125 0.000 -0.061750
112.47975 0.000 -0.015750
112.5 0.000 0.000
100.000625 29.750 -0.02225
100.019375 29.75 -0.129125
100.061875 29.75 -0.246125
100.1285 29.750 -0.369250
100.219375 29.75 -0.495125
100.33675 29.750 -0.620750
100.481875 29.75 -0.746000
100.652875 29.75 -0.870625
100.848625 29.75 -0.992500
101.068125 29.75 -1.109875
101.31025 29.75 -1.221250
101.573875 29.75 -1.324750
101.857875 29.75 -1.419375
102.16075 29.75 -1.503250
102.48075 29.75 -1.574250
102.817625 29.75 -1.629625
103.17125 29.75 -1.668250
103.543375 29.75 -1.688125
103.936 29.75 -1.690750
104.347125 29.75 -1.680875
104.774125 29.75 -1.658875
105.215125 29.75 -1.626375
105.6675 29.75 -1.585375
106.128125 29.75 -1.537875
106.593 29.75 -1.485125
107.058125 29.75 -1.428125
107.51975 29.75 -1.366875
107.97475 29.75 -1.301500
108.42 29.75 -1.232375
108.852875 29.75 -1.159625
109.27075 29.75 -1.083875
109.671125 29.75 -1.005500
110.0515 29.75 -0.925250
110.409625 29.75 -0.843625
110.743375 29.75 -0.761125
111.05075 29.75 -0.678375
111.330125 29.75 -0.596000
111.579875 29.75 -0.514500
111.798625 29.75 -0.434500
111.9855 29.75 -0.356625
112.138875 29.75 -0.281250
112.259375 29.75 -0.205750
112.353125 29.75 -0.129625
112.427125 29.75 -0.061750
112.47975 29.75 -0.015750
112.5 29.75 0.000
5 1
36 2
112.500625 0.000 12.47775
112.5055 0.000 12.570125
112.533 0.000 12.640000
112.598625 0.00 12.678375
112.71475 0.000 12.693750
112.87575 0.000 12.698000
113.078375 0.000 12.69150
113.320125 0.000 12.67550
113.598375 0.000 12.65025
113.91025 0.000 12.615625
114.2525 0.000 12.570375
114.62575 0.000 12.509375
115.03475 0.000 12.433125
115.48 0.000 12.348375
115.959125 0.000 12.25900
116.46875 0.000 12.168500
117.0055 0.000 12.080250
117.564875 0.00 11.997375
118.142375 0.000 11.92275
118.7325 0.000 11.858875
119.329875 0.000 11.80825
119.9285 0.000 11.772500
120.522 0.000 11.753000
121.104 0.000 11.750750
121.668 0.000 11.766000
122.2075 0.000 11.798500
122.716125 0.00 11.847625
123.1875 0.000 11.911750
123.616 0.000 11.989000
123.99575 0.000 12.076625
124.321625 0.000 12.17200
124.586625 0.000 12.27225
124.781875 0.000 12.36750
124.9085 0.000 12.441500
124.978125 0.00 12.485625
125 0.000 12.500000
112.500625 29.75 12.47775
112.5055 29.75 12.570125
112.533 29.75 12.640000
112.598625 9.75 12.678375
112.71475 29.75 12.693750
112.87575 29.75 12.698000
113.078375 29.75 12.69150
113.320125 29.75 12.67550
113.598375 29.75 12.65025
113.91025 29.75 12.615625
114.2525 29.75 12.570375
114.62575 29.75 12.509375
115.03475 29.75 12.433125
115.48 29.75 12.348375
115.959125 29.75 12.25900
116.46875 29.75 12.168500
117.0055 29.75 12.080250
117.564875 29.75 11.997375
118.142375 29.75 11.92275
118.7325 29.75 11.858875
119.329875 29.75 11.80825
119.9285 29.75 11.772500
120.522 29.75 11.753000
121.104 29.75 11.750750
121.668 29.75 11.766000
122.2075 29.75 11.798500
122.716125 29.75 11.847625
123.1875 29.75 11.911750
123.616 29.75 11.989000
123.99575 29.75 12.076625
124.321625 29.75 12.17200
124.586625 29.75 12.27225
124.781875 29.75 12.36750
124.9085 29.75 12.441500
124.978125 29.75 12.485625
125 29.75 12.500000
6 1
46 2
112.500625 0.000 12.47775
112.519375 0.000 12.370875
112.561875 0.000 12.253875
112.6285 0.000 12.130750
112.719375 0.000 12.004875
112.83675 0.000 11.879250
112.981875 0.000 11.75400
113.152875 0.000 11.629375
113.348625 0.000 11.50750
113.568125 0.000 11.390125
113.81025 0.000 11.278750
114.073875 0.000 11.17525
114.357875 0.000 11.080625
114.66075 0.000 10.996750
114.98075 0.000 10.925750
115.317625 0.000 10.870375
115.67125 0.000 10.831750
116.043375 0.000 10.811875
116.436 0.000 10.809250
116.847125 0.000 10.819125
117.274125 0.000 10.841125
117.715125 0.000 10.873625
118.1675 0.000 10.914625
118.628125 0.000 10.962125
119.093 0.000 11.014875
119.558125 0.000 11.071875
120.01975 0.000 11.133125
120.47475 0.000 11.198500
120.92 0.000 11.267625
121.352875 0.000 11.340375
121.77075 0.000 11.416125
122.171125 0.000 11.49450
122.5515 0.000 11.574750
122.909625 0.000 11.656375
123.243375 0.000 11.738875
123.55075 0.000 11.821625
123.830125 0.000 11.90400
124.079875 0.000 11.98550
124.298625 0.000 12.06550
124.4855 0.000 12.143375
124.638875 0.000 12.21875

124.759375 0.000 12.29425
124.853125 0.000 12.370375
124.927125 0.000 12.43825
124.97975 0.000 12.484250
125 0.000 12.500000
112.500625 29.75 12.47775
112.519375 29.75 12.370875
112.561875 29.75 12.253875
112.6285 29.75 12.130750
112.719375 29.75 12.004875
112.83675 29.75 11.879250
112.981875 29.75 11.75400
113.152875 29.75 11.629375
113.348625 29.75 11.50750
113.568125 29.75 11.390125
113.81025 29.75 11.278750
114.073875 29.75 11.17525
114.357875 29.75 11.080625
114.66075 29.75 10.996750
114.98075 29.75 10.925750
115.317625 29.75 10.870375
115.67125 29.75 10.831750
116.043375 29.75 10.811875
116.436 29.75 10.809250
116.847125 29.75 10.819125
117.274125 29.75 10.841125
117.715125 29.75 10.873625
118.1675 29.75 10.914625
118.628125 29.75 10.962125
119.093 29.75 11.014875
119.558125 29.75 11.071875
120.01975 29.75 11.133125
120.47475 29.75 11.198500
120.92 29.75 11.267625
121.352875 29.75 11.340375
121.77075 29.75 11.416125
122.171125 29.75 11.494500
122.5515 29.75 11.574750
122.909625 29.75 11.656375
123.243375 29.75 11.738875
123.55075 29.75 11.821625
123.830125 29.75 11.904000
124.079875 29.75 11.985500
124.298625 29.75 12.065500
124.4855 29.75 12.143375
124.638875 29.75 12.218750
124.759375 29.75 12.294250
124.853125 29.75 12.370375
124.927125 29.75 12.438250
124.97975 29.75 12.484250
125 29.75 12.500000
7 1
2 2
70 29.75 -30.000
130 29.75 -30.000
70 29.75 30.000
130 29.75 30.000
8 1
2 2
70 30.000 -30.000
130 30.000 -30.000
70 30.000 30.000
130 30.000 30.000
9 1
2 2
98.6 29.75 -3.200000
98.6 30.000 -3.200000
98.6 29.75 14.400000
98.6 30.000 14.400000
10 1
2 2
98.6 29.75 -3.200000
98.6 30.000 -3.200000
125.8 29.75 -3.200000
125.8 30.000 -3.200000
11 1
2 2
125.8 29.75 -3.200000
125.8 30.000 -3.200000
125.8 29.75 14.400000
125.8 30.000 14.400000
12 1
2 2
98.600000 29.75 14.400000
98.60000 30.000 14.400000
125.80000 29.75 14.400000
125.8000 30.000 14.400000
Mesh generation
26 12
Curves segments
1 1 1
2 2 1
3 3 1
4 4 1
5 5 1
6 6 1
7 7 1
8 8 1
9 9 1
10 10 1
11 11 1
12 12 1
13 13 1
14 14 1
15 15 1
16 16 1
17 17 1
18 18 1
19 19 1
20 20 1
21 21 1
22 22 1
23 23 1
24 24 1
25 25 1
26 26 1
Surface Regions
1 1 1
6
1 -2 -3 4 -5 6
2 2 1
2
1 2
3 3 1
4
11 3 12 7
4 4 1
4
11 8 12 4
5 5 1
4
13 5 14 9
6 6 1
4
13 10 14 6
7 7 1
8
25 15 -19 -22 7 -8 9 -10
8 8 1
4
23 20 -16 -26
9 9 1
4
17 16 -18 -15
10 10 1
4
19 18 -20 -21
11 11 1
4
22 21 -23 -24
12 12 1
4
24 26 -17 -25

APPENDIX B-2

STARS-CFD Background Mesh Data File (*boxwing.bac*)

```
Background Mesh....boxwing
4       1       0       3       6
1       -1800   -100    -2400
        1       0       0       40
        0       1       0       40
        0       0       1       40
2       1800    -100    -2400
        1       0       0       40
        0       1       0       40
        0       0       1       40
3       0       -100    2400
        1       0       0       40
        0       1       0       40
        0       0       1       40
4       0       2400    0
        1       0       0       40
        0       1       0       40
        0       0       1       40
1       1       2       3       4
* Point Sources
* Line Sources
1. Leading Edge of Lower Wing
100.00000    0.00000     -0.02224    0.07   0.07   0.35
100.00000    30.00000    -0.02224    0.07   0.07   0.35
2. Leading Edge of Upper Wing
112.50063    0.00000     12.57013    0.07   0.07   0.35
112.50063    30.00000    12.57013    0.07   0.07   0.35
3. In the middle
112.50063    0.00000     6.00000     0.8    6      15.00000
112.50063    30.00000    6.00000     0.8    6      15.00000
* Triangle Sources
1. Source for lower wing
100.00000    0.00000     0.00000     0.5    1      3
100.00000    30.00000    0.00000     0.5    1      3
```

112.50000	0.00000	0.00000	0.5	1	3
2. Source for lower wing					
112.50000	0.00000	0.00000	0.5	1	3
100.00000	30.00000	0.00000	0.5	1	3
112.50000	30.00000	0.00000	0.5	1	3
3. Source for upper wing					
112.50063	0.00000	12.57013	0.5	1	3
112.50063	30.00000	12.57013	0.5	1	3
125.00000	0.00000	12.57013	0.5	1	3
4. Source for upper wing					
125.00000	0.00000	12.57013	0.5	1	3
112.50063	30.00000	12.57013	0.5	1	3
125.00000	30.00000	12.57013	0.5	1	3
5. Source for endplate					
98.60000	30.00000	14.40000	0.5	1	3
125.80000	30.00000	-3.20000	0.5	1	3
125.80000	30.00000	14.40000	0.5	1	3
6. Source for endplate					
98.60000	30.00000	14.40000	0.5	1	3
125.80000	30.00000	-3.20000	0.5	1	3
98.60000	30.00000	-3.20000	0.5	1	3

APPENDIX B-3

STARS-CFD Boundary Conditions Data File (*boxwing.bco*)

```
Fin Boundary Condition File
12   26
Surface Regions
1    2
2    3
3    1
4    1
5    1
6    1
7    1
8    1
9    1
10   1
11   1
12   1
Curve Segments
1    0
2    0
3    0
4    0
5    0
6    0
7    3
8    3
9    3
10   3
11   0
12   1
13   0
14   1
15   1
16   1
17   1
18   1
19   3
20   3
21   1
22   1
23   1
24   1
25   3
26   3
```

APPENDIX B-4

STARS-CFD Parameter Control File (*boxwing.cons*)

```
&control
 nout    = 50.
 nstep   = 1,
 ncycl   = 5000,
 nstpe   = 20,
 nsmth   = 0,
 smofc   = 0.25,
 cfl     = 0.20,
 mach    = 0.434,
 alpha   = 0.0,
 beta    = 0.0,
 relax   = 1.0,
 amplitude= 1.0,
 restart = 0,
/
```

APPENDIX C-1

Selig 1223 Airfoil Coordinate Data

X	Y
0.00005	-0.00178
0.00155	-0.01033
0.00495	-0.01969
0.01028	-0.02954
0.01755	-0.03961
0.02694	-0.04966
0.03855	-0.05968
0.05223	-0.06965
0.06789	-0.07940
0.08545	-0.08879
0.10482	-0.09770
0.12591	-0.10598
0.14863	-0.11355
0.17286	-0.12026
0.19846	-0.12594
0.22541	-0.13037
0.25370	-0.13346
0.28347	-0.13505
0.31488	-0.13526
0.34777	-0.13447
0.38193	-0.13271
0.41721	-0.13011
0.45340	-0.12683
0.49025	-0.12303
0.52744	-0.11881
0.56465	-0.11425
0.60158	-0.10935
0.63798	-0.10412
0.67360	-0.09859
0.70823	-0.09277
0.74166	-0.08671
0.77369	-0.08044
0.80412	-0.07402
0.83277	-0.06749
0.85947	-0.06089
0.88406	-0.05427
0.90641	-0.04768
0.92639	-0.04116
0.94389	-0.03476
0.95884	-0.02853
0.97111	-0.02250
0.98075	-0.01646
0.98825	-0.01037
0.99417	-0.00494
0.99838	-0.00126
1.00000	0.00000
0.00044	0.00561
0.00264	0.01120
0.00789	0.01427
0.01718	0.01550
0.03006	0.01584
0.04627	0.01532
0.06561	0.01404
0.08787	0.01202
0.11282	0.00925
0.14020	0.00563
0.17006	0.00075
0.20278	-0.00535
0.23840	-0.01213
0.27673	-0.01928
0.31750	-0.02652
0.36044	-0.03358
0.40519	-0.04021
0.45139	-0.04618
0.49860	-0.05129
0.54639	-0.05534
0.59428	-0.05820

0.64176	-0.05976
0.68832	-0.05994
0.73344	-0.05872
0.77660	-0.05612
0.81729	-0.05219
0.85500	-0.04706
0.88928	-0.04088
0.91966	-0.03387
0.94573	-0.02624
0.96693	-0.01822
0.98255	-0.01060
0.99268	-0.00468
0.99825	-0.00115
1.00000	0.00000

VITA

Tony Michael Buratti

Candidate for the Degree of

Masters of Science

Thesis: TOP-FUEL DRAGSTER WING DESIGN USING CFD AND ITS INFLUENCE ON VEHICLE DYNAMIC PERFORMANCE

Major Field: Mechanical Engineering

Biography:

Personal Data: Born in Oklahoma City, Oklahoma March 12, 1976. The son of Richard M. and Joyce K. Buratti.

Education: Graduated from John Marshall High School, Oklahoma City, Oklahoma in May 1994; received a Bachelor of Science degree in Mechanical Engineering in July 1998 from Oklahoma State University, Stillwater, Oklahoma. Completed requirements for the Masters of Science degree with a major in Mechanical at Oklahoma State University in December, 2000.

Experience: Field Engineer, Boeing Aerospace Operations, 1997-1998; Teaching Assistant, Oklahoma State University School of Mechanical and Aerospace Engineering, 1998-2000; Graduate Research Assistant, Oklahoma State University School of Mechanical Engineering, 1998-2000.

Professional Memberships: American Institute of Aeronautics and Astronautics, American Society of Mechanical Engineers, Society of Automotive Engineers, American Pool Players Association, Phi Kappa Phi, Tau Beta Pi, Pi Tau Sigma, and Golden Key National Honor Society.